An Overview of Global Leaf Area Index (LAI): Methods, Products, Validation, and Applications

Fang, Hongliang ; Baret, Frédéric ; Plummer, Stephen ; Schaepman-Strub, Gabriela

Abstract: Leaf area index (LAI) is a critical vegetation structural variable and is essential in the feedback of vegetation to the climate system. The advancement of the global Earth Observation has enabled the development of global LAI products and boosted global Earth system modeling studies. This overview provides a comprehensive analysis of LAI field measurements and remote sensing estimation methods, the product validation methods and product uncertainties, and the application of LAI in global studies. First, the paper clarifies some definitions related to LAI and introduces methods to determine LAI from field measurements and remote sensing observations. After introducing some major global LAI products, progresses made in temporal compositing and prospects for future LAI estimation are analyzed. Subsequently, the overview discusses various LAI product validation schemes, uncertainties in global moderate resolution LAI products, and high resolution reference data. Finally, applications of LAI in global vegetation change, land surface modeling, and agricultural studies are presented. It is recommended that (1) continued efforts are taken to advance LAI estimation algorithms and provide high temporal and spatial resolution products from current and forthcoming missions; (2) further validation studies be conducted to address the inadequacy of current validation studies, especially for underrepresented regions and seasons; and (3) new research frontiers, such as machine learning algorithms, light detection and ranging technology, and unmanned aerial vehicles be pursued to broaden the production and application of LAI.

DOI: https://doi.org/10.1029/2018rg000608

Reviews of Geophysics

REVIEW ARTICLE
10.1029/2018RG000608

An Overview of Global Leaf Area Index (LAI): Methods, Products, Validation, and Applications

Hongliang Fang[1], Frédéric Baret[2], Stephen Plummer[3], and Gabriela Schaepman-Strub[4]

[1]LREIS, Institute of Geographic Sciences and Natural Resources Research, Chinese Academy of Sciences, Beijing, China, [2]UMR1114 EMMAH, INRA, Centre PACA, Bâtiment Climat, Domaine Saint-Paul, CS 40509, Avignon, Cédex, France, [3]Science, Applications and Climate Department, European Space Agency Climate Office, Oxfordshire, UK, [4]Department of Evolutionary Biology and Environmental Studies, University of Zurich, Zürich, Switzerland

Key Points:
- LAI, one half the total leaf area per unit surface area, is a fundamental vegetation attribute and an essential climate variable
- The paper gives an overview of LAI field and remote sensing estimation methods, and LAI product validation, uncertainties, and applications
- Gaps in current studies and new frontiers are analyzed; recommendations for future LAI estimations and validations are given

Supporting Information:
- Supporting Information S1

Correspondence to:
H. Fang,
fanghl@lreis.ac.cn

Citation:
Fang, H., Baret, F., Plummer, S., & Schaepman-Strub, G. (2019). An overview of global leaf area index (LAI): Methods, products, validation, and applications. *Reviews of Geophysics*, *57*, 739–799. https://doi.org/10.1029/2018RG000608

Received 25 MAY 2018
Accepted 19 APR 2019
Accepted article online 29 APR 2019
Published online 16 JUL 2019

Abstract Leaf area index (LAI) is a critical vegetation structural variable and is essential in the feedback of vegetation to the climate system. The advancement of the global Earth Observation has enabled the development of global LAI products and boosted global Earth system modeling studies. This overview provides a comprehensive analysis of LAI field measurements and remote sensing estimation methods, the product validation methods and product uncertainties, and the application of LAI in global studies. First, the paper clarifies some definitions related to LAI and introduces methods to determine LAI from field measurements and remote sensing observations. After introducing some major global LAI products, progresses made in temporal compositing and prospects for future LAI estimation are analyzed. Subsequently, the overview discusses various LAI product validation schemes, uncertainties in global moderate resolution LAI products, and high resolution reference data. Finally, applications of LAI in global vegetation change, land surface modeling, and agricultural studies are presented. It is recommended that (1) continued efforts are taken to advance LAI estimation algorithms and provide high temporal and spatial resolution products from current and forthcoming missions; (2) further validation studies be conducted to address the inadequacy of current validation studies, especially for underrepresented regions and seasons; and (3) new research frontiers, such as machine learning algorithms, light detection and ranging technology, and unmanned aerial vehicles be pursued to broaden the production and application of LAI.

CONTENTS

1. Introduction

Leaf area index (LAI) quantifies the amount of leaf area in an ecosystem and is a critical variable in processes such as photosynthesis, respiration, and precipitation interception (Alton, 2016; Asner, Braswell, et al., 1998; S. Boussetta et al., 2013; Jarlan et al., 2008). As a fundamental attribute of global vegetation, LAI has been listed as an essential climate variable by the global climate change research community (GCOS, 2011).

Table 1 shows the definition of LAI and several closely related terms. LAI is generally defined as one half of the total green leaf area per unit horizontal ground surface area (J. M. Chen & Black, 1992; GCOS, 2011). In published studies, green LAI (GLAI) has been used to restrict the LAI definition to the green area active in photosynthesis and transpiration (N.H. Broge & Leblanc, 2001; Haboudane et al., 2004; Viña et al., 2011). LAI and GLAI are generally used equivalently in canopy reflectance models. In some studies, a green area index (GAI) is defined to account for the area of green organs, which include leaves, stems, branches, and fruits (Baret et al., 2010; N. H. Broge & Mortensen, 2002; Duveiller et al., 2011). GAI has been applied in agronomy to study photosynthesis, canopy light interception, and light use efficiency (Baret et al., 2010; Duveiller et al., 2011; Raymaekers et al., 2014). However, GAI is not equivalent to the photosynthetic area because nongreen leaves may also contribute to photosynthesis, and photosynthesis may terminate for green tissues under extreme conditions (Kolari et al., 2007; Sheue et al., 2012).

The plant area index (PAI) makes no distinction between green and nongreen elements, neither between leaves and other elements (Jonckheere et al., 2004; Weiss et al., 2004). To convert PAI to LAI, one simple approach is to subtract the woody area index (WAI), obtained in the leafless period, from the PAI obtained in the leafy period using optical sensors (i.e., LAI = PAI − WAI; J.M. Chen, 1996; Leblanc & Fournier, 2014). WAI is generally calculated as one half the total woody surface area, including branches and stems, per unit ground surface area (Gower et al., 1999; Law et al., 2001; Olivas et al., 2013; Weiskittel & Maguire, 2006).

In some land surface models (LSMs), the stem area index (SAI) represents the sum of all nonphotosynthetic vegetation, including stems, branches, and dead leaves (Gordon B. Bonan & Levis, 2006; Lawrence & Chase, 2007; X. Zeng et al., 2002). SAI can be calculated from either the developed surface area (Baret et al., 2010; Lang et al., 1991; Stenberg, 2006) or the projected area, as in some earlier studies (J. M. Chen & Black, 1992; Deblonde et al., 1994; Lang, 1987). The presence of SAI significantly affects the snow surface albedo because of the absorption of nonphotosynthetic vegetation, the decrease of gaps in illumination, and the increase in shadows (Tian, Dickinson, Zhou, Zeng, et al., 2004).

Optical methods to estimate LAI usually assume that leaves have infinitesimal size and are randomly distributed in the canopy volume (see section 2.3). However, actual canopy leaves have a finite dimension and are nonrandomly distributed in space (the clumping effect). Therefore, the "effective" LAI is quantified when derived from the directional gap fraction method, assuming the leaves are randomly distributed (Miller, 1967; Ryu, Nilson, et al., 2010). The effective LAI (LAI_{eff}) is defined as the LAI value that would produce the same indirect ground measurement as that observed, assuming a simple random foliage distribution (J. M. Chen et al., 2005). The relationship between LAI_{eff} and true LAI is defined as

$$\begin{aligned} LAI_{\mathrm{eff}}(\theta) &= \Omega(\theta)\times LAI, \quad \text{or} \\ PAI_{\mathrm{eff}}(\theta) &= \Omega(\theta)\times PAI, \end{aligned} \tag{1}$$

where $\Omega(\theta)$ is the canopy clumping index, which describes the nonrandomness of the leaf foliage distribution, and θ is the solar zenith angle.

Table 1
Definitions of LAI, GLAI, GAI, PAI, LAI_{eff}, and PAI_{eff}.

		Green leaves only	Green + Non-green leaves	Leaves only	Stems, branches, and nongreen leaves	Woody elements only	All elements	Clumping correction	References
LAI	Leaf area index		√	√				√	J. M. Chen and Black (1992), GCOS (2011), and Watson (1947)
GLAI	Green LAI	√		√				√	Broge and Leblanc (2001), Haboudane et al. (2004), and Viña et al. (2011)
GAI	Green area index	√					√	√	Baret et al. (2010), Broge and Mortensen (2002), and Duveiller et al. (2011)
SAI	Stem area index				√			√	Lang et al. (1991), Stenberg (2006), and Baret et al. (2010)
WAI	Woody area index					√		√	Gower et al. (1999), Law et al. (2001), Olivas et al. (2013), and Weiskittel and Maguire (2006)
PAI	Plant area index		√				√	√	Bréda (2003), Jonckheere et al. (2004), and Weiss et al. (2004)
LAI_{eff}	Effective LAI		√	√					Demarez et al. (2008), Fang et al. (2014), and Ryu, Nilson, et al. (2010)
PAI_{eff}	Effective PAI		√				√		J. M. Chen et al. (1991), J. J. Richardson et al. (2009), and F. Zhao et al. (2011)

Note. GCOS = Globe Climate Observing System.

For forest canopies, the understory and overstory LAIs need to be considered separately to estimate the different characteristics of vegetation. The overstory LAI indicates the ability of the canopy layer to intercept radiation and precipitation (Law & Waring, 1994). The understory LAI is generally composed of shrubs and herbaceous elements and is important for estimating the surface runoff and nutrient availability of the underlying soil (Arora, 2002; Sumnall, Fox, et al., 2016). The entire vertical LAI profile can be derived from the canopy transmittance at different heights (Kumagai et al., 2006; Olthof et al., 2003). The understory LAI can then be calculated by subtracting the overstory LAI from the total canopy LAI.

At the canopy level, LAI can be separated into the sunlit and shaded portions (J. M. Chen et al., 2003; J M. Chen et al., 2012). Sunlit leaves receive both diffuse and direct radiation, while shaded leaves receive diffuse light only, such that their photosynthetic rates will be significantly different. This property has been adopted in LSMs to distinguish the energy dependence of photosynthesis (Carrer et al., 2013; J M. Chen et al., 2012; Hilker et al., 2011). The partitioning of the total canopy LAI into sunlit and shaded portions is a function of Ω and θ (Bonan, 2002; B. Chen et al., 2007):

$$\begin{aligned} LAI_{\text{sun}}\theta &= \frac{1-P\theta\cdot\cos\theta}{G\theta} \\ LAI_{\text{shade}} &= LAI-LAI_{\text{sun}}, \end{aligned} \tag{2}$$

where $P(\theta)$ is the canopy gap fraction, $G(\theta)$ is the projection function, and LAI_{sun} and LAI_{shade} are the sunlit and shaded LAIs, respectively. By the same rationale, the projected LAI is defined as the projected area of green leaves or needles per unit horizontal ground surface area (Barclay & Goodman, 2000; Davi et al., 2008). These different definitions reflect the different purposes for which LAI is determined and used.

The objective of this study is to provide an overview of LAI field measurement and remote sensing estimation methods, global LAI product validation studies, and LAI applications. First, LAI field measurement and

Table 2
Major Field LAI Measurement Methods

Methods	Principle	Notes	References
Destructive	Destructive sampling and measurement of leaf area	Obtain true LAI. Usually labor intensive and limited by the number and distribution of samples. Allometric relationships are usually site specific.	Asner et al. (2003), Baret et al. (2010); Fang, Wei, and Liang (2012), and Majasalmi et al. (2013)
Litter traps	Collection and measurement of leaf litter area		
Allometric	Relationship between leaf area and other structural variables		
LAI-2200	The Miller formula (equation (7))	Efficient methods to obtain PAI_{eff} or LAI_{eff}. PAI and LAI can be derived with a clumping correction (equation (1))	Bréda (2003), Fournier and Hall (2017), Jonckheere et al. (2004), Weiss et al. (2004), and Woodgate et al. (2015)
TRAC	The Beer-Lambert equation (equation (5))		
DCP & DHP	Classification and gap fraction estimation (equations (5) and (7))		

Note. DCP = digital cover photography; DHP = digital hemispherical photography; TRAC = Tracing Radiation and Architecture of Canopies; LAI = leaf area index; PAI = plant area index; PAI_{eff} = effective PAI; LAI_{eff} = effective LAI.

remote sensing estimation methods (sections 2 and 3) are provided, and then, various LAI validation schemes are discussed, focusing on the uncertainties in the global LAI products and the high resolution reference data (section 4). Subsequently, the paper provides a synthesis of LAI applications in vegetation monitoring, land surface modeling, and agricultural studies (section 5). Finally, recommendations are provided on how to improve the global LAI products and their validation and application (section 6).

2. LAI Field Measurement

LAI field measurement methods, uncertainties, and remedies have been reviewed by many authors (Table 2). Field LAI is traditionally estimated by either direct or indirect methods (Bréda, 2003; Jonckheere et al., 2004; Weiss et al., 2004). The direct methods measure the leaf area and estimate LAI from harvested leaves or leaf litters. The indirect methods are based on (1) an allometric relationship with other canopy biophysical variables, for example, diameter at breast height (DBH) for tree canopies, or (2) a logarithmic relationship with the canopy transmittance or gap fraction measurements.

2.1. Direct Measurement

LAI can be directly obtained by harvesting vegetation leaves through destructive sampling or collection of leaf litters and measuring their area (F. Baret et al., 2010; Nasahara et al., 2008). Leaf litters are collected using litter traps on the forest floor during the leaf-fall season and are sorted by species or by stem basal area (Nasahara et al., 2008). The leaf surface area can be measured using a leaf area meter or a scanner. The Li-3000 leaf area meter (LI-COR Inc., Lincoln, Nebraska, USA) is one of the most common instruments for this measurement. Alternatively, leaf area can be calculated through the specific leaf area (SLA, the leaf area per unit of dry leaf mass) in the laboratory. The SLA and total dry mass of each foliage age class are multiplied to calculate the LAI for the canopy (Baret et al., 2010).

$$\mathrm{LAI} = \mathrm{SLA} \times \mathrm{leaf\ mass} \tag{3}$$

SLA can only be obtained through destructive measurements, and dry leaf weights are generally used since fresh weights are subject to changes in leaf water content. When SLA is used to estimate the crop leaf area, the SLA is usually assumed to be constant or vary with plant age or season (Ali et al., 2017; R. Xu et al., 2010).

The destructive sampling method is more appropriate for short-stature ecosystems, for example, agriculture crops, grasslands, and tundra, while litter traps are more appropriate for deciduous forests. Direct measurement methods obtain the true LAI values and are often used as references for the indirect measurement techniques. Nevertheless, direct measurement methods are usually labor intensive when applied to a large area.

2.2. Estimation From Allometric Relationships

The allometric method estimates LAI based on an empirical regression with other easily measurable vegetation variables, for example, the DBH (Gower et al., 1999; le Maire et al., 2011; Majasalmi et al., 2013).

$$\log(LAI) = a\log(DBH) + b, \tag{4}$$

where a and b are regression coefficients derived from field measured LAI and DBH for different species, height, and management practices. In many studies, LAI is estimated as a product of the leaf length and width for different plant types and ages (Baret et al., 2010; Colaizzi et al., 2017; Homem Antunes et al., 2001).

The allometric relationship can be improved when additional biophysical parameters, such as canopy cover and canopy height, are included in the model (Döbert et al., 2015; Jensen et al., 2008; le Maire et al., 2011; Majasalmi et al., 2013; Olsoy et al., 2016). As an alternative, Turner et al. (2000) suggested estimating LAI from the sapwood cross-sectional area, because of their strong physiological relationship. Climatic variables, such as growing degree days and air temperature, have also been added to improve the model performance (Colaizzi et al., 2017; Yoshida et al., 2007). Although the approach is more commonly used for forests (Law et al., 2001; Vyas, et al., 2010), it has also been explored for crops (Colaizzi et al., 2017; Yoshida et al., 2007). Different allometric models may produce significantly different LAI estimates (Majasalmi et al., 2013).

2.3. Estimation From Indirect Optical Methods

2.3.1. General Principles

Indirect optical methods estimate LAI from the canopy gap fraction following the Beer-Lambert law (Nilson, 1971):

$$LAI = \frac{-\ln P(\theta)\cdot\cos(\theta)}{G(\theta)\cdot\Omega(\theta)}, \tag{5}$$

where $P(\theta)$ is the canopy gap fraction at zenith angle θ and $G(\theta)$ is the projection function that corresponds to the fraction of foliage projected on the plane normal to the solar direction. Miller (1967) simplified the inversion of equation (5) by showing that

$$\int_0^{\pi/2} G(\theta)\sin\theta \mathrm{d}\theta = 0.5, \tag{6}$$

for any leaf inclination distribution function. Assuming the foliage elements are randomly distributed in space ($\Omega = 1$), LAI can be estimated from the gap fraction at different view angles (Miller, 1967).

$$LAI_{\mathrm{eff}} = 2\int_0^{\pi/2} -\ln P(\theta)\cos\theta\sin\theta \mathrm{d}\theta. \tag{7}$$

Alternatively, $G(\theta)$ can be explicitly modeled from the leaf inclination distribution function $f(\theta_L)$. Assuming the leaf azimuth distribution is uniform, the computation of $G(\theta)$ is expressed by (Warren Wilson, 1960)

$$\begin{aligned} G(\theta) &= \int_0^{\pi/2} A(\theta,\theta_L) f(\theta_L)\mathrm{d}\theta_L \\ A(\theta,\theta_L) &= \cos\theta\cos\theta_L + \sin\theta\sin\theta_L\cos(\theta - \theta_L). \end{aligned} \tag{8}$$

Among existing leaf inclination distribution function models, the ellipsoidal distribution has been widely used (Mailly et al., 2013; W. M. Wang et al., 2007; Weiss et al., 2004). In this case, $f(\theta_L)$ is described as a function of the ratio of the horizontal to vertical axes of the ellipse (Campbell, 1986, 1990).

The canopy clumping index (Ω) in equation (5) can be estimated through the nonrandom distribution of gap fractions or gap sizes. The gap fraction-based Ω is calculated using the logarithmic gap fraction averaging method (the LX method; Lang & Xiang, 1986):

$$\Omega_{\mathrm{LX}}(\theta) = \frac{\ln\overline{P(\theta)}}{\overline{\ln P(\theta)}}. \tag{9}$$

Similarly, the gap size-based Ω is calculated using the logarithmic gap size averaging method (the CC method; J. M. Chen & Cihlar, 1995; Leblanc, 2002).

$$\Omega_{cc}(\theta) = \frac{\ln[F_m(0,\theta)]}{\ln[F_{mr}(0.\theta)]} \frac{[1-F_{mr}(0,\theta)]}{[1-F_m(0,\theta)]}, \quad (10)$$

where $F_m(0, \theta)$ is the measured accumulated gap fraction larger than zero, that is, the canopy gap fraction, and $F_{mr}(0, \theta)$ is the gap fraction for the canopy when nonrandom large gaps have been removed. The LX and CC methods can be integrated (hence the CLX method), to combine the advantages of both methods (Leblanc et al., 2005).

2.3.2. Major Devices

Several extensive review papers have covered the devices for LAI field measurements (e.g., Bréda, 2003; Jonckheere et al., 2004; Weiss et al., 2004). A number of instruments, such as digital cover photography (DCP), digital hemispherical photography (DHP), the LAI-2200 (or the predecessor LAI-2000; LI-COR Inc., Lincoln, Nebraska, USA) plant canopy analyzer, AccuPAR LP-80 ceptometer (Decagon Devices Inc., Pullman, Washington, USA), and the tracing radiation and architecture of canopies (TRAC; Third Wave Engineering, Ontario, Canada), have been used to estimate LAI. The LAI-2200 has five concentric conical rings (7°, 23°, 38°, 53°, and 68°) recording the incident light. The gap fraction is calculated from concurrent below and above canopy readings

$$P(\theta) = e^{\left(\overline{\ln P_o(\theta)}\right)} = e^{\left(\frac{1}{N}\sum_{j=1}^{N} \ln\frac{B_j}{A_j}\right)}, \quad (11)$$

where B_j and A_j are the jth ($j = 1 \ldots N$) below and above canopy readings, respectively. Consequently, LAI is estimated from equation (7). The LAI_{eff} estimated by LAI-2200 can be converted to LAI using Ω estimated by other methods.

Digital photography, including both DCP and DHP, provides a permanent recording of field condition and offers the ability to analyze images at different exposures (Chianucci & Cutini, 2012; Fournier & Hall, 2017). Both downward and upward pictures can be taken for short and high canopies. A thresholding process is necessary to separate the foliage from the soil background (downward view) or the sky (upward view). Several public programs, for example, CAN-EYE (Weiss & Baret, 2014), CIMES (Gonsamo et al., 2011), GLA (Frazer et al., 1999), and SOLARCALC (Mailly et al., 2013), and commercial ones, for example, HemiView (Delta-T Devices Ltd, Cambridge, UK) and WinScanopy (Regent Instruments, Quebec City, Canada), are available to process photographs. They provide manual interactive or automatic methods to determine the canopy gap fraction and estimate LAI_{eff} (equations (5) and (7); Frazer et al., 1999; Gonsamo et al., 2011; Mailly et al., 2013; Weiss & Baret, 2014). The true LAI can be derived after the canopy clumping effect is corrected (equation (1)).

The TRAC sensor records the transmitted direct light at high frequency and is often used for forest LAI measurement. TRAC accounts for not only canopy gap fraction but also the canopy gap size distribution. In essence, TRAC estimates LAI_{eff} based on the Miller formula (equation (7)). The standard TRAC algorithm estimates Ω with the CC method (equation (10)), which can be used to convert LAI_{eff} to LAI (J. M. Chen & Cihlar, 1995; Leblanc, 2002).

For needleleaf forest, LAI is calculated as (J.M. Chen, 1996)

$$LAI = (1-\alpha)\cdot PAI_{eff}\cdot\gamma_E/\Omega_E. \quad (12)$$

Ω_E is the element clumping index, which quantifies the effect of foliage clumping at scales larger than shoots, γ_E is the needle-to-shoot area ratio, which quantifies the effect of foliage clumping within shoots, and α is the woody-to-total-plant-area ratio, used to represent the contribution of woody material to the total area, including nongreen leaves, branches, and tree trunks. For broadleaf forests, γ_E equals unity. When no distinction is made between green leaves and other nonphotosynthetic elements, the actual quantity measured by optical methods is PAI.

The indirect optical method generally assumes that (1) foliage is black and does not transmit light and (2) individual leaf size is small compared with the canopy and the sensor field of view. LAI-2200 and DHP prefer diffuse measurement conditions, for example, in twilight or overcast days. In contrast, a clear blue sky with unobstructed sun is optimal for TRAC, as it requires distinct sun flecks and shadows. DHP is easy to operate

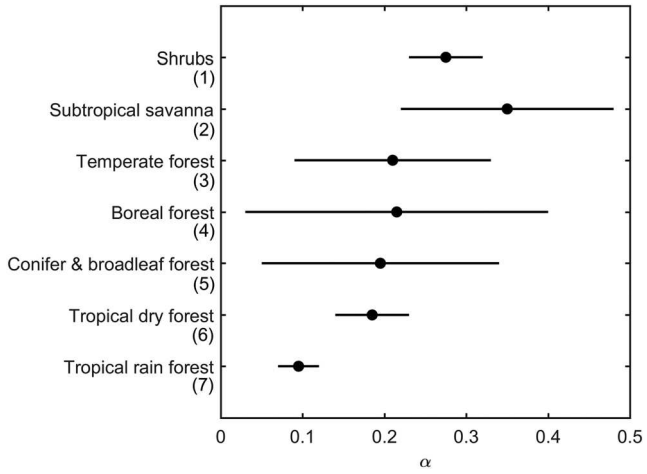

Figure 1. The range of typical values of woody-to-total-plant-area ratio (α, equation (12)) for different vegetation types. (1) Sonnentag et al. (2007); (2) Asner, Wessman, et al. (1998); (3) Deblonde et al. (1994) and Z. Li et al. (2018); (4) J. M. Chen (1996) and Weiskittel and Maguire (2006); (5) Gower et al. (1999), Z. Liu et al. (2015), and Ma et al. (2016); (6) Kalácska et al. (2005); and (7) Olivas et al. (2013).

and can simultaneously obtain canopy transmittance, leaf angle distribution, canopy coverage, and the clumping index (Chianucci & Cutini, 2012; Demarez et al., 2008; Macfarlane et al., 2007). New ways of field methods are currently under development, such as the use of wireless sensor networks (Qu, Han, et al., 2014; Qu, Zhu, et al., 2014) and smartphone applications (Confalonieri et al., 2013; Qu et al., 2016).

2.3.3. Sampling Strategy

The field sampling process is critical for field data quality. A variety of sampling designs, including random sampling (Majasalmi et al., 2012; Weiss et al., 2004), systematic sampling (Burrows et al., 2002; Law et al., 2001; Nackaerts et al., 2000), stratified sampling (López-Serrano et al., 2000; Yin, Li, Zeng, et al., 2016; Y. Zeng et al., 2014), and their combinations, has been explored in LAI field measurements. For close and homogeneous canopies, the discrepancies between different sampling schemes are small. The impact of random sampling errors may be reduced by averaging across multiple plots or measurement points. The stratified sampling method was found to be more appropriate for heterogeneous areas (López-Serrano et al., 2000; Y. Zeng et al., 2014). Recently, Jiapaer et al. (2017) found that the regular grid sampling is best for LAI-2000 sampling in the scattered forest. As a combination, the stratified random sampling method provides flexibility to local sample size variation and adaptability to the global accuracy requirement (Clark et al., 2008; Mayaux et al., 2006; Stehman et al., 2012).

The number of samples is determined by the size of the study area and the accuracy requirement. Various statistical analysis approaches can be used to select the site-specific sampling number needed in random and systematic sampling (Jiapaer et al., 2017; Majasalmi et al., 2012). Majasalmi et al. (2012) found that 12 LAI-2000 measurements are sufficient to obtain an accuracy of 0.15 and 0.06 for a boreal forest using random and systematic sampling methods, respectively. For crops, about 5 to 15 individual measurements are generally required for each elementary sampling unit (ESU), whereas about one to three ESUs are usually taken per crop type (Garrigues, Shabanov, et al., 2008; Weiss et al., 2004). Moreover, a few studies have dedicated to LAI temporal sampling (Fang et al., 2014; Fang et al., 2018; Raymaekers et al., 2014; Ryu et al., 2012). However, there is still no consensus on the measurement methods and sampling scales and frequencies.

2.4. Uncertainties in Field Measurements

Uncertainties in LAI field measurements usually stem from the measurement methods, the clumping effect process, and the inclusion/exclusion of woody and understory vegetation. Earlier studies have found severe underestimation in LAI-2000 (up to 50%), especially for forest, compared to the direct harvest method (Broadhead et al., 2003; Kalácska et al., 2005; Olivas et al., 2013), mainly due to the clumping effect and the outer ring errors (Pearse et al., 2016). The potential systematic errors between LAI-2200 and DHP can range from 10–15% for crops (Fang et al., 2014; Verger, Martinez, et al., 2009) to 10–20% for forests (A. D. Richardson et al., 2011; Woodgate et al., 2015). The range of errors is slightly higher than the empirical 10% assigned to field LAI by a few modelers (Fox et al., 2009; Williams et al., 2005).

Several field LAI databases have been constructed by compiling individual plot- and site-based LAI measurements over the past few decades (Asner et al., 2003; Baret, Morissette, et al., 2006; Fang, Wei, & Liang, 2012; Iio et al., 2014). Most field LAI data are obtained by indirect optical methods (supporting information Table S3). Field optical measurements generally estimate the total PAI, which includes contributions from the woody component. WAI values can be separately measured in leaf-off seasons (Fang et al., 2003; Kalácska et al., 2005; Leblanc & Chen, 2001) or with a near-infrared (NIR) camera (Chapman, 2007; Zou et al., 2009). Figure 1 shows the range of typical woody-to-total-plant-area ratio (α in equation (12)), with lower values for the tropical forest and higher values for savanna. This wide range of α values suggests the range of errors that could be introduced in the LAI indirect estimates without a proper woody correction.

The assumption about clumping parameters remains a large source of uncertainty (R. A. Fernandes et al., 2003; Garrigues, Lacaze, et al., 2008; A. D. Richardson et al., 2011). To be comparable with satellite LAI

products, PAI_{eff} or LAI_{eff}, estimated by the optical methods, needs to be converted to true LAI ($LAI = LAI_{eff} / \Omega$). Among the optical instruments, DCP (Ryu et al., 2012), DHP (Fang et al., 2014; Leblanc et al., 2005; van Gardingen et al., 1999), LAI-2200 (Fang et al., 2014; Fang et al., 2018), and TRAC (J. M. Chen & Cihlar, 1995) have been used to take canopy gap measurements and estimate Ω. The choice of a specific method varies for different biome types and ground conditions (Demarez et al., 2008; Gonsamo & Pellikka, 2009; Pisek et al., 2011). However, the Ω values estimated by different methods may differ by 10–15% (Fang et al., 2014; Pisek et al., 2011). For broadleaf forests, a few studies have found that the PAI_{eff} and LAI values are similar because the clumping effects are compensated by the contribution of woody structures (Fournier et al., 2003; Schlerf et al., 2005). In general, field LAI measurements may achieve uncertainties of <1.0 by conforming to instrument measurement standards and performing a clumping correction (Fang, Wei, & Liang, 2012; R. A. Fernandes et al., 2003; Garrigues, Lacaze, et al., 2008).

3. Remote Sensing Methods

3.1. General Principles

Estimation of LAI from remote sensing data has been extensively explored during the past few decades (Baret, 2015; J. M. Chen, 2018; Houborg et al., 2007; Verrelst, Camps-Valls, et al., 2015; Zheng & Moskal, 2009). LAI is mainly derived from passive optical sensors, the active light detection and ranging (LiDAR) instrument, and microwave sensors using empirical transfer and model inversion methods.

3.1.1. Empirical Transfer Functions

LAI can simply be estimated through empirical relationships with canopy reflectance or vegetation indices (VIs; Broge & Leblanc, 2001; Gitelson, 2004; Kimura et al., 2004; Viña et al., 2011; F. Yang et al., 2012). Many studies have highlighted the effectiveness of the NIR band for LAI estimation for crops (Houborg et al., 2009; Shibayama, Sakamoto, Takada, Inoue, Morita, Takahashi, et al., 2011; Shibayama, Sakamoto, Takada, Inoue, Morita, Yamaguchi, et al., 2011) and forests (Kobayashi et al., 2007). The NIR band is particularly useful for LAI estimation in densely vegetated areas where the VIs may saturate (Houborg et al., 2009; Houborg & Boegh, 2008). Kobayashi et al. (2010, 2007) found that the NIR band can be used to estimate the overstory LAI in the larch forest in Siberia. On the other hand, some earlier studies reported that the shortwave infrared band is better than other bands for forest LAI mapping (Aragão et al., 2005; Cohen, Maiersperger, Yang, et al., 2003; Eklundh et al., 2001; R. Pu et al., 2005). However, the single-band method is sensitive to the atmospheric conditions and background setting for low vegetation densities (Houborg & Boegh, 2008; Kobayashi et al., 2010; Mannschatz et al., 2014). Therefore, some studies recommend to estimate LAI with multiple bands (Cohen, Maiersperger, Gower, et al., 2003; Eklundh et al., 2003; Martínez et al., 2009).

The vegetation index (VI) method overcomes the limitations of single bands through the different forms of band combinations and is currently the most commonly used empirical method to estimate LAI. The advantage of the VI approach is its simplicity and ease of usage. The most commonly used VIs include the ratio VI (Darvishzadeh et al., 2009; Deng et al., 2006), normalized difference VI (NDVI; Jesús Delegido, et al., 2011; Kamal et al., 2016; Serbin et al., 2013; Tillack et al., 2014; Tong & He, 2013), the enhanced VI (EVI; Houborg et al., 2007; A. Huete et al., 2002), and the soil-adjusted VI (SAVI; Biudes et al., 2014; X. Gao et al., 2000). Hyperspectral reflectance data and hyperspectral indices have been widely explored in LAI estimation (K.-S. Lee et al., 2004; L. Liang et al., 2015; Locherer et al., 2015; Verger, Baret, & Camacho, 2011). The principle component analysis is usually applied to explore the relationship between the principle components of the spectral bands and LAI (S. Chaurasia & Dadhwal, 2004; F. Yang et al., 2012). However, some studies reported that hyperspectral data are not necessarily better than broadband data in the LAI estimation (Broge & Leblanc, 2001; Broge & Mortensen, 2002; Weiss et al., 2000).

The statistical relationship is commonly built with a simple linear, polynomial, exponential, or logarithmic model (J. Qi et al., 1994). The coefficients of the model can be derived through the ordinal least square regression (Cohen, Maiersperger, Gower, et al., 2003; Curran & Hay, 1986), the partial least-squares regression (X. Li, Zhang, et al., 2014; Serbin et al., 2013), and the canonical correlation analysis (Cohen, Maiersperger, Gower, et al., 2003). Other more sophisticated regression methods have also been investigated, such as the kernel ridge regression, the look-up table method (LUT), the neural network (NN) method, the random forest regression, and the support vector regression (Durbha et al., 2007; Kira et al., 2016; L. Liang

et al., 2015; E. Pasolli et al., 2012; F. Yang et al., 2012). The Gaussian process regression method, which builds a nonlinear regression as a linear combination of spectra mapped to high-dimensional space, has been demonstrated as a promising alternative to the traditional empirical approach (Campos-Taberner et al., 2016; Lazaro-Gredilla et al., 2014; Verrelst, Muñoz, et al., 2012; Verrelst, Alonso, et al., 2012).

The strength and generality of the empirical LAI-reflectance and LAI-VI relationships are limited by many external factors, including vegetation type, sun-surface-sensor geometry, leaf chlorophyll content, background reflectance, and atmospheric quality (Table 3). A general solution is to include these factors in statistical models or to develop new VIs that are sensitive to LAI but are robust to these factors (Table 3). The major challenge is that there is no universal LAI-reflectance or LAI-VI relationship applicable to diverse vegetation types, because the empirical coefficients depend primarily on vegetation types. In practice, an LAI-VI transfer function can be developed for each vegetation type, for example, coniferous, deciduous, mixed forests, and nonforest types (Deng et al., 2006). The majority of developed algorithms from statistical methods generally do not separate for estimation of GAI, GLAI, LAI_{eff}, LAI, PAI_{eff}, or PAI (Table 1); therefore, novel models need to be developed to estimate each individual variable (Delegido, et al., 2015; Malenovský et al., 2008). New VIs are needed to overcome the complex background and atmospheric effects and mitigate leaf pigment effects (L. Liang et al., 2015; Q. Xie et al., 2018). The selection of optimal bands for VIs may change with the season (Heiskanen, Rautiainen, Stenberg, Eigemeier, et al., 2012), and separate relationships can be developed before and after the mature stage (Bacour et al., 2002; Q. Wang et al., 2005).

3.1.2. Model Inversion Method

Canopy reflectance models relate fundamental canopy, for example, LAI, and leaf properties, to the scene reflectance for a given sun-surface-sensor geometry (Goel & Thompson, 2000; S. Liang, 2004). These models vary in degrees of complexity and may be grouped into four categories: kernel-based, turbid medium, geometrical, and computer simulation models. The kernel-based model estimates the directional reflectance of a land surface on the basis of the sun-surface-sensor geometry, bowl/bell shape, and backward/forward scattering shape of the anisotropic reflectance pattern (X. Huang, Jiao, et al., 2013; Rahman et al., 1993; Roujean et al., 1992). The turbid medium model simulates the canopy as turbid parallel layers above a ground surface (Kuusk, 2001). Turbid medium models are best suited for dense canopies with small vegetation elements, for example, grasses, agricultural crops, and forests. A widely used model in this category is the PROSAIL model (Berger et al., 2018; Jacquemoud et al., 2009), which combines the PROSPECT leaf optical properties model (Jacquemoud & Baret, 1990) and the Scattering by Arbitrarily Inclined Leaves canopy bidirectional reflectance model (Verhoef, 1984). In geometric optical models, the canopy architecture is described with different geometric objects (e.g., cones, spheroids, ellipsoids, and cubes), according to a given distribution and optical properties (J. Chen et al., 2000; J. M. Chen & Leblanc, 1997; X. Li & Strahler, 1985). Computer simulation models rely on an explicit description of the canopy architecture and trace photon interactions with the canopy and the environment (Disney et al., 2006; Roupsard et al., 2008). For example, the Discrete Anisotropic Radiative Transfer (Gastellu-Etchegorry et al., 2004, 2015) and Radiosity Applicable to Porous Individual Objects (H. Huang, Qin, et al., 2013; H. Huang et al., 2018) models are two such models that are under continuous development and maintenance, with features to simulate layered inhomogeneous canopies, urban landscapes, and airborne measurements.

Because of the complexity of the model, LAI is usually estimated from the canopy reflectance through a model inversion method (Richter, Atzberger, et al., 2012; Verrelst, Camps-Valls et al., 2015). Given a set of reflectance, the inversion process determines the set of canopy biophysical variables, so that the computed reflectances best fit the remote sensing reflectances. Classical inversion methods include the numerical optimization technique (Houborg & Boegh, 2008; Lewis et al., 2012), the NN approach (Baret et al., 2013; Fang & Liang, 2003), and the LUT approach (D. Huang et al., 2008; Verrelst et al., 2014). Both NN and LUT methods are easy to use once the database is generated from a range of properly configured input variables. For both methods, the number of simulations are enormous when all the combinations of parameters are considered. For the LUT method, it has been recommended to choose 100,000 reflectance realizations and use the best 50 cases to achieve a most efficient retrieval (Darvishzadeh, et al., 2008; Richter et al., 2011; Verrelst et al., 2014; Weiss et al., 2000). Other machine learning algorithms, such as the Bayesian network algorithm (V.C.E Laurent et al., 2012; Qu, Zhang, et al., 2014; Quan et al., 2015; Yao et al., 2008), the support vector

Table 3
A Summary of Major Effects in LAI Field Measurement and Remote Sensing Estimation From Statistical and Model Inversion Methods

Effects	Description	Field and empirical mitigation methods	Modeling methods
Atmospheric effect	Atmospheric conditions limit the field LAI measurements, affect LAI estimation from remote sensing data, and usually lead to product gaps.	Conduct field measurement under optimal conditions. Estimate LAI from atmospherically corrected surface reflectance data (Turner et al., 1999). Develop VI that can reduce the atmospheric impact, for example, ARVI (Kaufman & Tanré, 1992) and ISR (R. A. Fernandes et al., 2003). Fill LAI data gaps for the user community (section 3.4).	Estimate LAI from surface reflectance data through the model inversion method or estimated from the TOA radiance or reflectance data coupling the atmospheric RT modeling process (Fang & Liang, 2003; Houborg et al., 2009; Laurent et al., 2014; Shi et al., 2016).
Background effect	Remote sensing information contains mixed information from the background and vegetation. Proper characterization of the background is vital to obtain realistic LAI estimation.	Use VI that can suppress the background effect (Diaz & Blackburn, 2003; Gonsamo & Chen, 2014; Y. Qi et al., 2014), for example, the SAVI (A. R. Huete, 1988) or RSR (J. M. Chen et al., 2002). Include background information in the VI formulation (Pisek et al., 2010; D. Zhao, Yang, et al., 2012). Use different statistical relationships for different vegetation densities (Houborg & Boegh, 2008; Villa et al., 2014).	Use typical soil reflectances (S. Jacquemoud et al., 1992) or simulated soil reflectances (Price, 1990) in RT models. Use background reflectance estimated from RS to retrieve the overstory LAI (Pisek et al., 2010). More attentions are necessary for complicated water and snow backgrounds (Manninen, Korhonen, Riihelä, et al., 2012; Vaesen et al., 2001).
Chlorophyll effect	Leaf C_{ab} affects the canopy optical properties and thus the LAI estimation. Conventional VI method may be compromised for canopies having different C_{ab} contents (Blackburn, 1999).	Develop and use VIs that are more sensitive to LAI than to C_{ab}, for example, the enhanced vegetation index 2 (Y. Fu et al., 2013), or more efficient in estimating both C_{ab} and LAI, for example, the photochemical reflectance index (A. A. Gitelson et al., 2017). Estimate LAI and C_{ab}, separately, with different VIs (le Maire et al., 2008; Stagakis et al., 2010; D. Vyas et al., 2013).	Couple leaf optical models that explicitly includes C_{ab}, for example, PROSPECT (S. Jacquemoud & Baret, 1990), in the model simulation. Jointly retrieve C_{ab} and LAI using a regular model inversion approach (Gascon et al., 2004; Houborg et al., 2015; Laurent et al., 2014).
Classification effect	Errors in land cover classification affect the canopy RT model parameterization and LAI estimation methods that require the a priori classification information (Fang, Li, et al., 2013; Serbin et al., 2013).	Biome-specific empirical functions (D.P. Turner et al., 1999) and LUT configurations (Houborg et al., 2009) have been developed for LAI retrieval. Alternatively, the NN methods have been used in the GEOV1 (F. Baret et al., 2013) and GLASS (Zhiqiang Xiao et al., 2014) products, which do not rely on the classification information. Uncertainties in the input classification map, especially confusion between herbaceous and woody vegetation, can fatally impact LAI retrievals (Y. Tian et al., 2000). However, the impact can be smaller if similar biomes, for example, grasses and cereal crops, are confused (Fang, Li, et al., 2013; R. B. Myneni et al., 2002). Essentially, the accuracy of the land cover maps needs to be improved.	
Clumping effect	The clumping effect, indicated by the clumping index (CI), affects the LAI field measurements, remote sensing modeling and parameter retrieval. CI is scale-dependent and tends to increase with the increasing spatial resolution (Chianucci, Macfarlane, et al., 2015; Damm et al., 2015).	Estimate CI and perform clumping correction using optical instruments (section 2.3). Estimate CI from remote sensing data using various shape indicators (J. M. Chen et al., 2005; Lacaze et al., 2002) and vegetation indices (Roujean & Lacaze, 2002; Thomas et al., 2011).	The clumping effect is considered in many canopy reflectance models (section 3.1). A few CI products have been derived from POLDER, MODIS, and MISR (J. M. Chen et al., 2005; L. He et al., 2016; Wei & Fang, 2016).
Directional effect	Land surface reflectance and VI values are different when calculated from different sun-surface-sensor geometries. This affects the modeling and estimation of LAI from directional observations.	Simple application of global VI-LAI relationship will lead to large errors (Breunig et al., 2011; Y. Kang et al., 2016). Use BRDF-adjusted VIs and develop new directional based indices (Deng et al., 2006; Lacaze et al., 2002; Pocewicz et al., 2007).	It is a common practice to model the directional reflectance through an RT process for the coupled soil and canopy system (Houborg et al., 2009; S. Jacquemoud et al., 1992; Kuusk, 1998). LAI is then retrieved from the directional reflectance through various model inversion methods (Table 4).
Saturation effect	Surface reflectance and VI stagnant even with the increasing of LAI	Use narrow band reflectance and VI (D. J. Diner et al., 1999; Gemmel & McDonald, 2000) or develop new	No effective methods to solve the intrinsic problem. Some nonparametric machine-learning algorithms, for example, the

Table 3 *(continued)*

Effects	Description	Field and empirical mitigation methods	Modeling methods
	(Y. Fu et al., 2013; Gower et al., 1999). This happens for both field measurement and remote sensing estimation.	VI to reduce the sensitivity to the saturation effect, for example, the Wide Dynamic Range Vegetation Index (Anatoly A. Gitelson, 2004).	Gaussian processes regression, are reported to partly overcome the effect (Verrelst, Rivera, et al., 2015).
Scaling effect	The LAI estimation methods are only valid for a particular spatial scale, causing problems in comparing LAI values estimated from different scales, for example, field measurements and high and low resolution remote sensing measurements. See relevant reviews (J. Chen, 1999; F. Gao et al., 2014; Garrigues et al., 2006a; H. Wu & Li, 2009).	Quantify and correct the scaling bias, based on the nonlinearity of the transfer functions and the spatial heterogeneity (J. Chen, 1999; Garrigues et al., 2006a; Garrigues et al., 2006b; Z. Hu & Islam, 1997; X. Zhang et al., 2006). Use linear transfer functions based on different VI intervals. Collect sufficient amount of field data in homogeneous and large sites in validation studies.	The magnitude of the scaling bias increases with the model nonlinearity and the surface heterogeneity. Develop scale-dependent models (Yuhong Tian et al., 2003) and use scale dependency in LAI retrieval (R. B. Myneni et al., 2002). The theory of canopy spectral invariants may help improve the scaling property of the 3-D RT models and make the algorithm feasible for different spatial resolutions (Stenberg et al., 2013).
Shadow effect	Shadows from soil, leaf and canopy, terrain, cloud, and instrument hardware affect the LAI field measurements and remote sensing modeling and retrieval. The shadow effect is scale-dependent and tends to increase with the increasing spatial resolution (Damm et al., 2015).	Estimate the fraction of shadow from LiDAR (Hilker et al., 2011) or from satellite imagery using spectral mixture analysis (B. Hu et al., 2004; Peddle et al., 1999). Use a shadow correction factor based on measurement geometry (Wright et al., 2014) or the needle-to-shoot area ratio for conifer forests (Heiskanen, Rautiainen, Stenberg, Mõttus, et al., 2012). Include the correction factor in empirical models (Peddle et al., 1999).	The contribution of shadowed and illuminated components have been explicitly modeled in component-based models (Gascon et al., 2004; W. H. Qin & Xiang, 1994), kernel-driven models (Roujean et al., 1992), turbid medium models (Verhoef, 1984), and geometric-optic models (Q. Wang et al., 2013).
Snow effect	The presence of snow below or on the canopy affects field measurement, remote sensing modeling and parameter retrieval, product validation, and their applications.	Discriminate vegetation from snow cover using spectral unmixing methods (Verrelst et al., 2010). Develop new vegetation indices, for example, the NDPI (Cong Wang et al., 2017) and PPI (H. X. Jin & Eklundh, 2014), to suppress the snow impact on canopy LAI estimation (B. Hu et al., 2004). Ground snow cover may help forest LAI measurement (T. Manninen, Korhonen, Voipio, et al., 2012).	The impact of snow on surface reflectance has been considered in various models (Baker et al., 2017; Ni & Woodcock, 2000; Pulliainen et al., 2015). The dynamics of snow also needs to be modeled and the snow status labeled in the product quality layer.
Temporal effect	Broadly means (1) the temporal variation of field measurement conditions; (2) the variation of vegetation in RT modeling and LAI retrieval; (3) temporal mismatch between field and RS data in product validation; and (4) uncertainties in interpolation/extrapolation of LAI products.	Develop and use automatic field measurement methods. Separate statistical models for different growing phases (B. Lee et al., 2017; Potithep et al., 2013). Select temporally resistant bands (Heiskanen,Rautiainen, Stenberg, Eigemeier, et al., 2012) and include the temporal factor in statistical models (Guindin-Garcia et al., 2012).	Parameterize RT models with temporally variable values. Temporal filtering (section 3.3) and multisensor fusion (Table 6) to increase the product temporal resolutions and accuracies.
Texture effect	Soil texture, an important soil property, influences the soil reflectance (see the background effect; Thomasson et al., 2001).	Simple relationship can be built between LAI and NDVI and SR texture measures (Kraus et al., 2009; Moskal & Franklin, 2004). Combination of spectral features with texture features improves LAI mapping for meter resolution images, for example, WorldView-2 (Ruiliang Pu & Cheng, 2015) and IKONOS (Colombo et al., 2003; Z. Gu et al., 2012; Johansen & Phinn, 2006) and for radar images (Wong & Fung, 2013).	
Topographic effect	Topography affects the field LAI measurement, remote sensing modeling, and LAI retrieval. Topography is a critical factor in LiDAR signal processing	Follow the instrument guidelines for field measurements at slopes. Perform topographic corrections for field measured (Gonsamo & Pellikka, 2008; María Luisa et al., 2008) and remote sensing data (Gonsamo & Chen, 2014; Hantson & Chuvieco, 2011; Soenen et al., 2005). Include topographical variables, for example, elevation and slope, in the statistical models (Aragão et al., 2005). Build LAI statistical	

Table 3 *(continued)*

Effects	Description	Field and empirical mitigation methods	Modeling methods
	and parameter estimation (Drake et al., 2002; C. Li, Xu, et al., 2016).	model for different slope, aspect, and evaluation classes (White et al., 1997). Select proper LiDAR metrics for LAI estimation (M. Sumnall, Peduzzi, et al., 2016). Topography is generally considered in 3-D RT models, for example, DART (J. P. Gastellu-Etchegorry et al., 2004) but has been neglected in many other models.	
Woody effect	The presence of woody and other nonphotosynthetic vegetation components will interfere with LAI field measurement, remote sensing modeling, and parameter retrieval.	Similar to LAI, WAI can be estimated from direct measurement (Olivas et al., 2013; Weiskittel & Maguire, 2006), multispectral imager (Chapman, 2007; Zou et al., 2009), DHP (Kalácska et al., 2005; Sánchez-Azofeifa et al., 2009), LAI-2000 (Cutini et al., 1998; Fang et al., 2003; Leblanc & Chen, 2001), and terrestrial LiDAR (L. Ma et al., 2016). Empirical WAI estimation with spectral VIs (Jesús Delegido et al., 2015; X. Gao et al., 2000). Woody correction based on field measured WAI or a typical woody-to-total area ratio (equation (12) and Figure 1).	Stem and branch properties are considered by several forest RT models (J. M. Chen & Leblanc, 1997; Kuusk & Nilson, 2000). WAI is a required input in 3-D computer simulation models (J.-P. Gastellu-Etchegorry et al., 2016; N.V. Shabanov et al., 2003). The woody-to-total area ratio estimated from ground optical instruments, for example, DHP, can be used to simulate remote sensing observations with a 3-D RT model (Leblanc & Fournier, 2014; Woodgate et al., 2016).

Note. ARVI = atmospherically resistant vegetation index; BRDF = bidirectional reflectance distribution function; C_{ab} = leaf chlorophyll content; ISR = simple infrared ratio; RSR = reduced simple ratio; RT = radiative transfer; SAVI = soil adjusted vegetation index; TOA = top of atmosphere; VI = vegetation index; WAI = woody area index; LAI = leaf area index; LUT = look-up table; NN = neural network; GEOV1 = Geoland2/BiopPar version 1; DART = Discrete Anisotropic Radiative Transfer; GLASS = Global Land Surface Satellite; POLDER = POLarization and Directionality of the Earth's Reflectances; MODIS = Moderate Resolution Imaging Spectroradiometer; MISR = Multi-angle Imaging Spectro-Radiometer; LiDAR = Light Detection and Ranging; NDPI = normalized difference phenology index; PPI = plant phenology index; SR = simple ratio.

machine regression algorithm (Durbha et al., 2007; Fortin et al., 2014; Omer et al., 2016), and the Gaussian process regression method (García-Haro et al., 2018; Verrelst, Rivera, et al., 2015), have also been explored in a number of inversion studies. The choice of a particular retrieval method depends on the mathematical properties of the function to be minimized.

LAI inversion from a canopy reflectance model is usually ill-posed, meaning that the numerical solution does not depend continuously on the data and, thus, may result in unstable and inaccurate inversion performance (Jacquemoud, 1993; Kimes et al., 2000). Various regularization strategies have been proposed to increase the robustness of the estimates, including the use of alternative cost functions, prior parameter constraints, multiple best solutions, and added noise for measurements and models (Banskota et al., 2013; Leonenko et al., 2013b; Rivera et al., 2013; Verrelst et al., 2014). There is a high degree of flexibility in selecting the most robust optimization functions (Leonenko et al., 2013a, 2013b; Rivera et al., 2013). Leonenko et al. (2013b) made an overview of different forms of cost functions and found that the minimum contrast estimates performed better than the traditional least squares estimation in the LAI retrieval.

Three different sources of prior information have been examined: (1) input uncertainties and model variability, (2) statistics of the canopy spectral and structural properties, and (3) knowledge about the background characterization (Baret & Buis, 2008; Combal et al., 2002; Ganguly, Nemani, et al., 2014; Xiaowen Li, et al., 2001). For the NN method, it is recommended to construct a training data set based on the distribution of the variables (Atzberger & Richter, 2012; Bacour et al., 2006; Baret, Pavageau, et al., 2006; Verger, Baret, & Camacho, 2011). Some studies consider the LAI temporal evolution as a dynamic constraint (Houborg et al., 2007; Kötz et al., 2005; Xiao, Liang, et al., 2011). The dynamic LAI change has also been used in LAI retrieval with the data assimilation (DA) methods, for example, in JRC-TIP (Pinty et al., 2011), GA-TIP (Mathias Disney et al., 2016), Earth Observation Land Data Assimilation (Lewis et al., 2012), and Xiao, Wang, et al. (2011). Other than the pixel-based methods, the object-based inversion methods set spatial constraints for a particular land cover type or pixel patch (Atzberger & Richter, 2012; Houborg & Boegh, 2008). Both spatial and temporal constraints can be integrated in the inversion process (Lauvernet et al., 2008).

3.1.3. LiDAR and Microwave Estimation

The application of LiDAR for the retrieval of forest inventory parameters and structural characteristics has been extensively reviewed in many studies (Bergen et al., 2009; Dassot et al., 2011; Hall et al., 2011; van Leeuwen & Nieuwenhuis, 2010; K. G. Zhao, et al., 2011). LAI is mainly estimated from LiDAR data by means of correlation with the gap fraction (equation (5); Griebel et al., 2015; Moorthy et al., 2008; J. J. Richardson et al., 2009; F. Zhao, Strahler, et al., 2012; K. Zhao et al., 2015). The gap fraction is not directly measured by laser scanning but derived from various laser-based metrics, such as the laser penetration index (S.-Z. Luo, Wang, Zhang, et al., 2013; Solberg et al., 2006) and the above and below ratio index (M. Sumnall, Peduzzi, et al., 2016). LAI is also estimated through an allometric relationship with forest biophysical parameters derived from LiDAR, such as canopy cover (Jensen et al., 2008; Korhonen et al., 2011; Olsoy et al., 2016), canopy height (S. Z. Luo et al., 2015; Riaño et al., 2004), and foliage density (Olsoy et al., 2016; K. Zhao & Popescu, 2009). The spaceborne LiDAR currently available from the Geoscience Laser Altimeter System, onboard the ICESat satellite, offers an opportunity to derive a global footprint LAI (Garcia et al., 2012; S. Z. Luo, Wang, Li, et al., 2013; H. Tang et al., 2016).

Several physical radiative transfer models have been developed to simulate the LiDAR waveform under specific forest stand representation and LiDAR specifications (J.-P. Gastellu-Etchegorry et al., 2016; Ni-Meister et al., 2001; North et al., 2010; G. Q. Sun & Ranson, 2000). For example, the Discrete Anisotropic Radiative Transfer model has incorporated a quasi-Monte Carlo ray tracing approach to simulate LiDAR waveforms, with one three-dimensional (3-D) vegetation canopy for any LiDAR sensor configuration (J.-P. Gastellu-Etchegorry et al., 2016). A simulated 3-D canopy allows the simulation of the effects of LiDAR penetration and the relationship between LAI and LiDAR metrics under different conditions (Koetz et al., 2007; Morsdorf et al., 2009). Subsequently, LAI can be retrieved from LiDAR data using the model inversion method (Bye et al., 2017; Koetz et al., 2006; H. Ma, Song, et al., 2015; Tang et al., 2012).

LiDAR allows the characterization of the vertical LAI profile at different canopy heights (Detto et al., 2015; H. Ma, Song, et al., 2015; M. J. Sumnall, Fox, et al., 2016; Takeda et al., 2008; Tang et al., 2016). For example, Tang et al. (2012) retrieved the vertical profiles of LAI at 0.3-m height intervals from the Laser Vegetation Imaging Sensor data and showed moderate agreement between LiDAR and field-derived LAI ($R^2 = 0.63$, root mean squared error [RMSE] = 1.36). The canopy woody and foliage parts may be separated based on different LiDAR scattering properties (F. Zhao, et al., 2011). Automated LiDAR can provide cost-effective consecutive PAI and LAI estimates (Culvenor et al., 2014; Griebel et al., 2015). Information from different LiDAR platform types, that is, ground-based, airborne, and spaceborne, can be combined to improve the joint retrieval of forest biophysical parameters (Benjamin Koetz et al., 2007; Tansey et al., 2009; van Leeuwen & Nieuwenhuis, 2010). Furthermore, both passive optical and LiDAR data can be combined to yield improved estimations of biophysical parameters (Z. Fu et al., 2011; Hilker et al., 2008; Jensen et al., 2008; Benjamin Koetz et al., 2007; H. Ma et al., 2014).

Quality assessment of the LiDAR LAI mainly relies on comparison with other indirect optical methods (Table S1). In general, the LiDAR LAI estimations are in good agreement with those obtained from LAI-2200 (Hill et al., 2006; M. J. Sumnall, Fox, et al., 2016; F. Zhao, et al., 2011), DHP (Hopkinson et al., 2013; Solberg et al., 2006; F. Zhao, Strahler, et al., 2012), and TRAC (Jensen et al., 2008; H. Ma, Song, et al., 2015). The relative differences between the LiDAR-based LAI estimations and those obtained from LAI-2200 and DHP are generally within 10% (Hancock et al., 2014; Woodgate et al., 2015). Errors reported in the retrieval of LAI from discrete return terrestrial laser scanner (TLS) range between 0.2 and 0.3 (Table S1). For example, the TLS-based LAI_{eff} estimated from Zheng et al. (2013) explained about 90% (RMSE = 0.01) of the DHP estimated values. Good results have been found near the 60° zenith angles (Culvenor et al., 2014; Jupp et al., 2009), where the leaf projection function G ($\theta = 57.5°$) can be set to 0.5 in the LAI_{eff} estimation (equation (5)). A critical pitfall is that the LiDAR measurements generally do not separate LAI, LAI_{eff}, PAI, and PAI_{eff} (Table S1), which poses great uncertainties for the LAI estimation (Takeda et al., 2008). In some cases, the LiDAR-derived LAI_{eff} was directly compared with the true LAI because of the unknown clumping index (Ω) values (Jensen et al., 2008; Moorthy et al., 2008), although an analogous gap fraction method can be used to estimate Ω (e.g., Alonzo et al., 2015).

The microwave radar data have the potential to fill the acquisition gaps (e.g., cloud cover) in the optical data. LAI is estimated through the empirical relationship with the radar backscattered signal (σ).

$$LAI = a \times \sigma + b, \tag{13}$$

where a and b are the correlation coefficients. The relationship has been applied to estimate LAI for crops (Fieuzal & Baup, 2016; Hosseini et al., 2015; H. Xu & Steven, 1996) and forests (J. Chen et al., 2009; Manninen et al., 2013). Very good correlations have been reported for rice canopies ($R^2 > 0.80$; J. Chen et al., 2006; Inoue et al., 2002, 2014; Kumar et al., 2013). However, few studies have explored the LAI retrieval through the inversion of radar physical models (Tao et al., 2016). LAI estimation from radar data remains a challenge. Current methods are specific to the data set and are difficult to be generalized, because of the impact of observational conditions, sensor configuration, canopy structure, and the underlying soil. The combined use of optical and radar information may allow the improvement of regional LAI retrieval (Wong & Fung, 2013).

3.2. Major Global LAI Products

Over the past two decades, a number of global moderate resolution (250 m to 7 km) LAI products have been generated (Table 4). Over the long term, the National Oceanic and Atmospheric Administration (NOAA) Advanced Very High-Resolution Radiometer (AVHRR) is the only data source to generate global LAI since the early 1980s (Table 5). Figure 2 shows an example of the global mean LAI, derived from the Moderate Resolution Imaging Spectroradiometer (MODIS) and the Geoland2/BiopPar version 1 (GEOV1) from 2003 to 2013 in January and July, respectively. The two products are generally consistent, and the small differences are mainly attributed to the impact of the input reflectances, retrieval algorithms, the clumping effect processing, and the usage of a priori information (R. B. Myneni et al., 2002; Pisek et al., 2010; Weiss et al., 2007). Large discrepancies exist for very dense canopies, for example, the evergreen broadleaf forest (Aragão et al., 2005; N. V. Shabanov et al., 2005), mainly because of the complexity of the ecosystem and frequent cloud and aerosol contamination (Hilker et al., 2012). Differences have also been found for nongrowing seasons, particularly for the needleleaf forests during the winter period (Fang, Wei, Jiang, et al., 2012; Garrigues, Lacaze, et al., 2008; Tian, Dickinson, Zhou, & Shaikh, 2004).

Several LAI products provide uncertainty information in the form of quantitative quality indicators (QQIs), distributed together with the products. The MODIS QQIs are calculated from the standard deviation over all acceptable LUT solutions (D. Huang et al., 2008). The GEOV1 QQIs are computed using the NN training data set and reflect the sensitivity of the product to input reflectance uncertainties (Baret et al., 2013). The JRC-TIP and GA-TIP QQIs are derived from prior probability density functions of the LAI_{eff} and model uncertainties and denote the monthly dispersion of the LAI values (Mathias Disney et al., 2016; Pinty et al., 2011). Generated as diagnostic summaries, these QQI layers represent the theoretical uncertainties as a function of the input data, model imperfections, and the inversion process (Baret et al., 2007; Knyazikhin et al., 1999; Pinty et al., 2011).

The uncertainties are higher in the tropical (20° S–15° N) and boreal regions (~60° N) and in summer, given the higher LAI values in those areas and seasons (middle of Figure 2). The higher uncertainties in the boreal regions are partly caused by the low solar zenith angle, snow and cloud contamination, and the understory effect (Pisek et al., 2010; Weiss et al., 2007). The spatial distribution of relative uncertainties differs from those of the absolute uncertainties. The highest relative uncertainties are generally located in the ecological transition zones, such as the sparsely vegetated western areas of the Americas, Sahel, South Africa, central Asia and Australia, and the savanna areas (right of Figure 2). The mixed land cover types in these zones complicate the LAI modeling and retrieval, suggesting a need for further studies, especially because of the sensitivity of those areas to climate change and various disturbances. The LAI product uncertainties and the spatial and temporal variability are largely related to the LAI values (Fang, Jiang, et al., 2013). It should be noted that the uncertainties reported by the products differ from the validation uncertainties required by the user community (section 4).

Synergistic LAI products have been created by combining an ensemble of existing products (Table 6). The purposes of data synergy are to (1) improve the data quality, continuity, and consistency (Chai et al., 2012; D. Wang & Liang, 2011, 2014) and (2) reveal the strengths and weaknesses of each individual LAI. In addition to those in Table 6, similar data fusion studies have been performed for high-resolution Landsat, Satellite Pour l'Observation de la Terre (SPOT) high-resolution visible, and Sentinel-2 sensors (S. Li, Ganguly, et al., 2015; Mousivand et al., 2015; Soudani et al., 2006). Combing LAI with different

Reviews of Geophysics

10.1029/2018RG000608

Table 4
Characteristics of Global Moderate-Resolution LAI Products

Products	Version	Sensor	Spatial resolution	Temporal resolution	Algorithms	LAI T/E	Uncertainty	Notes	References
CYCLOPES	V3.1	SPOT/VEGETATION	1/112°	10-day (1997–2007)	NN (red, NIR, SWIR, and SZA)	T	Yes	Clumping at the plant and canopy scales not specifically represented	Baret et al. (2007)
EUMETSAT Polar System	V1	MetOp/AVHRR	1.1 km	10-day (2015–)	Gaussian process regression	T	Yes	LAI retrieved from normalized spectral reflectance factor with the Gaussian process regression method	García-Haro et al. (2018)
GA-TIP	V1	SPOT/VEGETATION and EnviSAT/MERIS	1 km	8-day (2002–2011)	Data assimilation retrieval from albedo (GlobAlbedo)	E	Yes	LAI_{eff} product, needs validation	Disney et al. (2016)
GEOV2	V2	SPOT/VEGETATION, MODIS	1/112°	10-day (1999–)	NN (red, NIR, SWIR, and SZA)	T	Yes	Integration of MODIS and CYCLOPES LAI products	Baret et al. (2013)
GLASS	V3	SPOT/VEGETATION, MODIS	1 km	8-day (2000–)	NN (red and NIR)	T	No	Trained from MODIS and CYCLOPES LAI products, spatially continuous	Xiao et al. (2014)
GLOBCARBON	V2	SPOT/VEGETATION, ENVISAT/ATSR	1 km	Monthly (1998–2006)	Empirical VI-LAI relationship	T	No	Product obsolete	Deng et al. (2006)
GLOBMAP	V2	MODIS	500 m	8-day (2000–)	Empirical VI-LAI relationship	T	No	Product derived from empirical method	Liu, Liu, et al. (2012)
JRC-TIP	V1	MODIS	0.01°	16-day (2000–)	Data assimilation retrieval from albedo (MODIS)	E	Yes	LAI_{eff} product, needs validation	Pinty et al. (2011)
MERIS	V1	EnviSAT/MERIS	300 m	10-day (2003–2011)	NN (13 bands, observation geometry, and atmosphere characteristics)	T	Yes	Gap-free 300-m LAI product	Tum et al. (2016)
MISR	V2	MISR	1.1 km	Daily (2000–)	LUT (red and NIR)	T	Yes	Product under validated and seldomly used	Diner et al. (2008)
MODIS	C6	MODIS	500 m	4-day (2000–)	LUT (red and NIR)	T	Yes	Widely used product, contains temporal variability	Huang et al. (2008)
PROBA-V	V1	PROBA-V	300 m	10-day (2014–)	NN (blue, red, NIR, and observation geometry)	T	Yes	Also known as GEOV3, a continuation of GEOV1/GEOV2	Baret et al. (2016)
University of Toronto (UofT)	V2	MODIS, MISR	250 m	10-day (2003)	Empirical VI-LAI relationship	T		Provide overstory LAI for forest and total LAI for other vegetation	Gonsamo and Chen (2014)
VIIRS	V1	SNPP/VIIRS	500 m	8-day (2012–)	LUT (red and NIR)	T	Yes	Interim product between EOS and JPSS	K. Yan et al. (2018)

Note. "LAI T/E" refers to true (T)/effective (E) LAI. LUT = look-up table; NIR = near-infrared; NN = neural network method; SWIR = shortwave infrared; SZA = solar zenith angle; VI = vegetation index; LAI = leaf area index; EnviSAT = Environment Satellite; EOS = Earth Observing System; GLASS = Global Land Surface Satellite; GLOBCARBON = The global carbon project; GLOBMAP = The global mapping project; JPSS = Joint Polar Satellite System; MERIS = MEdium-Resolution Imaging Spectrometer; MISR = Multiangle Imaging Spectro-Radiometer; PROBA = Project for On-Board Autonomy; VIIRS = Visible Infrared Imaging Radiometer Suite. CYCLOPES (http://www.theia-land.fr/), EUMETSAT Polar System (http://landsaf.meteo.pt/), GEOV2 (http://land.copernicus.eu/global/), GLASS (http://glass-product.bnu.edu.cn/ or http://glcf.umd.edu/), GLOBMAP (http://modis.cn/globalLAI/), MERIS (https://doi.org/10.15489/ak90g1wty909), MISR (https://eosweb.larc.nasa.gov/project/misr/misr_table), MODIS (https://lpdaac.usgs.gov/), PROBA-V (http://land.copernicus.eu/global/), UofT (http://ortelius.geog.utoronto.ca/data/Research/chenres/2003_global_1km/), and VIIRS (https://lpdaac.usgs.gov/). See the Committee on Earth Observation Satellites LPV website (https://lpvs.gsfc.nasa.gov/LAI/LAI_home.html) for a more updated LAI list.

Table 5
Examples of Global Long-Term LAI Products Derived From NOAA AVHRR Data

Products	Spatial resolution	Temporal resolution	Algorithms	Training data pair	Training area property	LAI T/E	Uncertainty	Validation scheme	Source	References
AVH15C1	0.05°	Daily (1982–)	Artificial NN	MODIS LAI vs. (LTDR red, NIR, NDVI, and SZA)	Global and class-wise	T	Bias = 0.23 RMSE = 1.13	II	Table 3	Claverie et al. (2016)
GEOV1	0.05°	Daily (1981–)	Back-propagation NN	GEOV1 LAI vs. (LTDR V3 red and NIR)	BELMANIP2 sites (F. Baret, Morissette, et al., 2006)	T				Verger et al. (2013)
GLASS	0.05°	8-day (1981–)	General regression NN	GLASS LAI vs. (LTDR V3 red and NIR)	BELMANIP2 sites (F. Baret, Morissette, et al., 2006)	T	Bias = −0.22 R^2 = 0.81 RMSE = 0.78	II	Figure 3	Xiao, Liang, et al. (2016)
GLOBMAP	8 km	Half-month (1981–)	VI-LAI relationship	MODIS LAI vs. GIMMS NDVI	Global and pixel-wise	T	R^2 = 0.36 RMSE = 1.65	II	Figure 12	Liu, Liu, et al. (2012)
LAI3g	1/12°	15-day (1981–)	Feed-forward NN	MODIS BNU LAI vs. (GIMMS NDVI3g, land cover, lat/long)	Global and for each month	T	RMSE = 0.68	II	Figure 2	Z. Zhu et al. (2013)

Note. "LAI T/E" refers to true (T)/effective (E) LAI. LUT = look-up table; NIR = near-infrared; NN = neural network method; SZA = solar zenith angle; VI = vegetation index; LAI = leaf area index; BELMANIP = Benchmark Land Multisite Analysis and Intercomparison of Products; GLASS = Global Land Surface Satellite; GLOBMAP = The global mapping project. The training data pair using the overlapping MODIS and AVHRR period to build a relationship to estimate long term LAI from AVHRR data. AVH15C1 (https://www.ncdc.noaa.gov/), GLASS (http://glass-product.bnu.edu.cn/ or http://glcf.umd.edu/), GLOBMAP (http://modis.cn/globalLAI/), and LAI3g (http://sites.bu.edu/cliveg/). See the Committee on Earth Observation Satellites LPV website (https://lpvs.gsfc.nasa.gov/LAI/LAI_home.html) for a more updated LAI list.

spatial and temporal resolutions is a common requirement from the user community (Fang, Liang, Townshend, et al., 2008; Verger et al., 2013; Yuan et al., 2011). F. Gao et al. (2006) proposed a spatial and temporal adaptive reflectance fusion model to blend both high-frequency MODIS and high-resolution Landsat data. The spatial and temporal adaptive reflectance fusion model uses changes in the MODIS pixels as a template to predict changes in the Landsat pixels. Several studies in the fusion of MODIS and Landsat have already illustrated the capability to generate high temporal and spatial resolution LAI data (F. Gao et al., 2012; Houborg et al., 2016; M. Q. Wu et al., 2012; H. K. Zhang et al., 2014).

3.3. Temporal Compositing

The irregular nature of the LAI time series, characterized by a combination of outlying values and data gaps, is linked to uncertainties in measurements and retrieval processes and has caused considerable difficulties for process models. Numerous methods have been designed to remove outliers and fill gaps and to improve the time series (Kandasamy et al., 2017; Verger et al., 2013).

3.3.1. Statistical Filtering Approach

The statistical filtering approach adjusts outliers and infills data gaps, using available observations and a priori guesses. Because of its simplicity and straightforwardness, the statistical filtering approach has been the dominant method for LAI temporal compositing. In this group, temporal filters are wildly used to generate continuous LAI products. One simple method is to remove outliers using predefined thresholds, for example, in the best index slope extraction algorithm (Doktor et al., 2009; L. Y. Sun & Schulz, 2017) or through an iterative interpolation process (Julien & Sobrino, 2010; Moreno et al., 2014). The most common method is to perform temporal smoothing by means of running averages or medians to suppress short-frequency variations. Other widely used temporal filtering methods include the asymmetric Gaussian model (Heumann et al., 2007; Jönsson & Eklundh, 2002), the double logistic filter (F. Gao et al., 2008; Z. Xiao et al., 2009), and the Savitzky-Golay filter (J. Chen et al., 2004; F. Gao et al., 2008). More sophisticated methods make use of Fourier- or wavelet-based filtering methods (Cihlar, 1996; Sellers et al., 1994).

The second group of statistical filtering methods is spatial filters, which uses pixel- or patch-level statistical data to remove noise and enhance surface features. Most commercial image processing software provides simple spatial filtering functions, such as nearest neighbor imputations, inverse distance weighted interpolation, and interpolation on triangulated irregular networks. For example, Kaptue Tchuente et al. (2010) used a simple interpolation method to fill the missing LAI values, using a weighted average of the same cover type within a specified range. Geostatistical methods, such as cokriging and stochastic simulation, have been used to extrapolate LAI field data at the landscape level (Burrows et al., 2002; Garrigues et al., 2001; Militino et al., 2017). To efficiently handle massive data sets, an approximate kriging method was proposed (Magnussen et al., 2008). Nevertheless, techniques based purely on spatial filtering are very limited in regions that have poor spatial coverage. Moreover, simple spatial filtering may fail to represent the spatial structure of the real landscapes (Berterretche et al., 2005). A significant number of efforts have been attempted to combine the advantages of both temporal and spatial filtering methods, by first replacing the outliers and

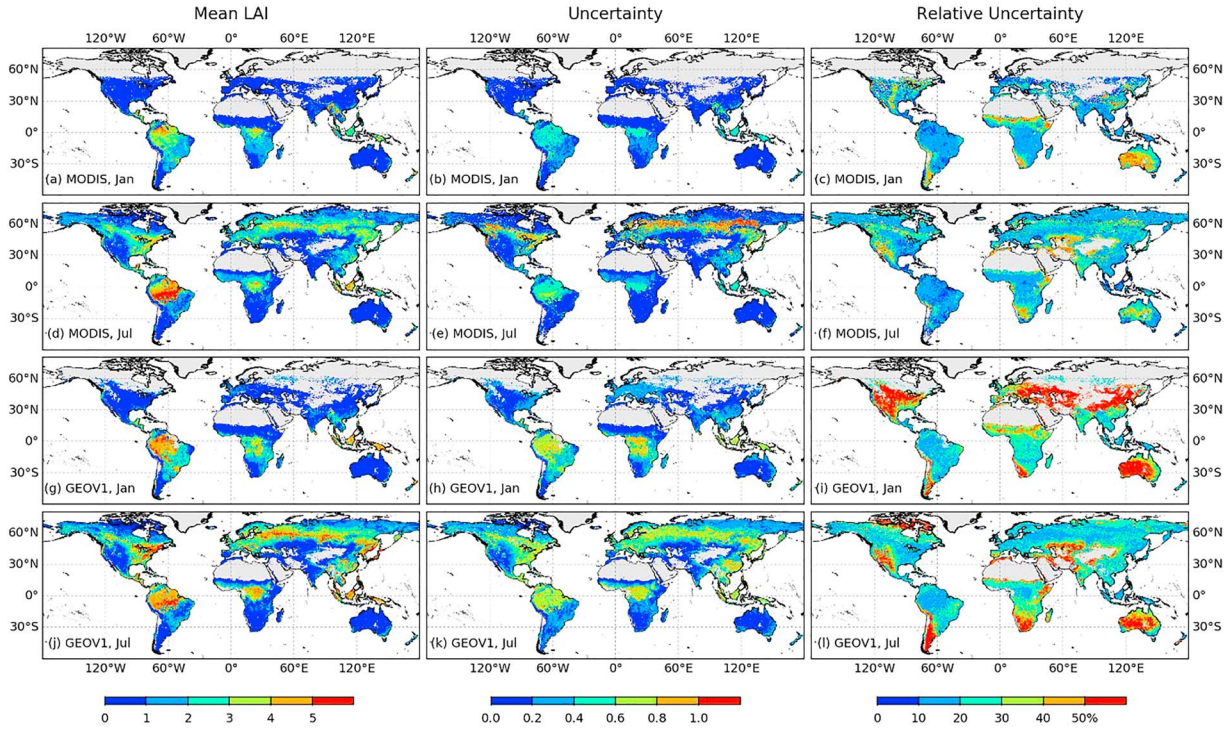

Figure 2. Global mean LAI (left), uncertainties (middle), and relative uncertainties (right) from MODIS (MOD15A2H, C6) and GEOV1 from 2003 to 2013 (0.05°) in January and July, respectively. The MODIS and GEOV1 uncertainties are derived from the standard deviation (LaiStdDev) and error (LAI_ERR) layers, respectively. The relative uncertainties are derived as a ratio of uncertainties to the mean LAI. LAI = leaf area index; MODIS = Moderate Resolution Imaging Spectroradiometer; GEOV1 = Geoland2/BiopPar version 1.

data gaps with a temporal filter, and if unsuccessful, a spatial filter will be activated (Borak & Jasinski, 2009; Fang, Liang, Townshend, et al., 2008; Verger et al., 2013; Yuan et al., 2011).

The quality of the composited LAI time series is evaluated by how accurately it reconstructs the full time series across temporal and spatial scales. The most straightforward criterion is to evaluate the filtered data for their completeness, smoothness, and accuracy by using field measurement data (Kandasamy et al., 2013, 2017; Pisek et al., 2010; Weiss et al., 2007). For example, Kandasamy et al. (2013, 2017) compared the performance of different statistical filters for MODIS and AVHRR LAI data, using field data from the Benchmark Land Multisite Analysis and Intercomparison of Products 2 sites. Quantitative performance metrics, such as the overall reconstruction error (J. Zhou et al., 2016), RMSE, the Akaike Information Criterion, and the Bayesian Information Criterion (Atkinson et al., 2012; Geng et al., 2014), were also used by some researchers in the performance assessment. Other studies have focused on how filtering methods can retain the key transition points and the robustness to noises in the time series (Geng et al., 2014; Hird & McDermid, 2009; R. G. Liu, Shang, et al., 2017).

All statistical filtering approaches involve a number of challenges. First, filtering approaches are limited to environments where the LAI time series follows regular vegetation cycles of growth and decline. Direct application of these approaches may be challenging for abrupt LAI changes (e.g., forest fire) or mixed pixels. Second, filtering algorithms originally designed for use with daily data may not be as effective with 8- or 10-day LAI data because the moving window algorithm is sensitive to the length of the sliding period. Adjustments have to be made to the filtering rules so that the algorithm works effectively with different temporal resolutions. Next, some filtering approaches, for example, the Savitzky-Golay and Fourier filters, are developed to make data adapt to the upper envelope. These algorithms would be limited in areas when the LAI products actually overestimate (Cohen, Maiersperger, Yang, et al., 2003; Fang & Liang, 2005). In practice, multiple filtering algorithms can be used jointly to improve the LAI data composition (Bradley et al., 2007; Frantz et al., 2017). Although the full time series can be completed reconstructed, none of the existing reconstruction models can outperform any other models under all situations (Hird & McDermid,

Table 6
LAI Products Derived From a Combination of Reflectance, Albedo, or LAI From Multiple Moderate-Resolution Sensors

Sensor/product	Fusion data	Fusion method	Validation scheme	Notes	Project/ Reference
MODIS/Terra+Aqua	Reflectance	Look-up table (LUT)	Data analysis	Terra-Aqua combination increases the number of high quality retrievals by 10–20% over woody vegetation.	MODIS (W. Yang et al., 2006)
MODIS/Terra+Aqua, Fengyun-3 MERSI	Reflectance	Spatial and spectral reflectance normalization and neural network LAI retrieval	III	The number of retrieved pixels increased from 78% and 88% for GEOV1 and MODIS to 98% for the fused product.	Yin, Li, Liu, et al. (2016)
MODIS and CYCLOPES	Reflectance and LAI	Neural networks and gap filling and temporal smoothing	III and II-Landsat	Improved the spatiotemporal continuity, consistency, and accuracy of the satellite products. Reduced 90% of the missing MODIS LAI.	Verger, Baret, & Weiss, (2011)
MODIS and CYCLOPES	Reflectance and LAI	Recurrent nonlinear autoregressive neural networks	III and II-Landsat	More continuous and higher quality compared to the original MODIS LAI.	Chai et al. (2012)
MODIS and CYCLOPES	LAI	Empirical orthogonal function	II	R^2 increases from 0.75 to 0.81, RMSE decreases from 1.04 to 0.71, compared to the original MODIS LAI. Improvement over CYCLOPES not significant.	D. Wang and Liang (2011)
MODIS and CYCLOPES	LAI	Optimal interpolation method	II	R^2 increases from 0.58 to 0.65; RMSE decreases from 0.93 to 0.79, compared to the original MODIS LAI. Compared to the reference data, the integrated LAI is not as good as CYCLOPES.	D. Wang and Liang (2014)
MODIS and CYCLOPES	LAI	GRNN between MODIS reflectance and the fused LAI (weighted average of individual LAIs)	I	Generated temporally continuous LAI profiles with improved accuracy compared with the individual LAI	GLASS (Zhiqiang Xiao et al., 2014)
MODIS and MISR	LAI	MultiResolution Tree (MRT)	II	Compared to MODIS, R^2 improved from 0.75 to 0.78; bias reduced from 0.28 to 0.14 and RMSE decreases from 1.04 to 0.82.	D. Wang and Liang (2010)
MODIS, MISR and SPOT VGT,	LAI	Ensemble Kalman filter	I	Improved temporal continuity and generated more accurate LAI	Liu et al. (2014)
ECOCLIMAP-II and GEOV1	LAI	Kalman filter	II	Compared to GEOV1, R^2 improved from 0.69 to 0.72; RMSE decreases from 0.86 to 0.85, while bias increases slightly from 0.02 to -0.14.	Munier et al. (2018)
MERIS, AATSR, ASAR, and SPOT HRV	LAI	Weighted average of optical and microwave LAI estimates	I	Produced slightly better LAI estimates than the optical and microwave estimates alone.	Manninen et al. (2005)
MERIS and SPOT VGT	Combined albedo	3-D RT model inversion	III	Output LAI values are temporally more stable than the MODIS LAI.	Disney et al. (2016)
ATSR and SPOT VGT	Intermediate LAI	LAI combination and smoothing	III	Relative uncertainties slightly higher than MODIS and CYCLOPES (Fang, Wei, Jiang, & et al., 2012).	GLOBCARBON Plummer et al. (2006)

Note. Different validation schemes are from Table 9. LAI = leaf area index; AATSR = Advanced Along-Track Scanning Radiometer; ASAR = Advanced Synthetic Aperture Radar; GLASS = Global Land Surface Satellite; GLOBCARBON = The global carbon project; HRV = high-resolution visible; MERIS = MEdium-Resolution Imaging Spectrometer; MERSI = MEdium Resolution Spectrum Imager; MISR = Multiangle Imaging Spectro-Radiometer.

2009; J. Zhou et al., 2016). There are no commonly accepted standards or criteria to intercompare different filters. Current filter intercomparison studies are limited because of the negligence of the impact of filter coefficients and the inherent differences in the LAI products. Designing the best way to infill the data gaps in both space and time while minimizing the original LAI product uncertainty is still a key task in global LAI data analysis, which demands comprehensive study.

3.3.2. Reconstruction Using Ancillary Data

The LAI temporal curve can be reconstructed based on the relationship with other ancillary variables. The most frequently used ancillary information is meteorological data, such as the growing degree days and radiation (Barr et al., 2004; R. Xu et al., 2010), air temperature (Koetz et al., 2005; L. Y. Sun & Schulz, 2017), thermal time (Duveiller et al., 2013; Lucas et al., 2015), and precipitation and potential evapotranspiration (ET; Tesemma et al., 2014, 2015). Indeed, multiple climatic variables can be jointly used to predict LAI (Iio et al., 2014; Pfeifer et al., 2012; Savoy & Mackay, 2015; L. Y. Sun & Schulz, 2017). Some researchers simply model the LAI temporal profile as a function of date (Cooter & Schwede, 2000; Z. Xiao et al., 2009). The temporal model is largely affected by the choice of the maximum and the seasonal variability of LAI. Others estimate the LAI time series from temporally continuous ancillary data, such as the fraction of absorbed photosynthetically active radiation (FPAR) from NOAA AVHRR (Los et al., 2000) and the reflectance data from MODIS (L. B. Guo et al., 2014; le Maire et al., 2011; Z. Xiao et al., 2009), Landsat (Z. Zhu et al., 2015), and FORMOSAT-2 (Bsaibes et al., 2009).

3.3.3. Dynamic Modeling Method

The other group of gap-filling techniques is referred to as the dynamic modeling method, which constrains a dynamic model with observations and uses the model to simulate the missing values. The dynamic model may be either a simple statistical model or a more sophisticated process model. The statistical model generally needs a priori background information. The most frequently used a priori information is the multiyear average or temporally fitted values (Fang, Liang, et al., 2008; Y. Gu et al., 2006; Verger et al., 2013; Z. Xiao et al., 2009). The accuracy of the dynamic modeling method is affected by the selection of model parameters and the dynamic model itself. Remote sensing LAI and processes models are integrated in various forms (section 5.2), where the continuous LAI happens to be a by-product since the main objective of the integration is for application.

3.4. Future Prospects

3.4.1. Improvement of Algorithms

Most of the new products to be derived from new missions, for example, European Space Agency Sentinels, National Aeronautics and Space Administration Decadal Survey, Joint Polar Satellite System, NOAA Geostationary Operational Environmental Satellites, and China Gaofen, are based on existing algorithms that have been demonstrated to be practical (M. Román et al., 2014). However, substantial biases in retrieval algorithms and model parameterization are often observed, and further improvement of algorithms, models, and parameterizations is necessary. The first issue is to reconcile the differences produced by different algorithms with the same input data (Pinty et al., 2004; Widlowski et al., 2015, 2007). This issue is broadly related to the model details, ancillary data dependence, and input data quality. A partnership among radiative transfer model developers has been created to perform a radiation transfer model intercomparison (RAMI) exercise, to identify crucial knowledge gaps that demonstrate the need for further model improvement (Widlowski et al., 2015). The latest phase of RAMI (RAMI-IV) shows that almost all simulated reflectances agree within a standard deviation of 2–6% (Widlowski et al., 2015). Similar experiments that apply a suite of algorithms over well-characterized reference sites should continue with open platform and community involvement for canopy model development and parameter retrieval.

Existing models mostly use typical soil reflectances from the spectral library (S. Jacquemoud et al., 1992) or derive them from soil reflectance models (Hapke, 1981; Price, 1990; Walthall et al., 1985). Contribution from more complicated background elements, for example, water and snow and understory vegetation, should be included in new modeling studies (Beget et al., 2013; G. Zhou et al., 2015). For algorithms that use ancillary land cover type as a priori information, errors in land cover will propagate to the LAI product and should be assessed formerly and be minimized where possible (J. Hu et al., 2003; Pocewicz et al., 2007). For algorithms that do not rely on land cover information, multiple sensors, multiple spectral bands, and observational geometry are likely to improve the retrieval accuracy (Baret et al., 2007; Q. Liu et al., 2014; Richter, Hank, et al., 2012; G. Yang et al., 2011). All algorithms will need to be adapted for future missions, particularly those

considering higher spatial and temporal resolutions and multiple data streams, rather than traditional single sensor approaches. It is unlikely that a single algorithm will be appropriate globally; instead, separate models may be considered for different biomes and can be exploited to build a database for global retrieval (Fang & Liang, 2005).

New retrieval algorithms and processing tools need to be developed to tackle the issues in the inversion process (Table 3). Alternative forms of band combinations and transfer models should be explored to find simple and robust LAI transfer functions. Hyperspectral band reflectances and VIs have demonstrated the capability to reduce the saturation effect and can be explored for operational LAI estimation (Canisius & Fernandes, 2012; D. J. Diner et al., 1999; Gemmel & McDonald, 2000; Houborg et al., 2009). Recent developments in machine learning and artificial intelligence algorithms, such as the deep learning algorithm, have shown potential and are worthwhile for further exploration (M. Campos-Taberner et al., 2016; Lazaro-Gredilla et al., 2014; L. P. Zhang et al., 2016). High-performance cloud platforms, such as the Google Earth Engine, have shown the capability to improve the efficiency of global variable retrieval (Manuel Campos-Taberner et al., 2018). Some locally optimized methods such as the Markov Chain Monte Carlo method (Q. Zhang, Xiao, et al., 2005) and the trust region method (J. Qin et al., 2008) warrant further examination before large-scale operational application.

3.4.2. Improvement of Temporal Coverage and Spatial Resolution

The long-term LAI products derived from AVHRR sensors since 1982 are gaining in prominence due to their ability to assess the LAI variation and quantify the future uptake of CO_2 by the world's vegetation (e.g., Table 12). Long-term spatiotemporal patterns and the main strengths and weaknesses of each data set need to be identified and compared with modeling results. The AVHRR orbit change and sensor degradation are two important sources of inconsistency (Jiang et al., 2017; Mao et al., 2016; Zaichun Zhu, Piao, et al., 2016). Further efforts should be made to reprocess and reanalyze the historical archives of AVHRR sensors to ensure compatibility and consistency with current records (GCOS, 2011). Extrapolation of an even longer LAI data set prior to the satellite era has been attempted (Boisier et al., 2014; Lawrence et al., 2012; Neilson, 1995), but attempts like this need climatic data for extrapolation purpose and are limited in explaining the climate change impact. Further studies of the long-term LAI change need to address several crucial companion questions: (1) Does the leaf spatial dispersion, that is, the clumping index, change with LAI, (2) how do the overstory and understory LAI values change, and (3) what are the long-term changes in foliage density and vegetation height?

Most global moderate resolution LAI products are mainly in kilometric resolutions (Table 4), and some hectometric (100–1,000 m) products have been developed over a few countries (Table 7). During the next few years, several high revisit frequency hectometric and decametric resolution (10–100 m) sensing systems will generate similar global LAI products. The hectometric products satisfy the GCOS requirement for a horizontal spatial resolution of 250 m (GCOS, 2016) and can be more easily validated with field measurements and higher spatial resolution imagery. The combination of these medium temporal resolution missions (e.g., Sentinel-2 and Landsat 8) with hectometric data (e.g., Sentinel-3) is expected to provide near daily LAI products (F. Gao et al., 2014). For many applications, however, it is vitally important to ensure traceability and consistency back to the kilometric LAI estimates because long time series are at least as important as higher spatial resolution.

3.4.3. Estimation From Active Sensors and UAV

The major advantage of LiDAR technology is its capability to characterize the vertical vegetation structure at different heights (M. J. Sumnall, Fox, et al., 2016; Tang et al., 2014). The LiDAR-based LAI estimates have been used in the validation of global moderate-resolution LAI products (Hill et al., 2006; Jensen et al., 2011; K. Zhao & Popescu, 2009). We expect the use of LiDAR LAI will increase with the growing availability of high-quality LAI data derived from LiDAR. The key issues are (1) the conversion of LAI_{eff} to LAI, which needs concurrent indirect optical measurements (Jensen et al., 2008; Moorthy et al., 2008), (2) the selection of proper LiDAR metrics for LAI estimation (M. Sumnall, Peduzzi, et al., 2016), and (3) building global LAI inventory derived from both the TLS and Airborne laser scanner databases. More field measurements and further development of LiDAR metrics are necessary (Hill et al., 2006; K. Zhao & Popescu, 2009).

Microwave radar data overcome some of the limitations of the remote sensing reflectance and LAI data, such as gaps during the growing season caused by cloudiness, and will be a tremendous new resource for LAI estimation. Microwave data are particularly powerful when combined with crop growth models in the

Table 7
Examples of Hectometric LAI Products Estimated from MODIS (250 m), MERIS (300 m), MERSI (250 m), and PROBA-V (300 m)

Sensor	Algorithms	LAI T/E	Country	Biome type	Scheme	N	Uncertainty	Field method	Source	References
MODIS	VI-LAI relationship	T	Canada	ENF and DBF	I	15	Bias = −0.3 R^2 = 0.689 RMAE = 30.7%	TRAC	Figure 4	Gonsamo and Chen (2014)
MODIS	PROSAIL inversion	T	Brazil	EBF	I	20	R^2 = 0.8 RMSE = 0.41	Destructive	Figure 5	le Maire et al. (2011)
MODIS	LUT-PROSAIL	T	Italy	Grass	I		Bias = 007 SD = 1.58 RMSE = 1.68	Destructive, allometric	Table 3	Pasolli et al. (2015)
MERIS	VI-LAI relationship	T	Canada	All	I	44	RMSE = 0.93 RRMSE = 53%	DHP	Table 3	Canisius and Fernandes (2012)
MERIS	NN	E	Netherlands	Grass	I	30	R^2 = 0.70 RMSE = 1.02 NRMSE = 16%	LAI-2000	Figure 4	Si et al. (2012)
MERIS	NN	E	VALERI sites	Crop, shrub, and mixed forest	II-SPOT HRV	6	RMSE = 0.471	DHP	Figure 10	Bacour et al. (2006)
MERSI	VI-LAI relationship	T	China	Grass	II-Landsat		R = 0.52 SD = 0.51	LAI-2000	Figure 5	L. Zhu et al. (2014)
PROBA-V	NN	GAI	Globe	All	II-Landsat		R^2 = 0.76[a] RMSE = 1.40	Destructive AccuPAR	Figure 4	Baret et al. (2016)

Note. "LAI T/E" refers to true (T)/effective (E) LAI. LUT = look-up table; VI = vegetation index; SD = standard deviation; RMAE = relative median absolute error; LAI = leaf area index; DBF = deciduous broadleaf forest; ENF = evergreen needleleaf forest; HRV = high-resolution visible; MERIS = MEdium-Resolution Imaging Spectrometer; MERSI = MEdium Resolution Spectrum Imager; PROBA = Project for On-Board Autonomy; VALERI = Validation of Land European Remote sensing Instruments.
[a]Based on simulated PROBA-V data (E. Roumenina et al., 2013).

assimilated estimation of the growing season LAI (Bach et al., 2001; Clevers & van leeuwen, 1996; Dente et al., 2008). However, their applicability at the global scale remains to be assessed.

Unmanned aerial vehicles (UAVs) provide an effective platform for field LAI estimation and act as a validation link between field and satellite data. Both reflective and LiDAR sensors can be affiliated with UAV (Q. Guo et al., 2017). In data acquisition, it is important to explore the optimal illumination conditions, flight configuration, and camera settings (Uto et al., 2013; Weiss & Baret, 2017). Motion pictures acquired on UAV allow 3-D scene building and LAI estimation (Mathews & Jensen, 2013; Weiss & Baret, 2017). LAI is generally estimated from UAV based on the same empirical transfer or model inversion methods as for other remote sensing data (Duan et al., 2014; Lelong et al., 2008; Verger et al., 2014). With the availability of more efficient data processing software, this technique is expected to become increasingly common in field studies.

3.4.4. Distribution of Product Quality Information

Due to the complex, multistage retrieval process from optical remote sensing data, a comprehensive quantitative assessment of the quality of LAI products is still lacking for satellite-derived LAI products. Given the importance of the associated uncertainty information, it is crucial for all existing and future global products to provide fully documented and traceable information on uncertainty. This requires the inclusion of a consistent quantified uncertainty layer in the product that is valuable and appropriate for use by the application community. Self-assessment serves as an internal validation process. New releases should represent improved confidence in LAI retrieval, which needs to be clearly transmitted to potential users. Considering the importance of the long time series for most applications, improvements in one product should be applied to the entire time series, which requires reprocessing the original imagery.

4. Product Validation and Evaluation

To meet the needs of global climate modeling studies, the Globe Climate Observing System (GCOS) has proposed a guideline that requires a maximum uncertainty of 15% for the LAI products (GCOS, 2016). Similar observational accuracy requirements have also been specified by the Global Terrestrial Observing System, the World Meteorological Organization, and the Global Monitoring for Environment and Security

Table 8
Observational Uncertainty Requirements for LAI Products From GCOS, GTOS, WMO, and GMES

Projects	Application	Uncertainty requirement[a]	References
GCOS	TOPC	10%-7%-5% Max (15%) Accuracy: max (20%, 0.5)	WMO[b] GCOS (2016) GCOS (2011)
GMES		Accuracy: 10%	Drusch et al. (2012)
GTOS		25%-15%	GTOS[c]
WMO	Agricultural meteorology	10%-7%-5%	WMO[b]
	Global NWP	20%-10%-5%	
	High resolution NWP	20%-10%-5%	
	Hydrology	20%-8%-5%	

Note. GCOS = Global Climate Observing System; GMES = Global Monitoring for Environment and Security; GTOS = Global Terrestrial Observing System; NWP = Numerical Weather Prediction; TOPC = Terrestrial Observation Panel for Climate; WMO = World Meteorological Organization; LAI = leaf area index. Accuracy requirements are denoted as a percentage of the maximum possible value for GCOS and as a percentage of the true value for GTOS and WMO. Data updated from Fang, Jiang, et al. (2013).
[a]Stated in terms of the threshold, the breakthrough, and the goal values. The GMES row shows the targeted precision for green LAI estimation. [b]WMO website—http://www.wmo-sat.info/oscar/requirements (Accessed on 16 March 2017). [c]GTOS web site—http://www.fao.org/gtos/tems/variable_show.jsp?VARIABLE_ID=80 (Accessed on 1 March 2012, obsolete).

(Table 8). In general, LAI application communities require a minimum relative accuracy of about 20% (Table 8). Characterization of the uncertainties associated with LAI products is, therefore, of vital importance for the downstream application community (Gobron & Verstraete, 2009; Lafont et al., 2012). A better understanding of the uncertainties embedded in current LAI products will improve the assimilation of LAI into modeling studies.

Validation is defined by the Committee on Earth Observation Satellites (CEOS) as "the process of assessing, by independent means, the quality of the data products" derived from the Earth observation systems (http://www.ceos.org/ourwork/workinggroups/wgcv/). The CEOS Land Product Validation (LPV) subgroup (http://lpvs.gsfc.nasa.gov/) has been charged to lead the comparison and evaluation of land surface products as well as the benchmarking of algorithms used to generate them. The mission of the LPV subgroup is to "coordinate the quantitative validation of satellite-derived products." The LPV subgroup focuses on "standardized intercomparison and validation across products from different satellite, algorithms, and agency sources" (http://lpvs.gsfc.nasa.gov/). Within this framework, a large number of LAI validation studies have been undertaken, from site to global scales.

4.1. Current Schemes

Table 9 summarizes the different schemes that have been used to validate satellite-derived LAI products.

4.1.1. Scheme I: Direct Field-to-Satellite LAI Comparison

The direct comparison method directly compares field measurements and satellite products. Field measurements, typically limited to a point or a very small area, are vital as they form the basis for all validation studies. Prior to National Aeronautics and Space Administration's Earth Observing System program (https://eospso.gsfc.nasa.gov/), most validation studies for AVHRR LAI products relied on the direct comparison method because of the scarcity of high-quality field LAI measurements and concurrent high-resolution satellite data (Buermann et al., 2002; H.-S. Kang et al., 2007; Nikolov & Zeller, 2006). This method is helpful when, for instance, a sufficient number of field points are available during a satellite overpass or when the field is spatially representative over the satellite pixel extent (Fang, Wei, & Liang, 2012). This method is often used when the high-resolution data are difficult to obtain from upscaling (see scheme II) or when the methods for estimating the high-resolution LAI are determined to be problematic. However, a major problem of the direct comparison method is the spatial scale mismatch between field measurements and remote sensing estimates. The errors are related to the spatial heterogeneity within the moderate-resolution pixels (Fang, Wei, & Liang, 2012). Furthermore, the areal coverage of the moderate-resolution LAI products is not constant over an aggregation period (e.g., 10 days for GEOV1), and pixel geolocation varies. Several methods have been proposed to mitigate the scaling and geolocation issues, including estimation of the mean or median LAI values of multiple pixels (e.g., a 3×3 array of pixels), employment of large field sampling units at the kilometric scale (e.g., J. L. Privette et al., 2002), and comparison of statistical distributions of in situ and satellite LAI (Pfeifer et al., 2014).

4.1.2. Scheme II: Comparison With Upscaled High-Resolution Reference Data

This scheme scales up the field-estimated LAI via high-resolution imagery to larger pixel sizes for comparison with moderate-resolution products, thus, bridging the scale differences between ground LAI measurement and moderate-resolution pixels. The upscaling process is mainly based on the establishment of a transfer function that relates field LAI measurements and high-resolution VIs or reflectance from satellite or airborne images (R. Fernandes et al., 2014; Morisette et al., 2006). Landsat and SPOT high-resolution visible have been the most common high-resolution satellite sensors. Selection of the optimal transfer function is usually biome- and site-specific (Cohen et al., 2006; R. A. Fernandes et al., 2003). Even within one land cover type, different weights can be assigned for each ESU, for example, in the Validation of Land

Table 9
Summary of LAI Product Validation and Evaluation Schemes

Schemes	Description	Advantages	Disadvantages	Examples
I. Direct field-satellite comparison	Makes direct comparison between field measurements and satellite LAI.	Flexible for quick assessment of the LAI retrieval algorithm and the product	Affected by the scale difference between field and pixel. Only feasible with sufficient number of ground points and for homogeneous regions. Difficult for global validation.	Alton (2016), Fang, Wei, & Liang et al. (2012), L. B. Guo et al. (2014), H.-S. Kang et al. (2007), Ogutu et al. (2011), and Sea et al. (2011)
II. Comparison with upscaled high-resolution reference data	Scales up LAI estimated from a dedicated field sampling via high resolution imagery to larger areas for comparison with moderate resolution products	Minimizes the scale difference between point and pixel. Commonly applied.	Affected by quality of the reference map, field measurements, clumping correction, transfer function, and upscaling methods.	Camacho et al. (2013), Claverie et al. (2013), Garrigues, Lacaze, et al. (2008), H. A. Jin et al. (2017), Raymaekers et al. (2014), and Xu, Li, et al. (2018)
III. Intercomparison of multiple satellite products	Intercompares different products with similar spatial and temporal resolutions	Efficient to describe the relative consistency and hence quality of multiple products assuming departure from the mean indicates lower quality.	Presents only the quality of one product relative to another product. Affected by LAI definitions, methodological differences, and characteristics of different sensors. Might require spatial and temporal resampling.	Fang, Jiang, et al. (2013), Garrigues, Lacaze, et al. (2008), Gessner et al. (2013), Kobayashi et al. (2010), Verger et al. (2008), and Xu, Li, et al. (2018)
IV. Comparison of the consistency with other related variables	Assesses the degree of consistency with other spectral, biophysical and climatic variables, for example, NDVI, FPAR, and albedo.	Permits analysis of the consistency of vegetation variables.	Difficult to interpret as all variables are affected by perturbations to different degrees.	Buermann et al. (2003), Biudes et al. (2014), Croft et al. (2014), McCallum et al. (2010), Yan et al. (2016), and Z. Zhu et al. (2013)
V. Comparison of satellite LAI with model simulated LAI	Compare LAI products with model simulated LAI.	Efficient to make an LAI-model comparison.	Affected by definition differences between modeled and satellite. Structural differences in LAI calculation between model and satellite.	Adiku et al. (2006), Anav, Murray-Tortarolo, et al. (2013), Di Bella et al. (2005), Murray-Tortarolo et al. (2013), Randerson et al. (2009), and Z. Zhu et al. (2013)
VI. Performance evaluation in process models	Integrate different LAI products into models, evaluate LAI products through their performance in modeled outputs	Allows comparison of multiple products in application models.	Affected by model limitations and uncertainties. Accuracy affected by other model parameters.	Calvet et al. (2014), Chu et al. (2011).), Ghilain et al. (2012), Ghilain et al. (2014), and Wythers et al. (2003)

Note. LAI = leaf area index.

European Remote sensing Instruments project (http://w3.avignon.inra.fr/valeri/), to generate the high-resolution reference LAI map. Besides the simple linear regression method, other model inversion methods can be used to derive the high-resolution reference LAI. The upscaling validation method has been widely used by the remote sensing community for data collection, analysis, and accuracy reporting. For global application, this scheme may be affected by several factors: (1) accuracy of the high-resolution reference data from different transfer functions, (2) error propagation introduced by scale mismatch and registration errors between high and moderate resolution LAI surfaces, and (3) labor intensity for conducting high-resolution remote sensing data processing and LAI estimation.

4.1.3. Scheme III: Intercomparison of Multiple Products

The purpose of the intercomparison is to determine the relative quality of the land products by quantifying the magnitude and locations of the differences and similarities between different products sharing similar spatial and temporal resolutions. The intercomparison approach, which does not require ground

measurements, has been used as a proxy in efforts aiming to assess the temporal and spatial consistency and statistical distribution within and between sensors (Garrigues, Lacaze, et al., 2008; Verger, Camacho, et al., 2009; Weiss et al., 2007). In this regard, it is an assessment of the differences in input data quality, methodology, assumptions, and dependencies in LAI estimation. Intercomparisons have been conducted at various scales ranging from site (Fang & Liang, 2005), regional and continental (Garrigues, Lacaze, et al., 2008; Gessner et al., 2013), to global scales (Fang, Jiang, et al., 2013; B. Xu, Park, et al., 2018). This scheme assumes that different satellite products represent the same physical quantity. The consensus estimated with this scheme is important but differs from the uncertainty information provided by error propagation analysis and validation (Fang, Jiang, et al., 2013). It is preferable to calculate the mean of multiple similar pixels and perform a comparison at the patch (multipixel) scale to account for the potential location mismatch between corresponding pixels and the uncertainties in the products (R. Myneni et al., 2005; Y. Wang et al., 2004). The value of this scheme is that it indicates areas and periods with higher discrepancies, in which future product development and validation studies may be focused.

4.1.4. Scheme IV: Comparison of Consistency With Other Related Variables

This method of evaluating LAI data sets involves assessing the degree of consistency with other spectral, biophysical, and climatic variables (W Buermann et al., 2002; Ganguly et al., 2008). The comparative analyses focus on the consistency of temporal profiles and data gap occurrences for major land cover types. Since NDVI has been widely used for LAI estimation, both LAI and NDVI products are frequently compared (Croft et al., 2014; Hadria et al., 2006). Given the known saturation issues with the NDVI-LAI relationship, LAI can be evaluated with other spectral data or VI products (e.g., enhanced VI and soil-adjusted VI; Biudes et al., 2014; Houborg et al., 2007). Some studies have found that LAI products show similar discrepancies to the FPAR products (McCallum et al., 2010; Seixas et al., 2009; Weiss et al., 2007). Other studies have evaluated the consistency between remote sensing LAI and key climatic variables that govern plant growth, such as land surface temperature, solar radiation, and precipitation (Buermann et al., 2002; Los et al., 2000; Lotsch et al., 2003; R. B. Myneni et al., 1996). Because remote sensing LAI products are usually generated without using climatic data, examining the statistical association between LAI and climatic variables can be considered as an independent means of LAI evaluation (Kai Yan et al., 2016; Z. Zhu et al., 2013). However, caution is advised in examining the relationship of LAI with these variables, which may be influenced by other external factors.

4.1.5. Scheme V: Comparison With Model-Simulated LAI

This scheme compares remote sensing products with climatic, ecological, and vegetation growth model simulations. The modeled LAI may be derived as a simple function of climatic variables or from a more complex vegetation dynamic model. The geographical and temporal patterns between modeled and satellite LAIs are generally consistent (Imbach et al., 2010; Szczypta et al., 2014; Z. Zhu et al., 2013), while some studies found that the maximum modeled LAI trails behind the satellite LAI (Randerson et al., 2009; Z. Zhu et al., 2013). Global comparison studies have found that current ecosystem models tend to overestimate LAI (Anav, Friedlingstein, et al., 2013; Anav, Murray-Tortarolo, et al., 2013; Z. Zhu et al., 2013), partly because of the overestimation of carbon fixation and allocation of biomass to leaves (Gibelin et al., 2006; A. D. Richardson et al., 2012). Similar overestimation phenomena have been reported for regional LSM simulations (Lafont et al., 2012; Murray-Tortarolo et al., 2013). Because of the complexity of the models, using such a scheme does not necessarily produce a quantitative estimation of the LAI product uncertainty. Instead, it highlights the inconsistent areas in which further refinement of land surface and remote sensing models is needed. Indeed, process models have mostly relied on field and remote sensing LAI for quality assessment and model improvement (Bao et al., 2014; Murray-Tortarolo et al., 2013; A. D. Richardson et al., 2012). Particular attention should be paid to the definitions of the variables used in process models, which should match those retrieved by the remote sensing methods. This is especially true for the mixed-type classes for which LAI definition and calculation may differ, in the consideration of 3-D vegetation structure, background contribution, and grid computation.

4.1.6. Scheme VI: Performance Evaluation in Process Models

This scheme evaluates different LAI data sets based on their performances in modeled outputs (Calvet et al., 2014; Wythers et al., 2003). For example, Chu et al. (2011).) found that the Global Land Surface Satellite LAI performed better than the MODIS LAI (C4) in modeling the climate impacts of large-scale revegetation in Queensland, Australia. This scheme is similar to scheme V and allows for an easy comparison among multiple products. However, despite its potential use, this scheme should be used with caution because the models suffer from the same limitations and uncertainties as those indicated for scheme V.

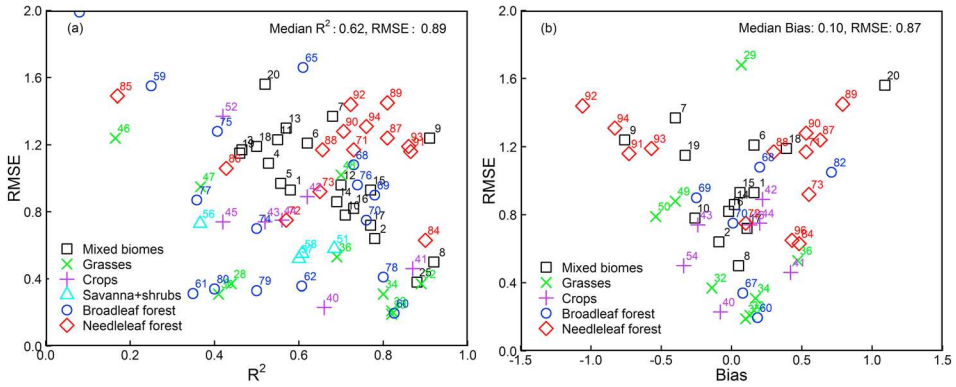

Figure 3. Statistical R-squared values (R^2) and (a) root-mean-squared error (RMSE) and bias and (b) RMSE from direct validation of moderate resolution leaf area index products. The numbers correspond to the reference number in Table S2.

Various schemes and state-of-the-art technologies have been explored by product developers, validation scientists, and science users in satellite data validation (Loew et al., 2017). The schemes are useful not only for LAI validation but also for other land surface variables and for improving LSMs. Schemes I and II can be considered direct validation schemes, while the other schemes are not strictly defined as validation schemes but are important for assessing the quality of LAI products. Poorly designed validation methods can lead to inconsistent validation results (R. Fernandes et al., 2014). It is important for the validation community to cross check results from different schemes.

4.2. Product uncertainties

4.2.1. LAI Uncertainties From the Literature

Figure 3 illustrates the uncertainties for major moderate-resolution LAI products, with data compiled from the literature (Table S2). The agreement between satellite LAI products and the reference data is generally good, and the associated median accuracy indicators are about $R^2 = 0.62$ and RMSE = 0.88 for all biome types (Table 10). The R^2 and RMSE values range between 0.08 and 0.92 and between 0.19 and 2.41, respectively. The median absolute errors are <0.10, and the relative errors are <8% (Table 10). The MODIS products, now in their sixth major reprocessing, have been investigated intensively during the past few decades and are commonly used as a benchmark for other LAI products. A review of the MODIS C5 validation studies suggests a median R^2 around 0.62 and an RMSE of 1.16. Carbon cYcle and Change in Land Observational Products from an Ensemble of Satellites (CYCLOPES) exhibits a performance similar to MODIS, scoring overall $R^2 = 0.61$ and RMSE = 0.87 (Table 10). CYCLOPES also shows a negative bias, which has been improved in the later GEOV1 (Baret et al., 2013).

Biome-specific uncertainties can be much lower, such as that for grassland or crops (Duveiller et al., 2011; Si et al., 2012). Good agreement was reported between satellite and reference LAI for grasslands, as confirmed

Table 10
Statistics of Moderate-Resolution Leaf Area Index Validation Results Reported in the Literature

All biomes	Statistics	Min	Median	Max	Biome types	Statistics	Min	Median	Max
Overall	R^2	0.08	0.615	0.92	Mixed biomes	R^2	0.416	0.68	0.92
	Bias	−1.59	0.1	1.65		RMSE	0.38	0.97	1.56
	RE (%)	−17	7.87	65	Grass	R^2	0.165	0.44	0.89
	RMSE	0.19	0.88	2.41		RMSE	0.19	0.48	1.68
	RRMSE (%)	23	36.6	98	Crops	R^2	0.42	0.59	0.87
MODIS	R^2	0.165	0.615	0.9		RMSE	0.23	0.74	1.37
	Bias	−1.18	0.13	1.65	Savanna + shrubs	R^2	0.293	0.6	0.684
	RMSE	0.21	1.16	2.41		RMSE	0.39	0.55	0.73
	RRMSE (%)	23	40.3	65.6	Broadleaf forest	R^2	0.08	0.5	0.826
CYCLOPES	R^2	0.358	0.608	0.92		RMSE	0.196	0.885	2.41
	Bias	−0.76	−0.175	0.05	Needleleaf forest	R^2	0.17	0.715	0.9
	RMSE	0.5	0.87	1.24		RMSE	0.63	1.17	1.49

Note. Data from Table S2. RE = relative error; RMSE = root mean squared error; RRMSE = relative RMSE.

by the lowest median RMSE (=0.48) among all biome types (Table 10). Satellite LAI products generally agree well with reference data for crops (median RMSE = 0.74), although larger deviations could occur because of field measurement and scaling differences (Stern et al., 2014). It has been rare to validate a specific crop type. Similarly, only a few studies have focused on the shrub type (Fang, Wei, & Liang, 2012; Hill et al., 2006).

Validation of the savanna LAI is difficult because of its complex biome composition (Fang, Li, et al., 2013). Early MODIS LAI validation showed reasonable agreement in both magnitude and seasonal variation for woodland savannas in Australia (Hill et al., 2006; Leuning et al., 2005) and Africa (J. L. Privette et al., 2002; Tian et al., 2002). Table 10 shows that the savanna RMSE uncertainty (0.55) is similar to that of grasses. This low uncertainty should be interpreted with reference to the small LAI values (~0.99) for savannas (Fang, Wei, & Liang, 2012). Recent MODIS (C5) validation studies have revealed an RMSE > 1.5 in the Amazon savanna transition zone (Biudes et al., 2014) and a small correlation with an R^2 of ~0.30 for the African savanna (Mayr & Samimi, 2015). These inconsistencies highlight the difficulties associated with savanna validation, which include heterogeneity of the landscape, difficulties in the completion and interpretation of ground measurements (Ryu, Sonnentag, et al., 2010), easy misclassification of the underlying land cover type (Fang, Li, et al., 2013), and scale differences between field measurement and satellite pixel sizes (Groenendijk et al., 2011).

The median R^2 and RMSE are 0.5 and 0.89 for broadleaf forests and 0.72 and 1.17 for needleleaf forests, respectively (Table 10). The MODIS LAI appears to capture changes in the overstory LAI reasonably well but fails to capture variations in the understory LAI (Biudes et al., 2014). This highlights the complexities in the LAI field measurement and product validation in tropical forests. Deciduous broadleaf forest is easy to measure in the field, using methods such as the litter fall method. For deciduous broadleaf forest, the bias and RMSE vary between 0.5 and 1.0 (Table S2). A large number of validation studies have been performed for the evergreen needleleaf forest in the northern midlatitudes. In contrast, only a limited number of studies were performed for deciduous needleleaf forest (Akitsu et al., 2015). The RMSE uncertainties vary between 0.5 and 1.5 for evergreen needleleaf forest, whereas for deciduous needleleaf forest, the bias is generally smaller than 1.0 (Table S2). Very good temporal consistency has been observed between MODIS C5 and GEOV1 for deciduous forests (R^2 > 0.70), with a smoother behavior for GEOV1 (Fang, Jiang, et al., 2013). However, there is a lack of validation studies for the evergreen broadleaf forest concentrated in the tropical regions (Clark et al., 2008).

4.2.2. Uncertainty Sources

Previous studies have identified three major contributors to LAI product uncertainties: (1) uncertainties in the input data, for example, surface reflectance or radiance (Mannschatz et al., 2014; Vermote et al., 2002; Y. Wang et al., 2001), (2) model uncertainties and problems of ill-posed retrieval (Deng et al., 2006; D. Huang et al., 2008; Knyazikhin et al., 1999; R. B. Myneni et al., 2002), and (3) errors in the ancillary information, for example, land cover type (DeFries & Los, 1999; Fang, Li, et al., 2013; Gonsamo & Chen, 2011). Each of these factors is assessed below.

The accuracy of LAI products is unavoidably driven by the input data. LAI products are estimated from surface reflectance, radiance, and albedo. The relative accuracy of the latest MODIS reflectance is generally within ±5% (Vermote et al., 2015) and <10% in the semiarid grassland (Fan et al., 2014). Over desert areas, the relative errors between Environment Satellite/medium-resolution imaging spectrometer, SPOT/VEGETATION, and MODIS are <3% (Lacherade et al., 2013). Uncertainties in the surface reflectance products are mainly attributed to aerosol and cloud contamination (Hagolle et al., 2005; Hilker et al., 2012). The relative uncertainty of the high-quality (full inversion) MODIS albedo products is generally within 10% (Pinty et al., 2011; M. O. Román et al., 2013) and <3% for the semiarid grassland (Fan et al., 2014). The overall accuracy of the input fractional vegetation cover, which is used to derive the Satellite Application Facility for Land Surface Analysis LAI, is around 20% (LSA SAF, 2008). Errors from input reflectance and albedo data, with favorable atmospheric correction conditions, are generally lower than those caused by ancillary data and model imperfections. Prior analysis of the NN inversion method showed that a reflectance error of ±10% will cause an error in 0.41 LAI units (Fang & Liang, 2003).

Two of the main difficulties in LAI retrieval are the intrinsic uncertainties in the radiative transfer modeling of light in canopies and the ill-posed inversion problem (Combal et al., 2001; Knyazikhin et al., 1999). The uncertainties may be driven mainly by the assumptions in the radiative transfer models, the inversion technique,

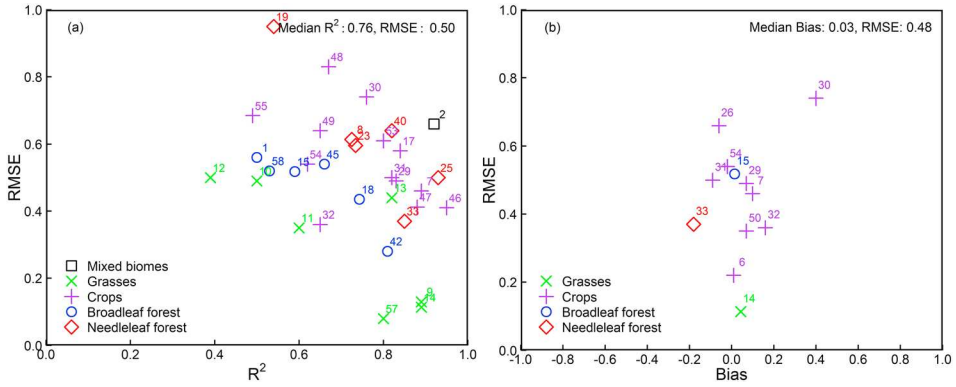

Figure 4. Uncertainties of high-resolution reference leaf area index data compared with field measurement data. (a) R^2-RMSE and (b) Bias-RMSE. The numbers correspond to the reference number in Table S3.

and the prior information used. These issues may be addressed by integrating various sources of prior information and by using multiple satellite data sets (Ganguly, Nemani, et al., 2014; Q. Liu et al., 2014). Most LAI estimation algorithms provide dispersion measures as outputs of the theoretical uncertainties (e.g., MODIS, CYCLOPES, GEOV1, JRC-TIP, and GA-TIP; Table 4). The MODIS uncertainty estimation is quantified as the standard deviation of all acceptable solutions from an LUT retrieval method (D. Huang et al., 2008; R. B. Myneni et al., 2002). The GEOV1 uncertainty information is derived from the NN training database and reflects the sensitivity of the product to the input reflectance values (F. Baret et al., 2013). Both of these uncertainties are fairly stable and are at a low level of <0.30 for the herbaceous vegetation types (Fang, Li, et al., 2013). In tropical regions, the MODIS uncertainty varies between 0.10 and 0.35, whereas the GEOV1 uncertainty is slightly higher. It is noted that the uncertainty information represents the model variation after multiple training and self-checking and reflects the sensitivity of the product to input reflectance values.

Land cover is used as an ancillary data constraint to make the inversion process more tractable. Although this speeds up the processing, land cover misclassification is one of the largest sources of uncertainty for LAI estimation (Fang, Li, et al., 2013; Gonsamo & Chen, 2011; Pisek et al., 2007). The overall accuracies are about 75% for the global MODIS C5 land cover data (Friedl et al., 2010) and 67.5% for GlobCover 2009 (Defourny et al., 2010). The land cover errors translate into the LAI uncertainty in two ways: (1) the selection of the wrong biome input and therefore the wrong algorithm or portion of an LUT and (2) the use of incorrect parameters where land cover types are similar, even if the algorithm is appropriate. Selection of the wrong algorithm can lead to errors of up to 40–50% for MODIS and the global mapping project (Gonsamo & Chen, 2011; R. B. Myneni et al., 2002), and inadequate parameterization of the radiative transfer scheme (e.g., vertical and horizontal heterogeneities, leaf single scattering albedo, and background reflectance) can introduce errors up to 20% for MODIS LAI (Serbin et al., 2013). Misclassification can easily occur among grasses/cereal crops and broadleaf crops because of their spectral and structural similarities (Pandya et al., 2006; Tan et al., 2005; P. Yang et al., 2007). However, misclassification between similar biomes generally induces small LAI errors (<30%; Fang, Li, et al., 2013; R. B. Myneni et al., 2002), whereas confusion between herbaceous and woody vegetation can significantly affect the LAI retrieval (Tian et al., 2000).

4.2.3. High-resolution reference LAI

An important issue related to the validation of moderate-resolution products is the quality of the high-resolution LAI reference data, which is generally derived using a transfer function calibrated over a set of field measurements. Recent studies related to LAI estimation using high-resolution remote sensing data were analyzed (Figure 4 and Table S3). The uncertainties of the reference data (median R^2 = 0.80, RMSE = 0.50, Figure 4 and Table 11) are significantly lower than those of the moderate-resolution products. In a few cases, the uncertainties of the reference data may be higher than those of the moderate-resolution LAI products (Z. Li, Tang, et al., 2014) because of the larger variability revealed by pixels of higher resolution. On the other hand, the relative errors of the reference data are approximately 13%, much higher than those for the moderate resolution LAI (~8%).

Table 11
Statistics of Reference Leaf Area Index Validation Results

All biomes	Statistics	Min	Median	Max	Biome types	Statistics	Min	Median	Max
Overall	R^2	0.39	0.8	0.97	Mixed biomes	R^2	0.92	0.92	0.92
	Bias	−0.18	0.014	0.4		RMSE	0.66	0.66	0.66
	RE (%)	−11.7	12.78	35.3	Grass	R^2	0.39	0.81	0.89
	RMSE	0.08	0.5	0.95		RMSE	0.08	0.35	0.5
	RRMSE (%)	2.1	22	37	Crops	R^2	0.49	0.787	0.97
Landsat	R^2	0.39	0.82	0.97		RMSE	0.22	0.55	0.83
	Bias	−0.18	0.029	0.4	Broadleaf forest	R^2	0.5	0.777	0.94
	RE (%)	−11.7	−0.045	17.56		RMSE	0.1	0.502	0.61
	RMSE	0.114	0.495	0.95	Needleleaf forest	R^2	0.45	0.734	0.93
	RRMSE (%)	20.2	24.89	26.82		RMSE	0.37	0.605	0.95

Note. Data from Table S3. RE = relative error; RMSE = root mean squared error; RRMSE = relative RMSE.

The overview of literature indicates that in early studies, the typical Landsat LAI reference map was within ±20% relative errors or within an absolute error smaller than 1.0 LAI for most biomes (Table S3). More recent studies indicate that $R^2 > 0.90$ and RMSE < 0.5 are attainable for crops (González-Sanpedro et al., 2008; J. Liu, Pattey, et al., 2012; Nigam et al., 2014; F. Vuolo et al., 2008) and forests (Kraus et al., 2009; Table S3). The accuracy error is generally <0.1 for crops (F. Gao et al., 2014; A. H. Li et al., 2013) and <0.2 for forests (Heiskanen et al., 2011; A. H. Li et al., 2013). Similar LAI uncertainty ranges have been reported in boreal forests (Duveiller et al., 2011; Heiskanen et al., 2011; Kraus et al., 2009). Having been the two main sources for generation of the reference LAI, Landsat and SPOT show similar predictive capability and can be combined to generate time series LAI (e.g., Heiskanen et al., 2011). Other high-resolution sensors such as Earth Observing-1 Advanced Land Imager, PROBA Compact High-Resolution Imaging Spectrometer, Advanced Spaceborne Thermal Emission and Reflection, and Huan Jing-1 (HJ-1) have shown the same uncertainty range (Table S3).

The uncertainties in the high-resolution reference data should ideally be smaller than those in the LAI products (Widlowski, 2015). In general, both field measurement and transfer function uncertainties need to be considered to improve the reference LAI accuracy (Ding et al., 2014; R. A. Fernandes et al., 2003; Garrigues, Lacaze, et al., 2008; A. H. Li et al., 2013). Prior to validation, it is important to examine the vegetation distribution within the pixel to check whether the field data are representative of the larger pixel (Fang, Wei, & Liang, 2012; Nikolov & Zeller, 2006). This can be realized by calculating the VI (e.g., NDVI) or reflectance variation from each of the high-resolution pixels within the larger moderate-resolution pixel (Fensholt et al., 2004; Iwata et al., 2013; Raymaekers et al., 2014; Y. Zeng et al., 2014). However, this method has been mostly used in low LAI areas because of the easy saturation of VI and reflectance in high LAI areas. As an alternative, geostatistical techniques have been effective in identifying spatially representative areas and mitigating the spatial mismatch between satellite pixels and reference data (Ding et al., 2014; Martinez et al., 2009, 2010). Using sampling schemes adapted to the spatial variability of the LAI (e.g., Validation of Land European Remote sensing Instruments) and by sampling sufficient numbers (>100) of ground measurements, the problem of scale differences in generating the reference data can be partly overcome (Nackaerts et al., 2000; Richter, Atzberger, et al., 2012).

It is noted that these uncertainties for the reference LAI represent general conditions and, therefore, cannot be used to describe the uncertainties at the pixel level. The pixel-level uncertainties can be estimated in a manner similar to the DA methods (Lewis et al., 2012; Pinty et al., 2011). In this case, the pixel-level precision uncertainties can be calculated as the differences between the LAI estimation and the multiyear mean value. The relative differences can also be computed to provide the relative errors for each pixel (Fang et al., 2007; Fang, Liang, Townshend, et al., 2008; Y. Gu et al., 2006; Xiao, Wang, et al., 2011). This topic should be an area for future development.

4.3. Recommendations

Existing sites already commissioned during previous validation studies need to be continued or reactivated to meet the validation requirement for the forthcoming sensors. CEOS LPV is compiling a list of core sites with long-term consistent observations and reference data staged at the On Line Validation Exercise

(http://calvalportal.ceos.org/web/olive/; Weiss et al., 2014). To help with the expansion of validation sites, the core sites should fully exploit current long-term and operational ecosystem networks, such as the Chinese Ecosystem Research Network (http://www.cern.ac.cn/), the Integrated Carbon Observation System (https://www.icos-ri.eu/), the Terrestrial Ecosystem Research Network (http://www.tern.org.au/), and the National Ecological Observatory Network (http://www.neoninc.org/). To assist the validation studies, other individual initiatives with proper metadata about the collection method, clump processing, woody component and understory consideration, and uncertainty calculation, should also be included (e.g., M. Ma, Che, et al., 2015; S. Wang et al., 2016). Field measurements need to be standardized in terms of field conditions, observation assumptions, and tools, to allow a rigorous evaluation and intercomparison of field data among the community (R. Fernandes et al., 2014). A clear distinction between the various LAI definitions (Table 1) is desirable in validation studies since most remote sensing products represent the true LAI (Table 4). Separate consideration of the overstory and understory LAI would enable more efficient validation of the storied LAI products (e.g., Y. Liu, Liu, et al., 2017) and the LiDAR-derived LAI vertical profiles (e.g., H. Tang et al., 2016). Over these sites, high-resolution reference data should be generated, using a standardized approach with traceable results and well-calibrated quality information.

The availability of field observations should be strongly fostered at the international level for underrepresented regions and seasons, when the potential improvements in LAI product quality are also large. Field LAI studies in the tropical and Arctic regions are critical for understanding the uncertainties and seasonal variation of LAI products (Doughty & Goulden, 2008; R. Myneni et al., 2007). However, field measurements are very scarce in these regions (Kalácska et al., 2004; Pfeifer et al., 2014; Verbyla, 2005), and product differences are large, primarily because of cloud and atmospheric effects (Fang, Jiang, et al., 2013). Sparsely vegetated areas in the arid and semiarid areas and savannas in ecological transition zones are also underrepresented (Fang, Jiang, et al., 2013; Gonsamo & Chen, 2014). More than 50% of the land surface has yearly LAI values <1.0 (F. Baret, Morissette, et al., 2006), with large relative errors and interannual variability (Fang, Jiang, et al., 2013). The relative RMSE target (15%) proposed by GCOS is influenced by the mean LAI values and may not reflect the overall uncertainty in low LAI regions. Therefore, further field measurement guidelines are warranted for these regions where the LAI values are sensitive to small changes in leaf cover over time.

Because of the ease of field work and satellite data availability, current field campaigns and validation studies are mainly conducted during the peak growing season (Fang, Jiang, et al., 2013; Heiskanen, Rautiainen, Stenberg, Mõttus, et al., 2012; Z. Wang et al., 2014). Nevertheless, the relative uncertainties are generally higher during the beginning and end of the growing season, when current validation studies are constrained (Camacho et al., 2013; Fang, Jiang, et al., 2013; Weiss et al., 2007). Continuous seasonal measurements and time series validation studies should be pursued, for example, by using high-frequency and automatic measurement tools (Baret et al., 2010; Qu, Zhu, et al., 2014; Ryu et al., 2012). With instrument improvement, more detailed measurement protocols need to be considered simultaneously to address the increasing demands for LAI validation studies.

Product validation is an ongoing process because of incremental improvements in the input data and the algorithms, new product releases, and product time series expansion. The ultimate goal is to achieve stage 4 validation, which requires systematic generation of real-time product quality information (Table A1). In reality, the validation of satellite products has lagged behind satellite product development. Many products have not been fully validated during their entire lifecycle (e.g., CYCLOPES and the global carbon project), before the next generation of satellite products become available. Similarly, the products generated from data synergy or temporal compositing are not fully validated, and their uncertainties are unspecified (Ganguly, Baret, et al., 2014). Extensive validation studies are warranted to ensure the quality and continuity for synergistic products and to fully characterize the potential error accumulation (Baret, Morissette, et al., 2006). Long-term LAI validation prior to 2000 is also limited by the scarcity of field data (J. Privette et al., 1998); direct validation has only been possible through comparison with field data extracted from the literature (Nikolov & Zeller, 2006; Scurlock et al., 2001). A practical solution is to conduct product intercomparison (Piao et al., 2015; Xiao et al., 2017) or make comparisons with climatic variables (Z. Zhu et al., 2013) and LSM simulations (Mao et al., 2013; Zaichun Zhu, Piao, et al., 2016).

More emphasis should be placed on the validation of LAI in future missions. With the increase in data sets from hectometric-resolution sensing systems, hectometric LAI products have been developed from MODIS

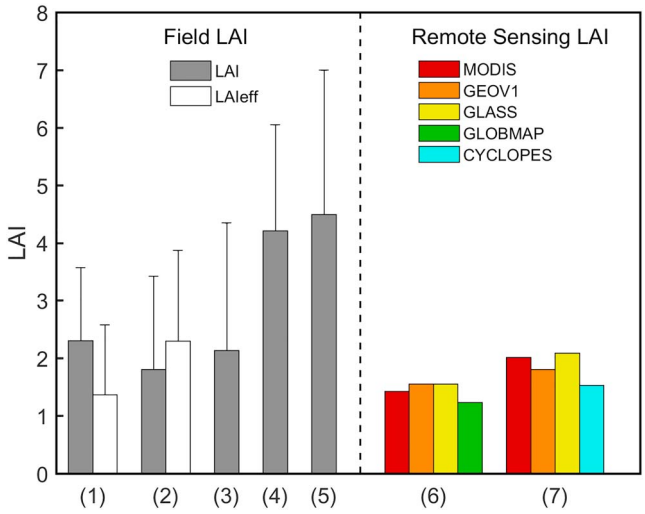

Figure 5. Global average LAI calculated from field and remote sensing data. The vertical bars show the standard deviation of the field data. (1) Table 3, Yan et al. (2016); (2) Table 1, Fang, Wei, & Liang (2012); (3) Table 2, Baret, Morissette, et al. (2006); (4) Table 2, Iio et al. (2014); (5) p. 202, Asner et al. (2003); (6) Table 3, Fang, Jiang, et al. (2013); and (7) Figure 4, for July, 2001, Yan et al. (2016). LAI = leaf area index; MODIS = Moderate Resolution Imaging Spectroradiometer; GEOV1 = Geoland2/BiopPar version 1; GLASS = Global Land Surface Satellite; GLOBMAP = The global mapping project; CYCLOPES = Carbon cYcle and Change in Land Observational Products from an Ensemble of Satellites.

(250 m), medium-resolution imaging spectrometer (300 m), MEdium Resolution Spectrum Imager (250 m), and PROBA-V (300 m; Table 7). At the hectometric resolution, direct comparison with ground measurements at spatially representative sites (scheme I, section 4.1.1) will become more realistic because of the similar scales between ESU samples and individual pixels (Gonsamo & Chen, 2014; Si et al., 2012). This may become even easier with the availability of frequent decametric resolution sensors, in which the pixel size is close to the size of the ground measurement. The availability of multiple decametric satellite sensors during the next decade will enable the generation of daily reference LAI based on its combination with calibrated transfer functions using continuous LAI measurements.

As a relatively new product, the spaceborne LiDAR product needs to be validated before it can be used to compare with the moderate-resolution LAI products. The LAI estimated from spaceborne LiDAR can be validated with field optical, TLS, and airborne LiDAR-derived LAI (Tang et al., 2014, 2016). The airborne LiDAR acts as a validation link between TLS and spaceborne data, and extensive work has been conducted to estimate LAI for forestry, exploiting the 3-D information obtained from airborne systems (Hyde et al., 2005; Ritchie, 1996). Methodologies based on LiDAR data sets have been developed to assess 3-D forest structures and for LAI estimates at the individual tree level with small footprint LiDAR (Alonzo et al., 2015). A few studies for nonforest vegetation types, such as wetland (Luo et al., 2015) and maize (Nie et al., 2016), have been performed, allowing full wall-to-wall validation using LiDAR data.

The traditional upscaling validation (scheme II, section 4.1.2) often treats the high-resolution LAI data as the reference truth and ignores the errors associated with the reference (R. Fernandes & Leblanc, 2005; Miralles et al., 2010). To fully calculate the output uncertainties, both product and reference uncertainties need to be considered (Miralles et al., 2010; Widlowski, 2015; Yu et al., 2012), with new methods such as the triple collocation method (Fang, Wei, Jiang, et al., 2012) and the Bayesian maximum entropy method (A. H. Li et al., 2013). Last but not least, the validation community need to communicate timely with users regarding the comprehensive quality of LAI products, not only for a range of vegetation types but also their spatial and temporal distributions.

5. LAI Applications

5.1. Global Vegetation Change

Field measurements show that the global average LAI values range from 1.98 (±1.61) to 2.31 (±1.26; Figure 5). The global remote sensing LAI products show a yearly average LAI of around 1.50, but the average LAI reaches around 2.0 during the peak growing season, which is comparable with the field data. Recently reported field LAI values are nearly half of those (4.5 ± 2.5) reported 16 years ago (Figure 5), mainly because of the significant number of high LAI values formerly collected in plantations (Asner et al., 2003).

5.1.1. LAI Phenology

A growing number of studies are using seasonal LAI products to investigate vegetation phenology in different regions (Che et al., 2014; Valderrama-Landeros et al., 2016; P. Zhang et al., 2004). For example, Valderrama-Landeros et al. (2016) built annual phenology maps from the CYCLOPES time series to assess deforestation in Mexico. Verger et al. (2016) derived the global baseline phenology from the LAI climatology estimated from 1-km SPOT-VEGETATION time series. The Spinning Enhanced Visible and InfraRed Imagery daily LAI is particularly useful for derivation of the growing season length, the asymmetric green-up and green-off length/rate, and the distinctive phenological features of cropland and natural vegetation (Guan et al., 2014). In general, the LAI becomes positive (LAI > 0) during the onset of greenness, and the seasonal maximum LAI may represent the time of maximum photosynthesis in the canopy (L. Y. Sun &

Table 12
Global Long-Term Remote Sensing LAI Trends During Different Time Periods

Region	Period	Product	LAI change	Source	Reference
Globe	2001–2017	MODIS C6	0.049 ± 0.023/10a[a] 0.060 ± 0.028/10a[b] 0.067 ± 0.034/10a[f] 0.040 ± 0.023/10a[g]	Figure 6	This study
Globe	2003–2011	GEOV1, MERIS, and MODIS C6	0.056 ± 0.010/10a[b]	Table 2	Jiang et al. (2017)
Globe	2002–2012	MODIS C6	−0.2 ± 0.4%/10a	Table 5	Alton (2018)
Globe	1982–2011	LAI3g, GLASS, GLOBMAP, and AVH15C1	0.053 ± 0.038/10a[b]	Table 2	Jiang et al. (2017)
Globe	1982–2009	LAI3g	6.93%[b]	Table 1	Mao et al. (2013)
Globe	1982–2014	LAI3g	0.032/a[c]	Figure S3	Zhu, Piao, et al. (2016)
Globe	1982–2011	LAI3g	0.038 ± 0.009/10a[a]	Figure S1a	Z. Zeng et al. (2018)
Globe	1982–2011	LAI3g	0.025 ± 0.0001/10a[a]	Figure 3	Forzieri et al. (2017)
Globe	1982–2011	LAI3g	8%[a]	Figure S1b	Z. Zeng et al. (2018)
Globe	1982–2009	LAI3g, GLASS, and GLOBMAP	0.068 ± 0.045/a[c]	Figure 1	Zhu, Piao, et al. (2016)
Globe	1982–2011	LAI3g, GLASS, GLOBMAP, and AVH15C1	(0.036,0.048, −0.008,0.048)/10a[a]	Figure 8	Xiao et al. (2017)
Globe	1999-2015	GEOV1	0.0275 ± 0.0235/a[a]	Figure 9	Munier et al. (2018)
30–75°N	1982–2011	LAI3g, GEOV1, and their average	0.143, 0.163, and 0.153[b]	Figure 1	Mao et al. (2016)
>30°N	1982–2009	Average of LAI3g, GLASS, and GLOBMAP	(0.03[e], 0.09[f], 0.05[g])/10a	Figure 1	Z. Zhu et al. (2017)
45–90°N	2002–2012	MODIS C6	2.7 ± 1.0%/10a	Table 5	Alton (2018)
China	1982–2009	LAI3g, GLASS, GLOBMAP, and their average	(0.035,0.127,0.048, 0.070)/10a[b]	Figure 2	Piao et al. (2015)

Note. See Tables 4 and 5 for products since 2000 and 1982, respectively. LAI = leaf area index; GLASS = Global Land Surface Satellite; GLOBMAP = The global mapping project; MERIS = MEdium-Resolution Imaging Spectrometer.
[a]Yearly average LAI. [b]Growing season (April–October) average LAI. [c]Growing season integrated LAI. [d]December-January-February (DJF). [e]March-April-May (MAM). [f]June-July-August (JJA). [g]September-October-November (SON).

Schulz, 2017). The start and end of the season can be identified using 30% and 40% thresholds, respectively, of the LAI amplitude values (Verger et al., 2016).

Validation of the LAI phenology can be performed through comparison with ground observations, high-resolution reference data, intercomparison with data derived from VIs, and comparison with the variation in climatic variables (Che et al., 2014; Valderrama-Landeros et al., 2016; Verger et al., 2016). A number of studies have reported that LAI is physically more meaningful and the derived phenological metrics are more accurate than those derived using the VI method (Verger et al., 2016; C. Wang, Li, et al., 2017; P. Zhang et al., 2004). Moderate-resolution LAI products are advantageous for global phenology studies because of their higher revisit cycles. With the availability of multiple high-resolutions satellite sensors, an increasing number of phenology studies are starting to use the high-resolution time series images, especially at local scales (El Hajj et al., 2009; Melaas et al., 2013; Senf et al., 2017; Zhe Zhu, Fu, et al., 2016). To appropriately use LAI in phenology studies, the original LAI curves need to be temporally filtered (section 3.3); differences in LAI data sets also need to be considered.

5.1.2. LAI and Climate Change

Global long-term satellite LAI products generally show positive values over a large proportion of vegetated areas since 1982 (Table 12). The global average growing season (April–October) LAI increased at a rate of about 0.060 ± 0.028 per decade from 2001 to 2017 (Figure 6 and Table 12). The greening trend in Eurasia is more obvious than that in North America (Kai Yan et al., 2016). The amplitude of greening in China is about 24% higher than the global value (0.070 per decade vs. 0.053 per decade; Jiang et al., 2017; Piao et al., 2015). The greening trend is largely explained by the climate change, CO_2 fertilization, atmospheric nitrogen deposition, and longer high-latitude growing seasons (Piao et al., 2015; Zaichun Zhu, Piao, et al., 2016). Differences exist among the LAI products in calculating the interannual variability and long-term trend, especially at regional scales (Fang, Jiang, et al., 2013; Jiang et al., 2017; Piao et al., 2015). Differences also exist in the predicted LAI using various process models (Mahowald et al., 2016). Long-term trends would be more convincing when remote sensing data agree with and model predictions (Mao et al., 2013; Piao et al., 2015).

Over a longer term, the global LAI has gradually increased since 1850, which is consistent with the change in global temperature (L. Chen & Dirmeyer, 2016; Lawrence et al., 2012). Lawrence et al. (2012) reported that

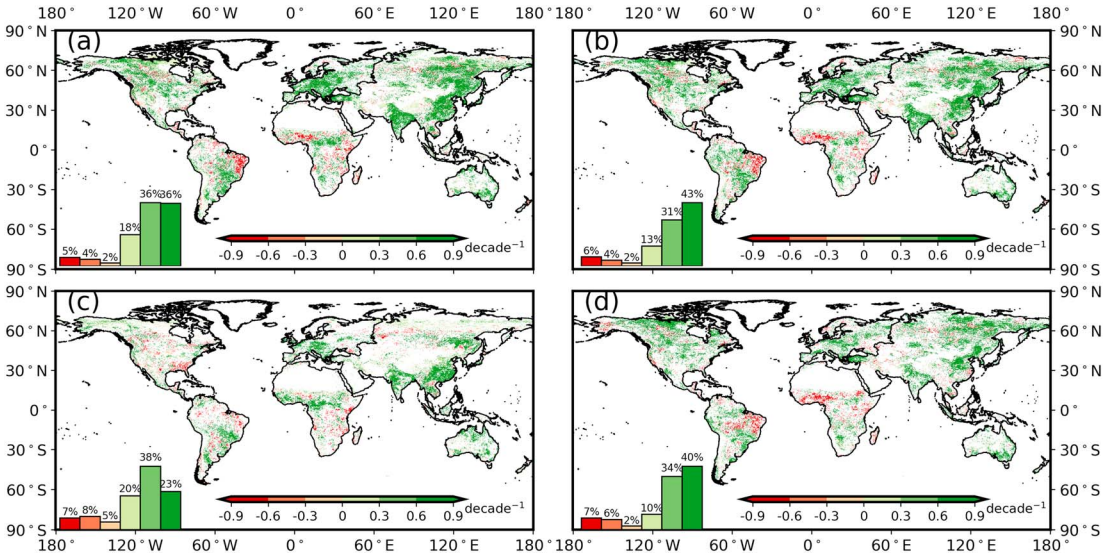

Figure 6. Maps of the linear trend of global leaf area index calculated from Moderate Resolution Imaging Spectroradiometer (MCD15A2H, C6; 2001–2017). (a) Yearly average, (b) growing season (April–October), (c) December-January-February, and (d) June-July-August. The histrogram shows the percentage of pixels for different category of changes. Pixels with $p \geq 0.1$ were excluded.

the global LAI has increased by about 0.11 compared to the preindustrial period (Table 13). The increasing LAI is partly mediated by anthropogenic land use and land cover change as a result of agricultural expansion and wood harvest. The negative effect of land use and land cover change is relatively small (–0.04) at the global scale (Lawrence et al., 2012), but it caused a 10% LAI decrease in Eurasia, north and south America, and southeast Asia (Boisier et al., 2014; L. Chen & Dirmeyer, 2016). The variations in LAI are more strongly affected by temperature changes at high latitudes. However, in tropical areas, these variations are more strongly influenced by moisture levels (Anav, Friedlingstein, et al., 2013; Anav, Murray-Tortarolo, et al., 2013; Forkel et al., 2014; Mahowald et al., 2016).

The global mean LAI is projected to increase in the 21st century under future climate change scenarios (Mahowald et al., 2016). Regional LAI varies under the impact of different environmental drivers (Lin et al., 2016; Mao et al., 2013; Tesemma et al., 2014). The increases in LAI are largest in midlatitude regions (~0.35), high-latitude regions, mountainous regions (e.g., Tibetan plateau), and the tropics (Mahowald et al., 2016). The increasing CO2 will decrease LAI in some areas, probably as a result of increased droughts (Duursma et al., 2016; Mao et al., 2013). In Australia, the mean annual LAI is projected to decrease as a result of decreasing precipitation (Tesemma et al., 2014).

Table 13
Centennial Change of LAI Reconstructed From Different Models

Region	Period	Model[a]	Climate	LAI change	Source	Reference
Globe	(1976–2005) to (1850–1879)	CCSM 4.0	Historical (1850–2005)	–0.04 (LULCC), 0.11 (climate + LULCC)	Table 6	Lawrence et al. (2012)
Eurasia, N. America, S. America, and SE Asia	1870–1992	Six AGCM/LSMs	LULCC	–10%	Figures 2 and 3	Boisier et al. (2014)
Globe	(2081–2100) to (1981–2000)	18 CMIP5 ESMs	RCP scenarios	0.16 (tropics), 0.35 (midlatitude), and 0.31 (high latitude)	Table 4	Mahowald et al. (2016)
Australia	2011–2100	CMIP5 GCM	RCP scenarios	–10% to –38% (crops), –5% to –24% (pasture), –2% to –11% (trees)	Table 3	Tesemma et al. (2014)

Note. AGCM = Atmospheric Global Circulation Model; CCSM = Community Climate System Model; CMIP5 = Coupled Model Intercomparison Project phase 5; ESMs = earth system models; GCM = global circulation models; LSMs = land surface models; LULCC = land use and land cover change; RCP = representative concentration pathways; LAI = leaf area index.
[a]See references in the last column for more details about the models.

LAI also presents an important feedback to climate change. Increasing LAI will decrease surface albedo and air temperature for snow-free regions, increase canopy ET, and decrease ground evaporation over tropical regions (Y. Tian, Dickinson, Zhou, & Shaikh, 2004; van den Hurk et al., 2003). Terrestrial carbon fluxes are strongly affected by changes in LAI, especially for the plant functional types that have high interannual variabilities (Kala et al., 2014). Global modeling studies have showed that the increased global LAI leads to an increase of 11.4 mm/year in the land ET, which accounts for more than 50% of the observed increase in the land ET over the last 30 years (Z. Z. Zeng et al., 2016).

5.2. Application in LSMs

Integration of remote sensing LAI products with LSMs has significantly improved the simulation of energy absorption, transpiration and interception, and ecosystem productivity prediction at seasonal and interannual time scales (Boussetta et al., 2015; Buermann et al., 2001; Guillevic et al., 2002; Jarlan et al., 2008). LAI is integrated with LSM through a simple direct forcing mode or a more sophisticated DA mode.

5.2.1. LAI in the Forcing Mode

In the direct forcing mode, LSM uses remote sensing LAI as initial conditions or input data to force the model to run in a more realistic way (M. Chen et al., 2015; Ge et al., 2008; Kala et al., 2014; Moore et al., 2010). In these models, LAI acts as the bridge to upscale the rate of leaf biophysical and biogeochemical processes, for example, leaf photosynthesis and stomatal conductance, to the canopy level (Mu et al., 2007; Niu et al., 2011; H. Yan et al., 2012). The canopy water storage capacity is calculated as a linear function of LAI (Bastiaanssen et al., 2012; Cui & Jia, 2014; van Dijk & Bruijnzeel, 2001). In a similar fashion, satellite-derived LAI data are directly used to calculate the canopy conductance (Cleugh et al., 2007; Mu et al., 2007; H. Yan et al., 2012). The MODIS LAI monthly climatology has improved simulation studies in land surface modeling (Boussetta et al., 2013; Jarlan et al., 2008; Weiss et al., 2012) and regional and global numerical weather predictions (Boussetta et al., 2013; Ge et al., 2008; Knote et al., 2009).

In the modeling of gross primary productivity (GPP), LAI is generally used to calculate the FPAR and the mean photosynthetically active radiation (PAR) incident on leaves to drive the canopy-level photosynthesis (Running et al., 2004; Y. Zhou et al., 2017):

$$\begin{aligned} \mathrm{GPP} &= \mathrm{FPAR}\times\mathrm{PAR}\times\mathrm{LUE}, \\ \mathrm{FPAR} &= e^{-k\cdot LAI}, \end{aligned} \tag{14}$$

where LUE is the light use efficiency and k is the light extinction coefficient. This equation is also used to calculate the incoming solar radiation and the below canopy PAR, which attenuates exponentially with LAI (Carrer et al., 2013). Alton (2016) found that GPP modeling is more sensitive to the LAI forcing (10–20% change) than to the land cover classification and the spatial resolution of simulation (<10%). In a similar study in Australia, Kala et al. (2014) found that changes in LAI more strongly affected the carbon fluxes than the sensible and latent heat fluxes, especially for croplands.

Some LSMs parameterize vegetation using a simple seasonally invariant LAI (G. B. Bonan, Levis, et al., 2002; Ford & Quiring, 2013; Sellers et al., 1986). However, the static LAI parameter tends to overestimate LAI and soil moisture during anomalously dry seasons (Ford & Quiring, 2013; Tesemma et al., 2015). Simulations with seasonally varying LAI represent a more realistic climatology and are recommended for LSM simulations (S. Boussetta et al., 2013; Ford & Quiring, 2013; A. Loew et al., 2014). It is noted that the LAI climatology created for each grid cell is different from the prescribed LAI for each plant functional type (Bonan, Levis, et al., 2002; Sellers et al., 1986). Moreover, LAI is generally defined for the vegetated fraction in LSMs, whereas the satellite LAI is defined for the whole pixel, including both vegetated and nonvegetated fractions (Bonan, Oleson, et al., 2002; Niu et al., 2011; X. Zeng et al., 2002).

5.2.2. LAI in the Assimilation Mode

Many studies have shown that DA of LAI improved the estimation of vegetation dynamics, water, energy, and chemical simulations (Table S4). The DA process constrains the model simulations with observations to improve estimation of the state variables. Generally, an optimal constraint is built upon the estimated measurement and model forecast errors through a sequential or a variational assimilation approach. The sequential assimilation constrains the model state to observations by a variance minimizing estimator, for example, an ensemble Kalman filter, and updates the model variable (e.g., LAI) each time a remote

Table 14
Examples of Setting LAI Uncertainties in Dynamic Process Models

Methods	LAI uncertainties	References
(a) Pixel-based		
	0.1–1.2	Boussetta et al. (2015)
(b) Percentage		
	10%	Boussetta et al. (2015), Curnel et al. (2011), and Viskari et al. (2015)
	13%	Xie, Wang, Bai, et al. (2017)
	20%	Jarlan et al. (2008), Rüdiger et al. (2010), Dewaele et al. (2017), and Albergel et al. (2017)
(c) Incremental values		
	0.2, 0.4, and 0.6 for LAI < 1, 2, and 3	Barbu et al. (2011) and Pauwels et al. (2007)
	0.01–0.40 and 0.4 for LAI < 2% and 20% otherwise (modeled LAI)	Nearing et al. (2012) Albergel et al. (2017)
(d) Constant value		
	0.3 for GEOV1	Barbu et al. (2013)
	1.0	Barbu et al. (2011) and Sabater et al. (2008)

Note. LAI = leaf area index.

sensing observation is available. A number of studies have proven the potential of ensemble Kalman filter assimilating LAI observations to correct the LSM states (Albergel et al., 2010; Pauwels et al., 2007; Rüdiger et al., 2010; Revill et al., 2013). Vazifedoust et al. (2009) showed that the assimilation of MODIS LAI results in better ET and crop yield forecasts at a regional level. The variational assimilation approach seeks an optimal fit between remote sensing and model estimates by adjusting the initial conditions or model parameters. The cost function is built by a maximum-likelihood estimator that calculates the distance of the model state to the observations and background. Boussetta et al. (2015) demonstrated the potential of assimilating the GEOV1 LAI into a LSM to improve the monitoring of extreme climate.

The underlying hypotheses of the DA studies are that the remote sensing LAI has greater accuracy than the simulated ones or that the LAI uncertainties can be properly quantified (Jongschaap, 2006). Because of the continuity of model simulation, intermittent remote sensing observations need to be processed (section 3.3) to match the model simulation dates (Jarlan et al., 2008; Pauwels et al., 2007; Rüdiger et al., 2010). Some DA studies have successfully coupled microwave radar and optical remote sensing data (Betbeder et al., 2016; Clevers & van leeuwen, 1996; Dente et al., 2008). Various ways to combine LAI with other variables, such as surface soil moisture (Albergel et al., 2010; Y. Xie, Wang, Sun, et al., 2017) and ET (Vazifedoust et al., 2009), have been proven to be successful in regional applications.

5.2.3. Configuration of LAI Uncertainties

Proper configuration of LAI uncertainties is critical because errors in LAI products could potentially propagate into the modeling processes (W. Buermann et al., 2001; Chase et al., 1996; van den Hurk et al., 2003). Various configurations of LAI uncertainties have been applied in LSMs (Table 14). LAI uncertainties are either assigned as constant values or using different uncertainties for different LAI values. More frequently, the LAI uncertainties are set as an empirical percentage (10–20%) of the LAI values (Fox et al., 2009; Jarlan et al., 2008; Rüdiger et al., 2010). The empirical quality settings in Table 14 are very similar to the LAI quality ranges reported in the literature (Table 10). In contrast to the overall uncertainty assignments, pixel-specific LAI uncertainties are expected to improve the model performance when the products are assimilated into climate and ecosystem models (Rüdiger et al., 2010). While LAI validation outputs have been recognized and exploited by the modeling community, a better representation of LAI uncertainty in LSMs is still desirable from the science user perspective. There is a clear disconnect between validation outputs and model settings, attributable mainly to the immature LAI validation stages (currently only stage 2) and insufficient quality information.

5.3. Agricultural Applications

Remote sensing LAI data have been widely applied in agriculture to assist the crop yield estimation (de Wit et al., 2012; Dente et al., 2008; Doraiswamy et al., 2005). Regression models have been developed to estimate crop yield from remote sensing LAI (Baez-Gonzalez et al., 2005; Y.-P. Wang et al., 2010; P. Zhang, Anderson,

et al., 2005). For example, Zhang, Anderson, et al. (2005) used the growing season MODIS LAI to estimate crop production at local, regional, and national levelss. Some studies indicate that GAI is more practical than LAI for crop yield estimation (N. Guindin-Garcia, 2010; Kouadio et al., 2012; Sakamoto et al., 2013). Under extreme weather conditions, the relationship between yield and LAI may not be adequate, and other agro-meteorological data, for example, temperature, reference ET, and radiation, need to be included in the prediction model.

More sophisticated methods integrate LAI with a crop simulation model (CSM) using the DA method to assist crop yield modeling and irrigation management. X. L. Jin et al. (2018) provided a recent review of crop models, remote sensing technology, and DA methods. Different DA methods to use LAI in CSMs, of various degrees of complexity and integration, have been proposed (Baret et al., 2000; Delécolle et al., 1992; Moulin et al., 1998). These methods are generally similar to those applied in the LSM (section 5.2) and include using remote sensing LAI directly in the CSM and updating, reinitializing and recalibrating CSMs based on LAI observations. A suite of crop growth models, for example, Decision Support System for Agrotechnology Transfer and WOrld FOod STudies, have been explored to improve simulations of land surface variables (Table S4). Jégo et al. (2012) reported that the crop model errors can be reduced by up to 20% if a variational assimilation approach was used.

Coupling satellite data with crop models remains challenging because of the low spatial resolution of satellite data and the traditionally point-based crop models. A practical DA protocol should be constructed using state-of-the-art remote sensing data for regional crop monitoring and yield estimation. Such a protocol would require good quality LAI data with a high temporal and spatial resolution and a wide geographic coverage (Pauwels et al., 2007). More thorough studies are needed to support agricultural decision making using LAI data.

5.4. General Guidelines

LAI has been increasingly applied in a number of new areas such as global land cover mapping (Xiao, Wang, et al., 2016), biodiversity tracking (Skidmore et al., 2015), forest management (J. Wang, Wang, et al., 2017), and urban landscaping (Chianucci, Puletti, et al., 2015). For all applications, it is important for users to understand the strengths and weaknesses of the product they are using. LAI validation studies (section 4) supply crucial information for process model evaluation and projection studies. Products with stage 2 to 4 validation can be used by the user community; however, provisional products require further refinement and validation and should be used with caution (Table A1). While many efforts have been made to evaluate a product based on its uncertainty, a more pertinent consideration for users would be whether or not the product is appropriate for its intended purpose. It is critical for the user community to understand the limitations of the product and provide feedback on the discrepancies between LAIs from the model and satellite data (Randerson et al., 2009). The most successful mechanism for this would be to involve the user community in the product development cycle.

6. Summary

LAI is a critical vegetation structural variable that is essential in the feedback of vegetation to the climate system. This paper provides a comprehensive overview of LAI field measurement and remote sensing estimation methods, product validations and uncertainties, and LAI application cases. In addition to the traditional direct and indirect methods, new cost-effective tools need to be investigated for long-term automatic field LAI measurements. Current moderate- and high-resolution satellite observation systems need to be continued with support from CEOS and space agencies. Further development of canopy reflectance models need to contain efficient modeling framework and accurate parameterization and be made publically available. Future LAI retrieval needs to capitalize new development in canopy reflectance models and new computing technologies (e.g., machine learning algorithms) and platforms. A new generation of analysis-ready products is expected to provide user-defined spatial and temporal resolutions with greater accuracy. The usage of LiDAR is expected to increase with the capability to provide the LAI vertical profile.

A summary of uncertainties of global LAI products show that the products are suitable for global vegetation change, land surface processes, agricultural production, and climatic studies. Further improvements can be made by enhancing the input information, canopy models, retrieval algorithms, and ancillary data.

Coordinated efforts of international agencies are required to establish long-term consistent validation networks enabling a comprehensive validation of the global products for current and future missions. Timely, accurate, and traceable product uncertainty information should be made regularly available to product users (stage 4 validation). Data producers and users need to communicate routinely to better understand the products and broaden their applications in various disciplines.

Appendix A: The CEOS WGCV Land Product Validation Hierarchy

The Committee on Earth Observation Satellites (CEOS) Working Group on Calibration and Validation (WGCV) Land Product Validation (LPV) subgroup has identified four validation levels for land products (Table A1).

Table A1
The Four Validation Stages Adopted by the Committee on Earth Observation Satellites Working Group on Calibration and Validation Land Product Validation subgroup (http://lpvs.gsfc.nasa.gov/)

Stage 1	Product accuracy is assessed from a small (typically <30) set of locations and time periods by comparison with in situ or other suitable reference data.
Stage 2	Product accuracy is estimated over a significant set of locations and time periods by comparison with reference in situ or other suitable reference data. Spatial and temporal consistency of the product and with similar products has been evaluated over globally representative locations and time periods. Results are published in the peer-reviewed literature.
Stage 3	Uncertainties in the product and its associated structure are well quantified from comparison with reference in situ or other suitable reference data. Uncertainties are characterized in a statistically rigorous way over multiple locations and time periods representing global conditions. Spatial and temporal consistency of the product and with similar products has been evaluated over globally representative locations and periods. Results are published in the peer-reviewed literature.
Stage 4	Validation results for stage 3 are systematically updated when new product versions are released and as the time series expands.

Note. The four stages correspond to the increasing spatial and temporal representativeness of samples used to perform direct validation (R. Fernandes et al., 2014).

Appendix B
Symbols and acronyms used in the paper.

3-D	Three dimension
α	Woody-to-total area ratio
A_j	The jth above canopy reading
B_j	The jth below canopy reading
γ_E	Needle-to-shoot area ratio
C_{ab}	Leaf chlorophyll content
$F_m(0, \theta)$	Measured accumulated gap fraction
$F_{mr}(0, \theta)$	Measured accumulated gap fraction excluding nonrandom large gaps
$f(\theta_L)$	Leaf inclination distribution function
G	Leaf projection function
θ	Solar zenith angle
θ_L	Leaf inclination angle
k	Light extinction coefficient.
P	Canopy gap fraction
P_o	Average light transmittance
σ	Radar backscattered signal
Ω	Clumping index
Ω_E	Element clumping index
AccuPAR	A PAR sensor
AVHRR	Advanced Very High-Resolution Radiometer
CC	The Chen and Cihlar (1995) method CEOS Committee on Earth Observation Satellites
CI	Clumping index
CLX	The combined CC and LX method
CYCLOPES	Carbon cYcle and Change in Land Observational Products from an Ensemble of Satellites

DA	Data assimilation
DBH	Diameter at breast height
DCP	Digital cover photography
DHP	Digital hemispherical photography
ECOCLIMAP	A database of land surface parameter
ESU	Elementary sampling unit
ET	Evapotranspiration
FPAR	Fraction of absorbed photosynthetically active radiation
GA-TIP	Global Albedo Two Stream Inversion
GAI	Green area index
GCOS	Globe Climate Observing System
GEOV1/2	Geoland2/BiopPar version 1/2
GLAI	Green LAI
GPP	Gross primary productivity
HJ-1	China's Huan Jing-1 satellite
IKONOS	A high-resolution satellite
JRC-TIP	Joint Research Center Two Stream Inversion Package
LAI	Leaf area index
LAI_{eff}	Effective LAI
LAI_{shade}	Shaded LAI
LAI_{sun}	Sunlit LAI
LiDAR	Light Detection and Ranging
LPV	Land Product Validation
LSM	Land surface model
LUT	Look-up table
LX	The Lang and Xiang (1986) method
MODIS	Moderate Resolution Imaging Spectroradiometer
NDVI	Normalized difference vegetation index
NIR	Near infrared
NN	Neural network
NOAA	National Oceanic and Atmospheric Administration
PAI	Plant area index
PAI_{eff}	Effective PAI
PAR	Photosynthetically active radiation
PROBA	Project for On-Board Autonomy
PROSAIL	A PROSPECT+SAIL model
PROSPECT	A leaf optical radiative transfer model
QQI	Quantitative quality indicator
RMSE	Root mean squared error
SAI	Stem area index
SLA	Specific leaf area
TLS	Terrestrial laser scanner
TRAC	Tracing Radiation and Architecture of Canopies
UAV	Unmanned aerial vehicle
VEGETATION	The medium resolution sensor aboard SPOT
VI	Vegetation index
WAI	Woody area index

Acknowledgments
The study was performed under the framework of CEOS LPV (http://lpvs.gsfc.nasa.gov/). H. F. was mainly supported by the Hundred Talent Program of the Chinese Academy of Sciences, the National Natural Science Foundation of China (41471295 and 41171333), and the National Key Research and Development Program of China (2016YFA0600201). The authors are thankful for C. Jiang, Y. Wang, S. Wei, and Y. Ye (CAS) who helped prepare the figures, and R. Fernandes (CCRS) and M. Román (NASA) who helped read an earlier draft of the manuscript. We thank the web teams who facilitated the distribution of the global LAI products.

References

Adiku, S. G. K., Reichstein, M., Lohila, A., Dinh, N. Q., Aurela, M., Laurila, T., et al. (2006). PIXGRO: A model for simulating the ecosystem CO_2 exchange and growth of spring barley. *Ecological Modeling*, *190*(3-4), 260–276. https://doi.org/10.1016/j.ecolmodel.2005.04.024

Akitsu, T., Nasahara, K., Kobayashi, H., Saigusa, N., Hayashi, M., Nakaji, T., et al. (2015). JAXA super sites 500: Large-scale ecological monitoring sites for satellite validation in Japan. Paper presented at the IGARSS 2015, Milan, Italy. https://doi.org/10.1109/IGARSS.2015.7326668

Albergel, C., Calvet, J. C., Mahfouf, J. F., Rüdiger, C., Barbu, A. L., Lafont, S., et al. (2010). Monitoring of water and carbon fluxes using a land data assimilation system: A case study for southwestern France. *Hydrology and Earth System Sciences*, *14*(6), 1109–1124. https://doi.org/10.5194/hess-14-1109-2010

Albergel, C., Munier, S., Leroux, D. J., Dewaele, H., Fairbairn, D., Barbu, A. L., et al. (2017). Sequential assimilation of satellite-derived vegetation and soil moisture products using SURFEX_v8.0: LDAS-Monde assessment over the Euro-Mediterranean area. *Geoscientific Model Development*, *10*(10), 3889–3912. https://doi.org/10.5194/gmd-10-3889-2017

Ali, A. M., Darvishzadeh, R., & Skidmore, A. K. (2017). Retrieval of specific leaf area from Landsat-8 surface reflectance data using statistical and physical models. *IEEE Journal of Selected Topics in Applied Earth Observations and Remote Sensing*, *10*(8), 3529–3536. https://doi.org/10.1109/JSTARS.2017.2690623

Alonzo, M., Bookhagen, B., McFadden, J. P., Sun, A., & Roberts, D. A. (2015). Mapping urban forest leaf area index with airborne lidar using penetration metrics and allometry. *Remote Sensing of Environment*, *162*(0), 141–153. https://doi.org/10.1016/j.rse.2015.02.025

Alton, P. B. (2016). The sensitivity of models of gross primary productivity to meteorological and leaf area forcing: A comparison between a Penman-Monteith ecophysiological approach and the MODIS Light-Use Efficiency algorithm. *Agricultural and Forest Meteorology*, *218*, 11–24. https://doi.org/10.1016/j.agrformet.2015.11.010

Alton, P. B. (2018). Decadal trends in photosynthetic capacity and leaf area index inferred from satellite remote sensing for global vegetation types. *Agricultural and Forest Meteorology*, *250-251*, 361–375. https://doi.org/10.1016/j.agrformet.2017.11.020

Anav, A., Friedlingstein, P., Kidston, M., Bopp, L., Ciais, P., Cox, P., et al. (2013). Evaluating the land and ocean components of the global carbon cycle in the CMIP5 Earth system models. *Journal of Climate*, *26*(18), 6801–6843. https://doi.org/10.1175/jcli-d-12-00417.1

Anav, A., Murray-Tortarolo, G., Friedlingstein, P., Sitch, S., Piao, S., & Zhu, Z. (2013). Evaluation of land surface models in reproducing satellite derived leaf area index over the high-latitude Northern Hemisphere. Part II: Earth system models. *Remote Sensing*, *5*(8), 3637–3661.

Aragão, L. E. O. C., Shimabukuro, Y. E., Espirito Santo, F. D. B., & Williams, M. (2005). Spatial validation of collection 4 MODIS LAI product in eastern Amazonia. *IEEE Transactions on Geoscience and Remote Sensing*, *43*(11), 2526–2534. https://doi.org/10.1109/TGRS.2005.856632

Arora, V. (2002). Modeling vegetation as a dynamic component in soil-vegetation-atmosphere transfer schemes and hydrological models. *Reviews of Geophysics*, *40*(2), 1006. https://doi.org/10.1029/2001RG000103

Asner, G. P., Braswell, B. H., Schimel, D. S., & Wessman, C. A. (1998). Ecological research needs from multiangle remote sensing data. *Remote Sensing of Environment*, *63*(2), 155–165. https://doi.org/10.1016/S0034-4257(97)00139-9

Asner, G. P., Scurlock, J. M. O., & Hicke, J. A. (2003). Global synthesis of leaf area index observations: Implications for ecological and remote sensing studies. *Global Ecology and Biogeography*, *12*, 191–205.

Asner, G. P., Wessman, C. A., & Archer, S. (1998). Scale dependence of absorption of photosynthetically active radiation in terrestrial ecosystems. *Ecological Applications*, *8*, 1003–1021.

Atkinson, P. M., Jeganathan, C., Dash, J., & Atzberger, C. (2012). Inter-comparison of four models for smoothing satellite sensor time-series data to estimate vegetation phenology. *Remote Sensing of Environment*, *123*, 400–417. https://doi.org/10.1016/j.rse.2012.04.001

Atzberger, C., & Richter, K. (2012). Spatially constrained inversion of radiative transfer models for improved LAI mapping from future Sentinel-2 imagery. *Remote Sensing of Environment*, *120*, 208–218. https://doi.org/10.1016/j.rse.2011.10.035

Bach, H., Schneider, K., Verhoef, W., Stolz, R., Mauser, W., Leeuwen, H., et al. (2001). Retrieval of geo- and biophysical information from remote sensing through advanced combination of a land surface process model with inversion techniques in the optical and microwave spectral range. Paper presented at the 8th International Symposium Physical Measurements & Signatures in Remote Sensing, Centre Paul Langevin, Aussois, France.

Bacour, C., Jacquemoud, S., Leroy, M., Hautecoeur, O., Weiss, M., Prévot, L., et al. (2002). Reliability of the estimation of vegetation characteristics by inversion of three canopy reflectance models on airborne POLDER data. *Agronomie*, *22*(6), 555–565. https://doi.org/10.1051/agro:2002039

Bacour, C., Weiss, M., Pavageau, K., Baret, F., & Béal, D. (2006). Neural network estimation of LAI, fAPAR, fCover and LAIxCab, from top of canopy MERIS reflectance data: Principles and validation. *Remote Sensing of Environment*, *105*(4), 313–325.

Baez-Gonzalez, A. D., Kiniry, J. R., Maas, S. J., Tiscareno, M. L., Macias, C. J., Mendoza, J. L., et al. (2005). Large-area maize yield forecasting using leaf area index based yield model. *Agronomy Journal*, *97*(2), 418–425. https://doi.org/10.2134/agronj2005.0418

Baker, E. H., Painter, T. H., Schneider, D., Meddens, A. J. H., Hicke, J. A., & Molotch, N. P. (2017). Quantifying insect-related forest mortality with the remote sensing of snow. *Remote Sensing of Environment*, *188*, 26–36. https://doi.org/10.1016/j.rse.2016.11.001

Banskota, A., Wynne, R., Thomas, V., Serbin, S., Kayastha, N., Gastellu-Etchegorry, J., & Townsend, P. (2013). Investigating the utility of wavelet transforms for inverting a 3-D radiative transfer model using hyperspectral data to retrieve forest LAI. *Remote Sensing*, *5*(6), 2639–2659.

Bao, Y., Gao, Y., Lü, S., Wang, Q., Zhang, S., Xu, J., et al. (2014). Evaluation of CMIP5 earth system models in reproducing leaf area index and vegetation cover over the Tibetan Plateau. *Journal of Meteorological Research*, *28*(6), 1041–1060. https://doi.org/10.1007/s13351-014-4023-5

Barbu, A. L., Calvet, J. C., Mahfouf, J. F., Albergel, C., & Lafont, S. (2011). Assimilation of soil wetness index and leaf area index into the ISBA-A-gs land surface model: Grassland case study. *Biogeosciences*, *8*(7), 1971–1986. https://doi.org/10.5194/bg-8-1971-2011

Barbu, A. L., Calvet, J. C., Mahfouf, J. F., & Lafont, S. (2013). Integrating ASCAT surface soil moisture and GEOV1 leaf area index into the SURFEX modelling platform: A land data assimilation application over France. *Hydrology and Earth System Sciences Discussions*, *10*(7), 9057–9103. https://doi.org/10.5194/hessd-10-9057-2013

Barclay, H. J., & Goodman, D. (2000). Conversion of total to projected leaf area index in conifers. *Canadian Journal of Botany*, *78*(4), 447–454.

Baret, F. (2015). Canopy biophysical variables retrieval from the inversion of reflectance models. In P. S. Thenkabail (Ed.), *Land resources monitoring, modeling, and mapping with remote sensing* (1st ed., Vol. 2, pp. 23–46). Boca Raton, FL: CRC Press.

Baret, F., & Buis, S. (2008). Estimating canopy characteristics from remote sensing observations: Review of methods and associated problems. In S. Liang (Ed.), *Advances in land remote sensing: System, modeling, inversion and application* (pp. 173–201). New York: Springer.

Baret, F., de Solan, B., Lopez-Lozano, R., Ma, K., & Weiss, M. (2010). GAI estimates of row crops from downward looking digital photos taken perpendicular to rows at 57.5° zenith angle: Theoretical considerations based on 3D architecture models and application to wheat crops. *Agricultural and Forest Meteorology*, *150*(11), 1393–1401. https://doi.org/10.1016/j.agrformet.2010.04.011

Baret, F., Hagolle, O., Geiger, B., Bicheron, P., Miras, B., Huc, M., et al. (2007). LAI, fPAR, and fCover CYCLOPES global products derived from VEGETATION part 1: Principles of the algorithm. *Remote Sensing of Environment*, *110*(3), 275–286. https://doi.org/10.1016/j.rse.2007.02.018

Baret, F., Morissette, J., Fernandes, R., Champeaux, J. L., Myneni, R., Chen, J., et al. (2006). Evaluation of the representativeness of networks of sites for the global validation and intercomparison of land biophysical products: Proposition of the CEOS-BELMANIP. *IEEE Transactions on Geoscience and Remote Sensing*, *44*(7), 1794–1803. https://doi.org/10.1109/TGRS.2006.876030

Baret, F., Pavageau, K., Béal, D., Weiss, M., Berthelot, B., & Regner, P. (2006). Algorithm theoretical basis document for MERIS Top of Atmosphere Land Products (TOA_VEG), Version 3 (Contract ESA AO/1-4233/02/I-LG). Retrieved from http://www.brockmann-consult.de/beam/software/plugins/toaveg-1.1.0/MERIS_ATBD_TOA_VEG_03_06.pdf

Baret, F., Weiss, M., Lacaze, R., Camacho, F., Makhmara, H., Pacholcyzk, P., & Smets, B. (2013). GEOV1: LAI, FAPAR essential climate variables and FCOVER global time series capitalizing over existing products. Part1: Principles of development and production. *Remote Sensing of Environment*, *137*, 399–309. https://doi.org/10.1016/j.rse.2012.12.027

Baret, F., Weiss, M., Troufleau, D., Prevot, L., & Combal, B. (2000). Maximum information exploitation for canopy characterisation by remote sensing. *Aspects of Applied Biology*, *60*, 71–82.

Baret, F., Weiss, M., Verger, A., & Smets, B. (2016). ATBD for LAI, FAPAR and FCOVER From PROBA-V Products at 300M Resolution (GEOV3) (IMAGINES_RP2.1_ATBD-LAI300M). Retrieved from http://fp7-imagines.eu/pages/documents.php

Barr, A. G., Black, T. A., Hogg, E. H., Kljun, N., Morgenstern, K., & Nesic, Z. (2004). Inter-annual variability in the leaf area index of a boreal aspen-hazelnut forest in relation to net ecosystem production. *Agricultural and Forest Meteorology*, *126*(3-4), 237–255.

Bastiaanssen, W. G. M., Cheema, M. J. M., Immerzeel, W. W., Miltenburg, I. J., & Pelgrum, H. (2012). Surface energy balance and actual evapotranspiration of the transboundary Indus Basin estimated from satellite measurements and the ETLook model. *Water Resources Research*, *48*, W11512. https://doi.org/10.1029/2011WR010482

Beget, M. E., Bettachini, V. A., Di Bella, C. M., & Baret, F. (2013). SAILHFlood: A radiative transfer model for flooded vegetation. *Ecological Modelling*, *257*(0), 25–35. https://doi.org/10.1016/j.ecolmodel.2013.02.025

Bergen, K. M., Goetz, S. J., Dubayah, R. O., Henebry, G. M., Hunsaker, C. T., Imhoff, M. L., et al. (2009). Remote sensing of vegetation 3-D structure for biodiversity and habitat: Review and implications for lidar and radar spaceborne missions. *Journal of Geophysical Research*, *114*, G00E06. https://doi.org/10.1029/2008JG000883

Berger, K., Atzberger, C., Danner, M., D'Urso, G., Mauser, W., Vuolo, F., & Hank, T. (2018). Evaluation of the PROSAIL model capabilities for future hyperspectral model environments: A review study. *Remote Sensing*, *10*(1), 85. https://doi.org/10.3390/rs10010085

Berterretche, M., Hudak, A. T., Cohen, W. B., Maiersperger, T. K., Gower, S. T., & Dungan, J. (2005). Comparison of regression and geostatistical methods for mapping leaf area index (LAI) with Landsat ETM+ data over a boreal forest. *Remote Sensing of Environment*, *96*(1), 49–61.

Betbeder, J., Fieuzal, R., & Baup, F. (2016). Assimilation of LAI and dry biomass data from optical and SAR images into an agro-meteorological model to estimate soybean yield. *IEEE Journal of Selected Topics in Applied Earth Observations and Remote Sensing*, *9*(6), 2540–2553. https://doi.org/10.1109/JSTARS.2016.2541169

Biudes, M. S., Machado, N. G., Danelichen, V. H. D., Souza, M. C., Vourlitis, G. L., & Nogueira, J. D. (2014). Ground and remote sensing-based measurements of leaf area index in a transitional forest and seasonal flooded forest in Brazil. *International Journal of Biometeorology*, *58*(6), 1181–1193. https://doi.org/10.1007/s00484-013-0713-4

Blackburn, G. A. (1999). Relationships between spectral reflectance and pigment concentrations in stacks of deciduous broadleaves. *Remote Sensing of Environment*, *70*, 224–237.

Boisier, J. P., de Noblet-Ducoudré, N., & Ciais, P. (2014). Historical land-use-induced evapotranspiration changes estimated from present-day observations and reconstructed land-cover maps. *Hydrology and Earth System Sciences*, *18*(9), 3571–3590. https://doi.org/10.5194/hess-18-3571-2014

Bonan, G. B. (2002). *Ecological climatology*. New York: Cambridge University Press.

Bonan, G. B., & Levis, S. (2006). Evaluating aspects of the community land and atmosphere models (CLM3 and CAM3) using a dynamic global vegetation model. *Journal of Climate*, *19*(11), 2290–2301. https://doi.org/10.1175/jcli3741.1

Bonan, G. B., Levis, S., Kergoat, L., & Oleson, K. W. (2002). Landscapes as patches of plant functional types: An integrating concept for climate and ecosystem models. *Global Biogeochemical Cycles*, *16*(2), 1021. https://doi.org/10.1029/2000GB001360

Bonan, G. B., Oleson, K. W., Vertenstein, M., Levis, S., Zeng, X., Dai, Y., et al. (2002). The land surface climatology of the NCAR community land model coupled to the NCAR Community Climate Model. *Journal of Climate*, *15*(22), 3123–3149. https://doi.org/10.1175/1520-0442(2002)015<3123:TLSCOT>2.0.CO;2

Borak, J. S., & Jasinski, M. F. (2009). Effective interpolation of incomplete satellite-derived leaf-area index time series for the continental United States. *Agricultural and Forest Meteorology*, *149*(2), 320–332.

Boussetta, S., Balsamo, G., Beljaars, A., Kral, T., & Jarlan, L. (2013). Impact of a satellite-derived leaf area index monthly climatology in a global numerical weather prediction model. *International Journal of Remote Sensing*, *34*(9-10), 3520–3542.

Boussetta, S., Balsamo, G., Dutra, E., Beljaars, A., & Albergel, C. (2015). Assimilation of surface albedo and vegetation states from satellite observations and their impact on numerical weather prediction. *Remote Sensing of Environment*, *163*(0), 111–126. https://doi.org/10.1016/j.rse.2015.03.009

Bradley, B. A., Jacob, R. W., Hermance, J. F., & Mustard, J. F. (2007). A curve fitting procedure to derive inter-annual phenologies from time series of noisy satellite NDVI data. *Remote Sensing of Environment*, *106*(2), 137–145.

Bréda, N. J. J. (2003). Ground-based measurements of leaf area index: A review of methods, instruments and current controversies. *Journal of Experimental Botany*, *54*, 2403–2417.

Breunig, F. M., Galvão, L. S., Formaggio, A. R., & Epiphanio, J. C. N. (2011). Directional effects on NDVI and LAI retrievals from MODIS: A case study in Brazil with soybean. *International Journal of Applied Earth Observation and Geoinformation*, *13*(1), 34–42. https://doi.org/10.1016/j.jag.2010.06.004

Broadhead, J. S., Muxworthy, A. R., Ong, C. K., & Black, C. R. (2003). Comparison of methods for determining leaf area in tree rows. *Agricultural and Forest Meteorology*, *115*(3-4), 151–161. https://doi.org/10.1016/s0168-1923(02)00212-5

Broge, N. H., & Leblanc, E. (2001). Comparing prediction power and stability of broadband and hyperspectral vegetation indices for estimation of green leaf area index and canopy chlorophyll density. *Remote Sensing of Environment*, *76*(2), 156–172.

Broge, N. H., & Mortensen, J. V. (2002). Deriving green crop area index and canopy chlorophyll density of winter wheat from spectral reflectance data. *Remote Sensing of Environment*, *81*, 45–57.

Bsaibes, A., Courault, D., Baret, F., Weiss, M., Olioso, A., Jacob, F., et al. (2009). Albedo and LAI estimates from FORMOSAT-2 data for crop monitoring. *Remote Sensing of Environment*, *113*(4), 716–729. https://doi.org/10.1016/j.rse.2008.11.014

Buermann, W., Anderson, B., Tucker, C. J., Dickinson, R. E., Lucht, W., Potter, C. S., & Myneni, R. B. (2003). Interannual covariability in Northern Hemisphere air temperatures and greenness associated with El Niño-Southern Oscillation and the Arctic Oscillation. *Journal of Geophysical Research*, *108*(D13), 4396. https://doi.org/10.1029/2002JD002630

Buermann, W., Dong, J., Zeng, X., Myneni, R., & Dickinson, R. (2001). Evaluation of the utility of satellite-based vegetation leaf area index data for climate simulations. *Journal of Climate*, *14*(17), 3536–3550.

Buermann, W., Wang, Y. J., Dong, J. R., Zhou, L. M., Zeng, X. B., Dickinson, R. E., et al. (2002). Analysis of a multiyear global vegetation leaf area index data set. *Journal of Geophysical Research*, *107*(D22), 4646. https://doi.org/10.1029/2001JD000975

Burrows, S. N., Ahl, D. E., Norman, J. H., Diak, G., Gower, S. T., Clayton, M. K., & Mackay, D. S. (2002). Application of geostatistics to characterize leaf area index (LAI) from flux tower to landscape scales using a cyclic sampling design. *Ecosystems*, *5*(6), 667–679.

Bye, I. J., North, P. R. J., Los, S. O., Kljun, N., Rosette, J. A. B., Hopkinson, C., et al. (2017). Estimating forest canopy parameters from satellite waveform LiDAR by inversion of the FLIGHT three-dimensional radiative transfer model. *Remote Sensing of Environment*, *188*, 177–189. https://doi.org/10.1016/j.rse.2016.10.048

Calvet, J.-C., Barbu, A., Carrer, D., Fairbairn, D., Gelati, E., & Meurey, C. (2014). Cross-validation of satellite products over France through their integration into a land surface model. Paper presented at the 4th International Symposium Recent Advances in Quantitative Remote Sensing, Torrent, Spain.

Camacho, F., Cernicharo, J., Lacaze, R., Baret, F., & Weiss, M. (2013). GEOV1: LAI, FAPAR essential climate variables and FCOVER global time series capitalizing over existing products. Part 2: Validation and intercomparison with reference products. *Remote Sensing of Environment*, *137*, 310–329. https://doi.org/10.1016/j.rse.2013.02.030

Campbell, G. S. (1986). Extinction coefficients for radiation in plant canopies calculated using an ellipsoidal inclination angle distribution. *Agricultural and Forest Meteorology*, *36*(4), 317–321. https://doi.org/10.1016/0168-1923(86)90010-9

Campbell, G. S. (1990). Derivation of an angle density function for canopies with ellipsoidal leaf angle distributions. *Agricultural and Forest Meteorology*, *49*(3), 173–176. https://doi.org/10.1016/0168-1923(90)90030-A

Campos-Taberner, M., Garcia-Haro, F. J., Camps-Valls, G., Grau-Muedra, G., Nutini, F., Crema, A., & Boschetti, M. (2016). Multitemporal and multiresolution leaf area index retrieval for operational local rice crop monitoring. *Remote Sensing of Environment*, *187*, 102–118. https://doi.org/10.1016/j.rse.2016.10.009

Campos-Taberner, M., Moreno-Martínez, Á., García-Haro, F., Camps-Valls, G., Robinson, N., Kattge, J., & Running, S. (2018). Global estimation of biophysical variables from Google Earth Engine Platform. *Remote Sensing*, *10*(8), 1167. https://doi.org/10.3390/rs10081167

Canisius, F., & Fernandes, R. (2012). Evaluation of the information content of Medium Resolution Imaging Spectrometer (MERIS) data for regional leaf area index assessment. *Remote Sensing of Environment*, *119*, 301–314. https://doi.org/10.1016/j.rse.2011.10.013

Carrer, D., Roujean, J.-L., Lafont, S., Calvet, J.-C., Boone, A., Decharme, B., et al. (2013). A canopy radiative transfer scheme with explicit FAPAR for the interactive vegetation model ISBA-A-gs: Impact on carbon fluxes. *Journal of Geophysical Research: Biogeosciences*, *118*, 888–903. https://doi.org/10.1002/jgrg.20070

Chai, L., Qu, Y., Zhang, L., Liang, S., & Wang, J. (2012). Estimating time-series leaf area index based on recurrent nonlinear autoregressive neural networks with exogenous inputs. *International Journal of Remote Sensing*, *33*(18), 5712–5731. https://doi.org/10.1080/01431161.2012.671553

Chapman, L. (2007). Potential applications of near infra-red hemispherical imagery in forest environments. *Agricultural and Forest Meteorology*, *143*(1–2), 151–156. https://doi.org/10.1016/j.agrformet.2006.12.006

Chase, T. N., Pielke, R. A., Kittel, T. G. F., Running, S. R., & Nemani, R. (1996). Sensitivity of a general circulation model to global changes in leaf area index. *Journal of Geophysical Research*, *101*(D3), 7393–7408.

Chaurasia, S., & Dadhwal, V. K. (2004). Comparison of principal component inversion with VI-empirical approach for LAI estimation using simulated reflectance data. *International Journal of Remote Sensing*, *25*(14), 2881–2887.

Che, M., Chen, B., Zhang, H., Fang, S., Xu, G., Lin, X., & Wang, Y. (2014). A new equation for deriving vegetation phenophase from time series of leaf area index (LAI) data. *Remote Sensing*, *6*(6), 5650–5670.

Chen, B., Chen, J. M., & Ju, W. (2007). Remote sensing-based Ecosystem-Atmosphere Simulation Scheme (EASS)—Model formulation and test with multiple-year data. *Ecological Modelling*, *209*, 277–300.

Chen, J. (1999). Spatial scaling of a remotely sensed surface parameter by contexture. *Remote Sensing of Environment*, *69*, 30–42.

Chen, J., Jönsson, P., Tamura, M., Gu, Z., Matsushita, B., & Eklundh, L. (2004). A simple method for reconstructing a high quality NDVI time-series data set based on the Savitzky-Golay filter. *Remote Sensing of Environment*, *91*(3-4), 332–344.

Chen, J., Li, X., Nilson, T., & Strahler, A. (2000). Recent advances in geometrical optical modelling and its applications. *Remote Sensing Reviews*, *18*, 227–262.

Chen, J., Lin, H., Huang, C., & Fang, C. (2009). The relationship between the leaf area index (LAI) of rice and the C-band SAR vertical/horizontal (VV/HH) polarization ratio. *International Journal of Remote Sensing*, *30*(8), 2149–2154.

Chen, J., Lin, H., Liu, A., Shao, Y., & Yang, L. (2006). A semi-empirical backscattering model for estimation of leaf area index (LAI) of rice in southern China. *International Journal of Remote Sensing*, *27*(24), 5417–5425.

Chen, J. M. (1996). Optically based methods for measuring seasonal variation of leaf area index in boreal conifer stands. *Agricultural and Forest Meteorology*, *80*(2-4), 135–163.

Chen, J. M. (2018). Remote sensing of leaf area index and clumping index. In S. Liang (Ed.), *Comprehensive remote sensing*, (pp. 53–77). Oxford: Elsevier.

Chen, J. M., Black, A., & Adams, R. S. (1991). Evaluation of hemispherical photography for determining plant area index and geometry of forest stand. *Agricultural and Forest Meteorology*, *56*, 129–143.

Chen, J. M., & Black, T. A. (1992). Defining leaf area index for non-flat leaves. *Plant, Cell and Environment*, *15*(4), 421–429.

Chen, J. M., & Cihlar, J. (1995). Plant canopy gap-size analysis theory for improving optical measurements of leaf-area index. *Applied Optics*, *34*, 6211–6222.

Chen, J. M., & Leblanc, S. G. (1997). A four-scale bidirectional reflectance model based on canopy architecture. *IEEE Transactions on Geoscience and Remote Sensing*, *35*(5), 1316–1337. https://doi.org/10.1109/36.628798

Chen, J. M., Liu, J., Leblanc, S. G., Lacaze, R., & Roujean, J.-L. (2003). Multi-angular optical remote sensing for assessing vegetation structure and carbon absorption. *Remote Sensing of Environment*, *84*(4), 516–525.

Chen, J. M., Menges, C. H., & Leblanc, S. G. (2005). Global mapping of foliage clumping index using multi-angular satellite data. *Remote Sensing of Environment*, *97*(4), 447–457. https://doi.org/10.1016/j.rse.2005.05.003

Chen, J. M., Mo, G., Pisek, J., Liu, J., Deng, F., Ishizawa, M., & Chan, D. (2012). Effects of foliage clumping on the estimation of global terrestrial gross primary productivity. *Global Biogeochemical Cycles*, *26*, GB1019. https://doi.org/10.1029/2010GB003996

Chen, J. M., Pavlic, G., Brown, L., Cihlar, J., Leblanc, S. G., White, H. P., et al. (2002). Derivation and validation of Canada-wide leaf area index maps using ground measurements and high and moderate resolution satellite imagery. *Remote Sensing of Environment*, *80*(1), 165–184. https://doi.org/10.1016/S0034-4257(01)00300-5

Chen, L., & Dirmeyer, P. A. (2016). Adapting observationally based metrics of biogeophysical feedbacks from land cover/land use change to climate modeling. *Environmental Research Letters*, *11*(3), 1–14. https://doi.org/10.1088/1748-9326/11/3/034002

Chen, M., Willgoose, G. R., & Saco, P. M. (2015). Investigating the impact of leaf area index temporal variability on soil moisture predictions using remote sensing vegetation data. *Journal of Hydrology*, *522*, 274–284. https://doi.org/10.1016/j.jhydrol.2014.12.027

Chianucci, F., & Cutini, A. (2012). Digital hemispherical photography for estimating forest canopy properties: Current controversies and opportunities. *Iforest-Biogeosciences and Forestry*, *5*, 290–295. https://doi.org/10.3832/ifor0775-005

Chianucci, F., Macfarlane, C., Pisek, J., Cutini, A., & Casa, R. (2015). Estimation of foliage clumping from the LAI-2000 Plant Canopy Analyzer: Effect of view caps. *Trees-Structure and Function*, *29*(2), 355–366. https://doi.org/10.1007/s00468-014-1115-x

Chianucci, F., Puletti, N., Giacomello, E., Cutini, A., & Corona, P. (2015). Estimation of leaf area index in isolated trees with digital photography and its application to urban forestry. *Urban Forestry & Urban Greening*, *14*(2), 377–382. https://doi.org/10.1016/j.ufug.2015.04.001

Chu, J., Syktus, J., McAlpine, C., Thatcher, M., Scarth, P., Jeffrey, S., et al. (2011). Validation of land surface products for modelling the climate impacts of large-scale revegetation in Queensland. Paper presented at the MODSIM2011,19th International Congress on Modelling and Simulation, Perth, Australia.

Cihlar, J. (1996). Identification of contaminated pixels in AVHRR composite images for studies of land biosphere. *Remote Sensing of Environment*, *56*(3), 149–163.

Clark, D. B., Olivas, P. C., Oberbauer, S. F., Clark, D. A., & Ryan, M. G. (2008). First direct landscape-scale measurement of tropical rain forest Leaf Area Index, a key driver of global primary productivity. *Ecology Letters*, *11*(2), 163–172. https://doi.org/10.1111/j.1461-0248.2007.01134.x

Claverie, M., Matthews, J., Vermote, E., & Justice, C. (2016). A 30+ year AVHRR LAI and FAPAR climate data record: Algorithm description and validation. *Remote Sensing*, *8*(3), 263. https://doi.org/10.3390/rs8030263

Claverie, M., Vermote, E. F., Weiss, M., Baret, F., Hagolle, O., & Demarez, V. (2013). Validation of coarse spatial resolution LAI and FAPAR time series over cropland in southwest France. *Remote Sensing of Environment*, *139*(0), 216–230. https://doi.org/10.1016/j.rse.2013.07.027

Cleugh, H. A., Leuning, R., Mu, Q. Z., & Running, S. W. (2007). Regional evaporation estimates from flux tower and MODIS satellite data. *Remote Sensing of Environment*, *106*(3), 285–304. https://doi.org/10.1016/j.rse.2006.07.007

Clevers, J. G. P. W., & van leeuwen, H. J. C. (1996). Combined use of optical and microwave remote sensing data for crop growth monitoring. *Remote Sensing of Environment*, *56*, 42–51.

Cohen, W. B., Maiersperger, T. K., Gower, S. T., & Turner, D. P. (2003). An improved strategy for regression of biophysical variables and Landsat ETM+ data. *Remote Sensing of Environment*, *84*, 561–571.

Cohen, W. B., Maiersperger, T. K., Turner, D. P., Ritts, W. D., Pflugmacher, D., Kennedy, R. E., et al. (2006). MODIS land cover and LAI collection 4 product quality across nine sites in the western hemisphere. *IEEE Transactions on Geoscience and Remote Sensing*, *44*(7), 1843–1857. https://doi.org/10.1109/TGRS.2006.876026

Cohen, W. B., Maiersperger, T. K., Yang, Z., Gower, S. T., Turner, D. P., Ritts, W. D., et al. (2003). Comparisons of land cover and LAI estimates derived from ETM+ and MODIS for four sites in North America: a quality assessment of 2000/2001 provisional MODIS products. *Remote Sensing of Environment*, *88*(3), 233–255. https://doi.org/10.1016/j.rse.2003.06.006

Colaizzi, P. D., Evett, S. R., Brauer, D. K., Howell, T. A., Tolk, J. A., & Copeland, K. S. (2017). Allometric method to estimate leaf area index for row crops. *Agronomy Journal*, *109*(3), 883–894. https://doi.org/10.2134/agronj2016.11.0665

Colombo, R., Bellingeri, D., Fasolini, D., & Marino, C. M. (2003). Retrieval of leaf area index in different vegetation types using high resolution satellite data. *Remote Sensing of Environment*, *86*, 120–131.

Combal, B., Baret, F., & Weiss, M. (2001). Improving canopy variables estimation from remote sensing data by exploiting ancillary information. Case study on sugar beet canopies. *Agronomie*, *22*(2), 205–215. https://doi.org/10.1051/agro:2002008

Combal, B., Baret, F., Weiss, M., Trubuil, A., Macé, D., Pragnère, A., et al. (2002). Retrieval of canopy biophysical variables from bidirectional reflectance using prior information to solve the ill-posed inverse problem. *Remote Sensing of Environment*, *84*(1), 1–15.

Confalonieri, R., Foi, M., Casa, R., Aquaro, S., Tona, E., Peterle, M., et al. (2013). Development of an app for estimating leaf area index using a smartphone. Trueness and precision determination and comparison with other indirect methods. *Computers and Electronics in Agriculture*, *96*(0), 67–74. https://doi.org/10.1016/j.compag.2013.04.019

Cooter, E. J., & Schwede, D. B. (2000). Sensitivity of the National Oceanic and Atmospheric Administration multilayer model to instrument error and parameterization uncertainty. *Journal of Geophysical Research*, *105*(D5), 6695–6707.

Croft, H., Chen, J. M., & Zhang, Y. (2014). Temporal disparity in leaf chlorophyll content and leaf area index across a growing season in a temperate deciduous forest. *International Journal of Applied Earth Observation and Geoinformation*, *33*(0), 312–320. https://doi.org/10.1016/j.jag.2014.06.005

Cui, Y., & Jia, L. (2014). A modified Gash model for estimating rainfall interception loss of forest using remote sensing observations at regional scale. *Water*, *6*(4), 993.

Culvenor, D. S., Newnham, G. J., Mellor, A., Sims, N. C., & Haywood, A. (2014). Automated in-situ laser scanner for monitoring forest leaf area index. *Sensors*, *14*(8), 14994–15008. https://doi.org/10.3390/s140814994

Curnel, Y., de Wit, A. J. W., Duveiller, G., & Defourny, P. (2011). Potential performances of remotely sensed LAI assimilation in WOFOST model based on an OSS Experiment. *Agricultural and Forest Meteorology*, *151*(12), 1843–1855. https://doi.org/10.1016/j.agrformet.2011.08.002

Curran, P. J., & Hay, A. M. (1986). The importance of measurement error for certain procedures in remote sensing at optical wavelengths. *Photogrammetric Engineering and Remote Sensing*, *52*, 229–241.

Cutini, A., Matteucci, G., & Mugnozza, G. S. (1998). Estimation of leaf area index with the Li-Cor LAI 2000 in deciduous forests. *Forest Ecology and Management*, *105*(1–3), 55–65. https://doi.org/10.1016/S0378-1127(97)00269-7

Damm, A., Guanter, L., Verhoef, W., Schläpfer, D., Garbari, S., & Schaepman, M. E. (2015). Impact of varying irradiance on vegetation indices and chlorophyll fluorescence derived from spectroscopy data. *Remote Sensing of Environment*, *156*, 202–215. https://doi.org/10.1016/j.rse.2014.09.031

Darvishzadeh, R., Atzberger, C., Skidmore, A. K., & Abkar, A. A. (2009). Leaf area index derivation from hyperspectral vegetation indices and the red edge position. *International Journal of Remote Sensing*, *30*(23), 6199–6218. https://doi.org/10.1080/01431160902842342

Darvishzadeh, R., Skidmore, A., Schlerf, M., & Atzberger, C. (2008). Inversion of a radiative transfer model for estimating vegetation LAI and chlorophyll in a heterogeneous grassland. *Remote Sensing of Environment*, *112*(5), 2592–2604. https://doi.org/10.1016/j.rse.2007.12.003

Dassot, M., Constant, T., & Fournier, M. (2011). The use of terrestrial LiDAR technology in forest science: Application fields, benefits and challenges. *Annals of Forest Science*, *68*(5), 959–974. https://doi.org/10.1007/s13595-011-0102-2

Davi, H., Baret, F., Huc, R., & Dufrêne, E. (2008). Effect of thinning on LAI variance in heterogeneous forests. *Forest Ecology and Management*, *256*(5), 890–899. https://doi.org/10.1016/j.foreco.2008.05.047

de Wit, A., Duveiller, G., & Defourny, P. (2012). Estimating regional winter wheat yield with WOFOST through the assimilation of green area index retrieved from MODIS observations. *Agricultural and Forest Meteorology*, *164*(0), 39–52. https://doi.org/10.1016/j.agrformet.2012.04.011

Deblonde, G., Penner, M., & Royer, A. (1994). Measuring leaf area index with the LI-COR LAI-2000 in pine stands. *Ecology*, *75*, 1507–1511.

Defourny, P., Bontemps, S., Obsomer, V., Schouten, L., Bartalev, S., Herold, M., et al. (2010). Accuracy assessment of global land cover maps: Lessons learnt from the GlobCover and GlobCorine Experiences. Paper presented at the 2010 European Space Agency Living Planet Symposium, Bergen, Norway.

DeFries, R. S., & Los, S. O. (1999). Implications of land-cover misclassification for parameter estimates in global land-surface models: An example from the simple biosphere model (SiB2). *Photogrammetric Engineering and Remote Sensing*, *65*(9), 1083–1088.

Delécolle, R., Maas, S. J., Guérif, M., & Baret, F. (1992). Remote sensing and crop production models: Present trends. *ISPRS Journal of Photogrammetry and Remote Sensing*, *47*, 145–161.

Delegido, J., Verrelst, J., Alonso, L., & Moreno, J. (2011). Evaluation of Sentinel-2 red-edge bands for empirical estimation of green LAI and chlorophyll content. *Sensors*, *11*(7), 7063–7081.

Delegido, J., Verrelst, J., Rivera, J. P., Ruiz-Verdú, A., & Moreno, J. (2015). Brown and green LAI mapping through spectral indices. *International Journal of Applied Earth Observation and Geoinformation*, *35*(Part B), 350–358. https://doi.org/10.1016/j.jag.2014.10.001

Demarez, V., Duthoit, S., Baret, F., Weiss, M., & Dedieu, G. (2008). Estimation of leaf area and clumping indexes of crops with hemispherical photographs. *Agricultural and Forest Meteorology*, *148*(4), 644–655. https://doi.org/10.1016/j.agrformet.2007.11.015

Deng, F., Chen, J. M., Plummer, S., Chen, M., & Pisek, J. (2006). Algorithm for global leaf area index retrieval using satellite imagery. *IEEE Transactions on Geoscience and Remote Sensing*, *44*(8), 2219–2229. https://doi.org/10.1109/TGRS.2006.872100

Dente, L., Satalino, G., Mattia, F., & Rinaldi, M. (2008). Assimilation of leaf area index derived from ASAR and MERIS data into CERES-Wheat model to map wheat yield. *Remote Sensing of Environment*, *112*(4), 1395–1407.

Detto, M., Asner, G. P., Muller-Landau, H. C., & Sonnentag, O. (2015). Spatial variability in tropical forest leaf area density from multi-return lidar and modeling. *Journal of Geophysical Research: Biogeosciences*, *120*, 294–309. https://doi.org/10.1002/2014JG002774

Dewaele, H., Munier, S., Albergel, C., Planque, C., Laanaia, N., Carrer, D., & Calvet, J. C. (2017). Parameter optimisation for a better representation of drought by LSMs: Inverse modelling vs. sequential data assimilation. *Hydrology and Earth System Sciences*, *21*(9), 4861–4878. https://doi.org/10.5194/hess-21-4861-2017

Di Bella, C., Seguin, B., Faivre, R., & Ruget, F. (2005). Using VEGETATION satellite data and the crop model STICS-Prairie to estimate pasture production at the national level in France. *Physics and Chemistry of the Earth*, *30*(1-3), 3–9.

Diaz, B. M., & Blackburn, G. A. (2003). Remote sensing of mangrove biophysical properties: Evidence from a laboratory simulation of the possible effects of background variation on spectral vegetation indices. *International Journal of Remote Sensing*, *24*(1), 53–73. https://doi.org/10.1080/01431160110115852

Diner, D. J., Asner, G. P., Davies, R., Knyazikhin, Y., Muller, J. P., Nolin, A. W., et al. (1999). New directions in Earth Observing: Scientific applications of multiangle remote sensing. *Bulletin of the American Meteorological Society*, *80*(11), 2209–2228. https://doi.org/10.1175/1520-0477(1999)080<2209:NDIEOS>2.0.CO;2

Diner, D. J., Martonchik, J. V., Borel, C., Gerstl, S. A. W., Gordon, H. R., Knyazikhin, Y., et al. (2008). Multi-angle Imaging Spectro-Radiometer (MISR) level 2 surface retrieval algorithm theoretical basis (JPL D-11401, Rev. E). Retrieved from http://eospso.gsfc.nasa.gov/sites/default/files/atbd/ATB_L2Surface43.pdf

Ding, Y., Ge, Y., Hu, M., Wang, J., Wang, J., Zheng, X., & Zhao, K. (2014). Comparison of spatial sampling strategies for ground sampling and validation of MODIS LAI products. *International Journal of Remote Sensing*, *35*(20), 7230–7244. https://doi.org/10.1080/01431161.2014.967889

Disney, M., Lewis, P., & Saich, P. (2006). 3D modelling of forest canopy structure for remote sensing simulations in the optical and microwave domains. *Remote Sensing of Environment*, *100*(1), 114–132.

Disney, M., Muller, J.-P., Kharbouche, S., Kaminski, T., Voßbeck, M., Lewis, P., & Pinty, B. (2016). A new global fAPAR and LAI dataset derived from optimal albedo estimates: Comparison with MODIS products. *Remote Sensing*, *8*(4), 275. https://doi.org/10.3390/rs8040275

Döbert, T. F., Webber, B. L., Sugau, J. B., Dickinson, K. J. M., & Didham, R. K. (2015). Can leaf area index and biomass be estimated from Braun-Blanquet cover scores in tropical forests? *Journal of Vegetation Science*, *26*(6), 1043–1053. https://doi.org/10.1111/jvs.12310

Doktor, D., Bondeau, A., Koslowski, D., & Badeck, F.-W. (2009). Influence of heterogeneous landscape on computed green-up dates based on daily AVHRR NDVI observations. *Remote Sensing of Environment*, *113*(12), 2618–2632.

Doraiswamy, P. C., Sinclair, T. R., Hollinger, S., Akhmedov, B., Stern, A., & Prueger, J. (2005). Application of MODIS derived parameters for regional crop yield assessment. *Remote Sensing of Environment*, *97*(2), 192–202.

Doughty, C. E., & Goulden, M. L. (2008). Seasonal patterns of tropical forest leaf area index and CO_2 exchange. *Journal of Geophysical Research*, *113*, G00B06. https://doi.org/10.1029/2007JG000590

Drake, J. B., Dubayah, R. O., Clarke, D. B., Knox, R. G., Blair, J. B., & Hofton, M. A. (2002). Estimation of tropical forest structural characteristics using large-footprint lidar. *Remote Sensing of Environment*, *79*, 305–319.

Drusch, M., Del Bello, U., Carlier, S., Colin, O., Fernandez, V., Gascon, F., et al. (2012). Sentinel-2: ESA's optical high-resolution mission for GMES operational services. *Remote Sensing of Environment*, *120*, 25–36. https://doi.org/10.1016/j.rse.2011.11.026

Duan, S.-B., Li, Z.-L., Wu, H., Tang, B.-H., Ma, L., Zhao, E., & Li, C. (2014). Inversion of the PROSAIL model to estimate leaf area index of maize, potato, and sunflower fields from unmanned aerial vehicle hyperspectral data. *International Journal of Applied Earth Observation and Geoinformation*, *26*(0), 12–20. https://doi.org/10.1016/j.jag.2013.05.007

Durbha, S. S., King, R. L., & Younan, N. H. (2007). Support vector machines regression for retrieval of leaf area index from multiangle imaging spectroradiometer. *Remote Sensing of Environment*, *107*(1-2), 348–361.

Duursma, R. A., Gimeno, T. E., Boer, M. M., Crous, K. Y., Tjoelker, M. G., & Ellsworth, D. S. (2016). Canopy leaf area of a mature evergreen Eucalyptus woodland does not respond to elevated atmospheric CO2 but tracks water availability. *Global Change Biology*, *22*(4), 1666–1676. https://doi.org/10.1111/gcb.13151

Duveiller, G., Baret, F., & Defourny, P. (2013). Using thermal time and pixel purity for enhancing biophysical variable time series: An interproduct comparison. *IEEE Transactions on Geoscience and Remote Sensing*, *51*(4), 2119–2127. https://doi.org/10.1109/TGRS.2012.2226731

Duveiller, G., Weiss, M., Baret, F., & Defourny, P. (2011). Retrieving wheat Green Area Index during the growing season from optical time series measurements based on neural network radiative transfer inversion. *Remote Sensing of Environment*, *115*(3), 887–896. https://doi.org/10.1016/j.rse.2010.11.016

Eklundh, L., Hall, K., Eriksson, J., Ardö, J., & Pilesjö, P. (2003). Investigating the use of Landsat thematic mapper data for estimation of forest leaf area index in southern Sweden. *Canadian Journal of Remote Sensing*, *29*, 349–362.

Eklundh, L., Harrie, L., & Kuusk, A. (2001). Investigating relationships between Landsat ETM+ sensor data and leaf area index in a boreal conifer forest. *Remote Sensing of Environment*, *78*, 239–251.

El Hajj, M., Bégué, A., Guillaume, S., & Martiné, J.-F. (2009). Integrating SPOT-5 time series, crop growth modeling and expert knowledge for monitoring agricultural practices—The case of sugarcane harvest on Reunion Island. *Remote Sensing of Environment*, *113*(10), 2052–2061.

Fan, L., Berger, F. H., Liu, H., & Bernhofer, C. (2014). Validating MODIS land surface reflectance products using ground-measured reflectance spectra—A case study in semi-arid grassland in Inner Mongolia, China. *International Journal of Remote Sensing*, *35*(5), 1715–1728. https://doi.org/10.1080/01431161.2014.882031

Fang, H., Jiang, C., Li, W., Wei, S., Baret, F., Chen, J. M., et al. (2013). Characterization and intercomparison of global moderate resolution leaf area index (LAI) products: Analysis of climatologies and theoretical uncertainties. *Journal of Geophysical Research: Biogeosciences*, *118*, 529–548. https://doi.org/10.1002/jgrg.20051

Fang, H., Li, W., & Myneni, R. B. (2013). The impact of potential land cover misclassification on MODIS leaf area index (LAI) estimation: A statistical perspective. *Remote Sensing*, *5*(2), 830–844. https://doi.org/10.3390/rs5020830

Fang, H., Li, W., Wei, S., & Jiang, C. (2014). Seasonal variation of leaf area index (LAI) over paddy rice fields in NE China: Intercomparison of destructive sampling, LAI-2200, digital hemispherical photography (DHP), and AccuPAR methods. *Agricultural and Forest Meteorology*, *198-199*, 126–141. https://doi.org/10.1016/j.agrformet.2014.08.005

Fang, H., & Liang, S. (2003). Retrieving leaf area index with a neural network method: Simulation and validation. *IEEE Transactions on Geoscience and Remote Sensing*, *41*(6), 2052–2062.

Fang, H., & Liang, S. (2005). A hybrid inversion method for mapping leaf area index from MODIS data: Experiments and application to broadleaf and needleleaf canopies. *Remote Sensing of Environment*, *94*(3), 405–424. https://doi.org/10.1016/j.rse.2004.11.001

Fang, H., Liang, S., Kim, H.-Y., Townshend, J. R., Schaaf, C. L., Strahler, A. H., & Dickinson, R. E. (2007). Developing a spatially continuous 1 km surface albedo data set over North America from Terra MODIS products. *Journal of Geophysical Research*, *112*, D20206. https://doi.org/10.1029/2006JD008377

Fang, H., Liang, S., & Kuusk, A. (2003). Retrieving leaf area index using a genetic algorithm with a canopy radiative transfer model. *Remote Sensing of Environment*, *85*(3), 257–270.

Fang, H., Liang, S., Townshend, J. R., & Dickinson, R. E. (2008). Spatially and temporally continuous LAI data sets based on an integrated filtering method: Examples from North America. *Remote Sensing of Environment*, *112*(1), 75–93.

Fang, H., Wei, S., Jiang, C., & Scipal, K. (2012). Theoretical uncertainty analysis of global MODIS, CYCLOPES and GLOBCARBON LAI products using a triple collocation method. *Remote Sensing of Environment*, *124*, 610–621. https://doi.org/10.1016/j.rse.2012.06.013

Fang, H., Wei, S., & Liang, S. (2012). Validation of MODIS and CYCLOPES LAI products using global field measurement data. *Remote Sensing of Environment*, *119*, 43–54. https://doi.org/10.1016/j.rse.2011.12.006

Fang, H., Ye, Y., Liu, W., Wei, S., & Ma, L. (2018). Continuous estimation of canopy leaf area index (LAI) and clumping index over broadleaf crop fields: An investigation of the PASTIS-57 instrument and smartphone applications. *Agricultural and Forest Meteorology*, *253-254*, 48–61. https://doi.org/10.1016/j.agrformet.2018.02.003

Fensholt, R., Sandholt, I., & Rasmussen, M. S. (2004). Evaluation of MODIS LAI, fAPAR and the relation between fAPAR and NDVI in a semi-arid environment using in situ measurements. *Remote Sensing of Environment*, *91*(3-4), 490–507.

Fernandes, R., & Leblanc, S. G. (2005). Parametric (modified least squares) and non-parametric (Theil-Sen) linear regressions for predicting biophysical parameters in the presence of measurement errors. *Remote Sensing of Environment*, *95*(3), 303–316. https://doi.org/10.1016/j.rse.2005.01.005

Fernandes, R., Plummer, S., Nightingale, J., Baret, F., Camacho, F., Fang, H., et al. (2014). Global leaf area index product validation good practices (Version 2.0). Retrieved from http://lpvs.gsfc.nasa.gov/documents.html

Fernandes, R. A., Butson, C., Leblanc, S. G., & Latifovic, R. (2003). Landsat-5 and Landsat-7 ETM+ based accuracy assessment of leaf area index products for Canada derived from SPOT-4 VEGETATION data. *Canadian Journal of Remote Sensing*, *29*(2), 241–258.

Fieuzal, R., & Baup, F. (2016). Estimation of leaf area index and crop height of sunflowers using multi-temporal optical and SAR satellite data. *International Journal of Remote Sensing*, *37*(12), 2780–2809. https://doi.org/10.1080/01431161.2016.1176276

Ford, T. W., & Quiring, S. M. (2013). Influence of MODIS-Derived Dynamic Vegetation on VIC-Simulated Soil Moisture in Oklahoma. *Journal of Hydrometeorology*, *14*(6), 1910–1921. https://doi.org/10.1175/JHM-D-13-037.1

Forkel, M., Carvalhais, N., Schaphoff, S., v. Bloh, W., Migliavacca, M., Thurner, M., & Thonicke, K. (2014). Identifying environmental controls on vegetation greenness phenology through model–data integration. *Biogeosciences*, *11*(23), 7025–7050. https://doi.org/10.5194/bg-11-7025-2014

Fortin, J. G., Anctil, F., & Parent, L. E. (2014). Comparison of multiple-layer perceptrons and least squares support vector machines for remote-sensed characterization of in-field LAI patterns—A case study with potato. *Canadian Journal of Remote Sensing*, *40*(2), 75–84. https://doi.org/10.1080/07038992.2014.928182

Forzieri, G., Alkama, R., Miralles, D. G., & Cescatti, A. (2017). Satellites reveal contrasting responses of regional climate to the widespread greening of Earth. *Science*, *356*(6343), 5. https://doi.org/10.1126/science.aal1727

Fournier, R. A., & Hall, R. J. (Eds) (2017). *Hemispherical photography in forest science: Theory, methods, applications* (Vol. 28). The Netherlands: Springer.

Fournier, R. A., Mailly, D., Walter, J.-M. N., & Soudani, K. (2003). Indirect measurements of forest canopy structure from in situ optical sensors. In M. A. Wulder, & S. E. Franklin (Eds.), *Remote sensing of forest environments—Concepts and case studies* (pp. 77–114). Boston: Kluwer Academic Publishers.

Fox, A., Williams, M., Richardson, A. D., Cameron, D., Gove, J. H., Quaife, T., et al. (2009). The REFLEX project: Comparing different algorithms and implementations for the inversion of a terrestrial ecosystem model against eddy covariance data. *Agricultural and Forest Meteorology*, *149*(10), 1597–1615. https://doi.org/10.1016/j.agrformet.2009.05.002

Frantz, D., Roder, A., Stellmes, M., & Hill, J. (2017). Phenology-adaptive pixel-based compositing using optical earth observation imagery. *Remote Sensing of Environment*, *190*, 331–347. https://doi.org/10.1016/j.rse.2017.01.002

Frazer, G. W., Canham, C. D., & Lertzman, K. P. (1999). Gap Light Analyzer (GLA), version 2.0: Imaging software to extract canopy structure and gap light transmission indices from true-color fisheye photographs, users manual and program documentation. Millbrook, NY. Retrieved from http://rem-main.rem.sfu.ca/forestry/downloads/Files/GLAV2UsersManual.pdf

Friedl, M. A., Sulla-Menashe, D., Tan, B., Schneider, A., Ramankutty, N., Sibley, A., & Huang, X. (2010). MODIS Collection 5 global land cover: Algorithm refinements and characterization of new datasets. *Remote Sensing of Environment*, *114*(1), 168–182. https://doi.org/10.1016/j.rse.2009.08.016

Fu, Y., Yang, G., Wang, J., & Feng, H. (2013). A comparative analysis of spectral vegetation indices to estimate crop leaf area index. *Intelligent Automation & Soft Computing*, *19*(3), 315–326. https://doi.org/10.1080/10798587.2013.824176

Fu, Z., Wang, J. D., Song, J. L., Zhou, H. M., Pang, Y., & Chen, B. S. (2011). Estimation of forest canopy leaf area index using MODIS, MISR, and LiDAR observations. *Journal of Applied Remote Sensing*, *5*. https://doi.org/10.1117/1.3594171

Ganguly, S., Baret, F., Myneni, R., Zhang, G., Milesi, C., & Hashimoto, H. (2014). Long-term data records of biophysical parameters from multiple satellite systems. Paper presented at the AGU, San Francisco. https://agu.confex.com/agu/fm14/meetingapp.cgi#Paper/5704

Ganguly, S., Nemani, R. R., Baret, F., Bi, J., Weiss, M., Zhang, G., et al. (2014). Green leaf area and fraction of photosynthetically active radiation absorbed by vegetation. In J. M. Hanes (Ed.), *Biophysical applications of satellite remote sensing*, (pp. 43–61). Berlin: Springer-Verlag. https://doi.org/10.1007/978-3-642-25047-7_2

Ganguly, S., Samanta, A., Schull, M. A., Shabanov, N. V., Milesi, C., Nemani, R. R., et al. (2008). Generating vegetation leaf area index Earth system data record from multiple sensors. Part 2: Implementation, analysis and validation. *Remote Sensing of Environment*, *112*(12), 4318–4332. https://doi.org/10.1016/j.rse.2008.07.013

Gao, F., Anderson, M. C., Kustas, W. P., & Houborg, R. (2014). Retrieving leaf area index from Landsat using MODIS LAI products and field measurements. *IEEE Geoscience and Remote Sensing Letters*, *11*(4), 773–777. https://doi.org/10.1109/lgrs.2013.2278782

Gao, F., Anderson, M. C., Kustas, W. P., & Wang, Y. (2012). Simple method for retrieving leaf area index from Landsat using MODIS leaf area index products as reference. *Journal of Applied Remote Sensing*, *6*, 063554. https://doi.org/10.1117/1.JRS.6.063554

Gao, F., Masek, J., Schwaller, M., & Hall, F. (2006). On the blending of the Landsat and MODIS surface reflectance: Predicting daily Landsat surface reflectance. *IEEE Transactions on Geoscience and Remote Sensing*, *44*(8), 2207–2218.

Gao, F., Morisette, J. T., Wolfe, R. E., Ederer, G., Pedelty, J., Masuoka, E., et al. (2008). An algorithm to produce temporally and spatially continuous MODIS-LAI time series. *IEEE Geoscience and Remote Sensing Letters*, *5*(1), 60–64. https://doi.org/10.1109/LGRS.2007.907971

Gao, X., Huete, A. R., Ni, W., & Miura, T. (2000). Optical-biophysical relationships of vegetation spectra without background contamination. *Remote Sensing of Environment*, *74*(3), 609–620.

Garcia, M., Popescu, S., Riano, D., Zhao, K. G., Neuenschwander, A., Agca, M., & Chuvieco, E. (2012). Characterization of canopy fuels using ICESat/GLAS data. *Remote Sensing of Environment*, *123*, 81–89. https://doi.org/10.1016/j.rse.2012.03.018

García-Haro, F. J., Campos-Taberner, M., Muñoz-Marí, J., Laparra, V., Camacho, F., Sánchez-Zapero, J., & Camps-Valls, G. (2018). Derivation of global vegetation biophysical parameters from EUMETSAT Polar System. *ISPRS Journal of Photogrammetry and Remote Sensing*, *139*, 57–74. https://doi.org/10.1016/j.isprsjprs.2018.03.005

Garrigues, S., Allard, D., Baret, F., & Weiss, M. (2006a). Influence of landscape spatial heterogeneity on the non-linear estimation of leaf area index from moderate spatial resolution remote sensing data. *Remote Sensing of Environment*, *105*(4), 286–298.

Garrigues, S., Allard, D., Baret, F., & Weiss, M. (2006b). Quantifying spatial heterogeneity at the landscape scale using variogram models. *Remote Sensing of Environment*, *103*, 81–96.

Garrigues, S., Allard, D., Weiss, M., Baret, F., Marni, S., & Jeanjean, H. (2001). Influence of spatial heterogeneity and scaling on leaf areda index estimates from remote sensing data. Paper presented at the 1st Int. Symp. Recent Advances on Quantitative Remote Sensing, Valencia, Spain.

Garrigues, S., Lacaze, R., Baret, F., Morisette, J. T., Weiss, M., Nickeson, J. E., et al. (2008). Validation and intercomparison of global Leaf Area Index products derived from remote sensing data. *Journal of Geophysical Research*, *113*, G02028. https://doi.org/10.1029/2007JG000635

Garrigues, S., Shabanov, N., Swanson, K., Morisette, J. T., Baret, F., & Myneni, R. (2008). Intercomparison and sensitivity analysis of leaf area index retrievals from LAI-2000, AccuPAR, and digital hemispherical photography over croplands. *Agricultural and Forest Meteorology*, *148*, 1193–1209.

Gascon, F., Gastellu-Etchegorry, J. P., Lefevre-Fonollosa, M. J., & Dufrene, E. (2004). Retrieval of forest biophysical variables by inverting a 3-D radiative transfer model and using high and very high resolution imagery. *International Journal of Remote Sensing*, *25*(24), 5601–5616.

Gastellu-Etchegorry, J. P., Martin, E., & Gascon, F. (2004). DART: A 3D model for simulating satellite images and studying surface radiation budget. *International Journal of Remote Sensing*, *25*(1), 73–96.

Gastellu-Etchegorry, J.-P., Yin, T., Lauret, N., Cajgfinger, T., Gregoire, T., Grau, E., et al. (2015). Discrete Anisotropic Radiative Transfer (DART 5) for modeling airborne and satellite spectroradiometer and LIDAR acquisitions of natural and urban landscapes. *Remote Sensing*, *7*(2), 1667–1701. https://doi.org/10.3390/rs70201667

Gastellu-Etchegorry, J.-P., Yin, T., Lauret, N., Grau, E., Rubio, J., Cook, B. D., et al. (2016). Simulation of satellite, airborne and terrestrial LiDAR with DART (I): Waveform simulation with quasi-Monte Carlo ray tracing. *Remote Sensing of Environment*, *184*, 418–435. https://doi.org/10.1016/j.rse.2016.07.010

GCOS. (2011). Systematic observation requirements for satellite-based products for climate, 2011 Update, Supplemental Details to the Satellite-Based Component of the Implementation Plan for the Global Observing System for Climate in Support of the UNFCCC (2010 Update). Retrieved from http://www.wmo.int/pages/prog/gcos/Publications/gcos-154.pdf

GCOS. (2016). The global observing system for climate: Implementation needs (GCOS-200). Retrieved from https://library.wmo.int/opac/doc_num.php?explnum_id=3417

Ge, J., Qi, J., & Lofgren, B. (2008). Use of vegetation properties from EOS observations for land-climate modeling in East Africa. *Journal of Geophysical Research*, *113*, D15101. https://doi.org/10.1029/2007JD009628

Gemmel, F., & McDonald, J. (2000). View zenith angle effects on the forest information content of three spectral indices. *Remote Sensing of Environment*, *72*, 139–158.

Geng, L., Ma, M., Wang, X., Yu, W., Jia, S., & Wang, H. (2014). Comparison of eight techniques for reconstructing multi-satellite sensor time-series NDVI data sets in the Heihe River Basin, China. *Remote Sensing*, *6*(3), 2024–2049.

Gessner, U., Niklaus, M., Kuenzer, C., & Dech, S. (2013). Intercomparison of leaf area index products for a gradient of sub-humid to arid environments in West Africa. *Remote Sensing*, *5*(3), 1235–1257.

Ghilain, N., Arboleda, A., Sepulcre-Canto, G., Batelaan, O., Ardo, J., & Gellens-Meulenberghs, F. (2012). Improving evapotranspiration in a land surface model using biophysical variables derived from MSG/SEVIRI satellite. *Hydrology and Earth System Sciences*, *16*(8), 2567–2583. https://doi.org/10.5194/hess-16-2567-2012

Ghilain, N., De Roo, F., & Gellens-Meulenberghs, F. (2014). Evapotranspiration monitoring with Meteosat Second Generation satellites: Improvement opportunities from moderate spatial resolution satellites for vegetation. *International Journal of Remote Sensing*, *35*(7), 2654–2670. https://doi.org/10.1080/01431161.2014.883093

Gibelin, A. L., Calvet, J. C., Roujean, J. L., Jarlan, L., & Los, S. O. (2006). Ability of the land surface model ISBA-A-gs to simulate leaf area index at the global scale: Comparison with satellites products. *Journal of Geophysical Research*, *111*, D18102. https://doi.org/10.1029/2005JD006691

Gitelson, A. A. (2004). Wide dynamic range vegetation index for remote quantification of biophysical characteristics of vegetation. *Journal of Plant Physiology*, *161*, 165–173.

Gitelson, A. A., Gamon, J. A., & Solovchenko, A. (2017). Multiple drivers of seasonal change in PRI: Implications for photosynthesis 2. Stand level. *Remote Sensing of Environment*, *190*, 198–206. https://doi.org/10.1016/j.rse.2016.12.015

Gobron, N., & Verstraete, M. M. (2009). Assessment of the status of the development of the standards for the terrestrial essential climate variables: Leaf area index (LAI). Retrieved from http://www.fao.org/gtos/doc/ECVs/T11/T11.pdf

Goel, N. S., & Thompson, R. L. (2000). A snapshot of canopy reflectance models and a universal model for the radiation regime. *Remote Sensing Reviews*, *18*, 197–225.

Gonsamo, A., & Chen, J. M. (2011). Evaluation of the GLC2000 and NALC2005 land cover products for LAI retrieval over Canada. *Canadian Journal of Remote Sensing*, *37*(3), 302–313. https://doi.org/10.5589/m11-039

Gonsamo, A., & Chen, J. M. (2014). Improved LAI algorithm implementation to MODIS data by incorporating background, topography, and foliage clumping information. *IEEE Transactions on Geoscience and Remote Sensing*, *52*(2), 1076–1088. https://doi.org/10.1109/tgrs.2013.2247405

Gonsamo, A., & Pellikka, P. (2008). Methodology comparison for slope correction in canopy leaf area index estimation using hemispherical photography. *Forest Ecology and Management*, *256*(4), 749–759. https://doi.org/10.1016/j.foreco.2008.05.032

Gonsamo, A., & Pellikka, P. (2009). The computation of foliage clumping index using hemispherical photography. *Agricultural and Forest Meteorology*, *149*(10), 1781–1787. https://doi.org/10.1016/j.agrformet.2009.06.001

Gonsamo, A., Walter, J. M. N., & Pellikka, P. (2011). CIMES: A package of programs for determining canopy geometry and solar radiation regimes through hemispherical photographs. *Computers and Electronics in Agriculture*, *79*(2), 207–215. https://doi.org/10.1016/j.compag.2011.10.001

González-Sanpedro, M. C., Le Toan, T., Moreno, J., Kergoat, L., & Rubio, E. (2008). Seasonal variations of leaf area index of agricultural fields retrieved from Landsat data. *Remote Sensing of Environment*, *112*(3), 810–824.

Gower, S. T., Kucharik, C. J., & Norman, J. M. (1999). Direct and indirect estimation of leaf area index, fAPAR, and net primary production of terrestrial ecosystems. *Remote Sensing of Environment*, *70*, 29–51.

Griebel, A., Bennett, L. T., Culvenor, D. S., Newnham, G. J., & Arndt, S. K. (2015). Reliability and limitations of a novel terrestrial laser scanner for daily monitoring of forest canopy dynamics. *Remote Sensing of Environment*, *166*, 205–213. https://doi.org/10.1016/j.rse.2015.06.014

Groenendijk, M., Dolman, A. J., Ammann, C., Arneth, A., Cescatti, A., Dragoni, D., et al. (2011). Seasonal variation of photosynthetic model parameters and leaf area index from global Fluxnet eddy covariance data. *Journal of Geophysical Research*, *116*, G04027. https://doi.org/10.1029/2011JG001742

Gu, Y., Bélair, S., Mahfouf, J.-F., & Deblonde, G. (2006). Optimal interpolation analysis of leaf area index using MODIS data. *Remote Sensing of Environment*, *104*(3), 283–296.

Gu, Z., Ju, W., Liu, Y., Li, D., & Fan, W. (2012). Applicability of spectral and spatial information from IKONOS-2 imagery in retrieving leaf area index of forests in the urban area of Nanjing, China. *Journal of Applied Remote Sensing*, *6*. https://doi.org/10.1117/1.JRS.6.063556

Guan, K., Medvigy, D., Wood, E. F., Caylor, K. K., Li, S., & Jeong, S. J. (2014). Deriving vegetation phenological time and trajectory information over Africa using SEVIRI Daily LAI. *IEEE Transactions on Geoscience and Remote Sensing*, *52*(2), 1113–1130. https://doi.org/10.1109/tgrs.2013.2247611

Guillevic, P., Koster, R. D., Suarez, M. J., Bounoua, L., Collatz, G. J., Los, S. O., & Mahanama, S. P. P. (2002). Influence of the interannual variability of vegetation on the surface energy balance—A global sensitivity study. *Journal of Hydrometeorology*, *3*(6), 617–629. https://doi.org/10.1175/1525-7541(2002)003<0617:iotivo>2.0.co;2

Guindin-Garcia, N. (2010). Estimating maize grain yield from crop biophysical parameters using remote sensing. (Ph.D.), University of Nebraska-Lincon. Retrieved from. http://digitalcommons.unl.edu/agronhortdiss/21/

Guindin-Garcia, N., Gitelson, A. A., Arkebauer, T. J., Shanahan, J., & Weiss, A. (2012). An evaluation of MODIS 8- and 16-day composite products for monitoring maize green leaf area index. *Agricultural and Forest Meteorology*, *161*, 15–25. https://doi.org/10.1016/j.agrformet.2012.03.012

Guo, L. B., Wang, J. D., Xiao, Z. Q., Zhou, H. M., & Song, J. L. (2014). Data-based mechanistic modelling and validation for leaf area index estimation using multi-angular remote-sensing observation time series. *International Journal of Remote Sensing*, *35*(13), 4655–4672. https://doi.org/10.1080/01431161.2014.919683

Guo, Q., Su, Y., Hu, T., Zhao, X., Wu, F., Li, Y., et al. (2017). An integrated UAV-borne lidar system for 3D habitat mapping in three forest ecosystems across China. *International Journal of Remote Sensing*, *38*(8-10), 2954–2972. https://doi.org/10.1080/01431161.2017.1285083

Haboudane, D., Miller, J. R., Pattey, E., Zarco-Tejada, P. J., & Strachan, I. B. (2004). Hyperspectral vegetation indices and novel algorithms for predicting green LAI of crop canopies: Modeling and validation in the context of precision agriculture. *Remote Sensing of Environment*, *90*, 337–352.

Hadria, R., Duchemin, B., Lahrouni, A., Khabba, S., Er-raki, S., Dedieu, G., et al. (2006). Monitoring of irrigated wheat in a semi-arid climate using crop modelling and remote sensing data: Impact of satellite revisit time frequency. *International Journal of Remote Sensing*, *27*(6), 1093–1117. https://doi.org/10.1080/01431160500382980

Hagolle, O., Lobo, A., Maisongrande, P., Cabot, F., Duchemin, B., & De Pereyra, A. (2005). Quality assessment and improvement of temporally composited products of remotely sensed imagery by combination of VEGETATION 1 and 2 images. *Remote Sensing of Environment*, *94*(2), 172–186. https://doi.org/10.1016/j.rse.2004.09.008

Hall, F. G., Bergen, K., Blair, J. B., Dubayah, R., Houghton, R., Hurtt, G., et al. (2011). Characterizing 3D vegetation structure from space: Mission requirements. *Remote Sensing of Environment*, *115*(11), 2753–2775. https://doi.org/10.1016/j.rse.2011.01.024

Hancock, S., Essery, R., Reid, T., Carle, J., Baxter, R., Rutter, N., & Huntley, B. (2014). Characterising forest gap fraction with terrestrial lidar and photography: An examination of relative limitations. *Agricultural and Forest Meteorology*, *189–190*, 105–114. https://doi.org/10.1016/j.agrformet.2014.01.012

Hantson, S., & Chuvieco, E. (2011). Evaluation of different topographic correction methods for Landsat imagery. *International Journal of Applied Earth Observation and Geoinformation*, *13*(5), 691–700. https://doi.org/10.1016/j.jag.2011.05.001

Hapke, B. (1981). Bidirectional reflectance spectroscopy 1. Theory. *Journal of Geophysical Research*, *86*(B4), 3039–3054.
He, L., Liu, J., Chen, J. M., Croft, H., Wang, R., Sprintsin, M., et al. (2016). Inter- and intra-annual variations of clumping index derived from the MODIS BRDF product. *International Journal of Applied Earth Observation and Geoinformation*, *44*, 53–60. https://doi.org/10.1016/j.jag.2015.07.007
Heiskanen, J., Rautiainen, M., Korhonen, L., Mõttus, M., & Stenberg, P. (2011). Retrieval of boreal forest LAI using a forest reflectance model and empirical regressions. *International Journal of Applied Earth Observation and Geoinformation*, *13*(4), 595–606. https://doi.org/10.1016/j.jag.2011.03.005
Heiskanen, J., Rautiainen, M., Stenberg, P., Eigemeier, E., Majasalmi, T., Mõttus, M., & Vesanto, V.-H. (2012). Narrowband vegetation indices in boreal forest LAI estimation: The effect of reflectance seasonality. *Geophysical Research Abstracts, 14*(EGU2012-8856-1). Retrieved from http://adsabs.harvard.edu/abs/2012EGUGA..14.8856H
Heiskanen, J., Rautiainen, M., Stenberg, P., Mõttus, M., Vesanto, V.-H., Korhonen, L., & Majasalmi, T. (2012). Seasonal variation in MODIS LAI for a boreal forest area in Finland. *Remote Sensing of Environment*, *126*, 104–115. https://doi.org/10.1016/j.rse.2012.08.001
Heumann, B. W., Seaquist, J. W., Eklundh, L., & Jönsson, P. (2007). AVHRR derived phenological change in the Sahel and Soudan, Africa, 1982-2005. *Remote Sensing of Environment*, *108*(4), 385–392.
Hilker, T., Coops, N. C., Hall, F. G., Nichol, C. J., Lyapustin, A., Black, T. A., et al. (2011). Inferring terrestrial photosynthetic light use efficiency of temperate ecosystems from space. *Journal of Geophysical Research*, *116*, G03014. https://doi.org/10.1029/2011JG001692
Hilker, T., Lyapustin, A. I., Tucker, C. J., Sellers, P. J., Hall, F. G., & Wang, Y. (2012). Remote sensing of tropical ecosystems: Atmospheric correction and cloud masking matter. *Remote Sensing of Environment*, *127*, 370–384. https://doi.org/10.1016/j.rse.2012.08.035
Hilker, T., Wulder, M. A., & Coops, N. C. (2008). Update of forest inventory data with lidar and high spatial resolution satellite imagery. *Canadian Journal of Remote Sensing*, *34*(1), 5–12. https://doi.org/10.5589/m08-004
Hill, M. J., Senarath, U., Lee, A., Zeppel, M., Nightingale, J. M., Williams, R. D. J., & McVicar, T. R. (2006). Assessment of the MODIS LAI product for Australian ecosystems. *Remote Sensing of Environment*, *101*, 495–518.
Hird, J. N., & McDermid, G. J. (2009). Noise reduction of NDVI time series: An empirical comparison of selected techniques. *Remote Sensing of Environment*, *113*(1), 248–258. http://doi.org/10.1016/j.rse.2008.09.003
Homem Antunes, M. A., Walter-Shea, E. A., & Mesarch, M. A. (2001). Test of an extended mathematical approach to calculate maize leaf area index and leaf angle distribution. *Agricultural and Forest Meteorology*, *108*(1), 45–53. https://doi.org/10.1016/S0168-1923(01)00219-2
Hopkinson, C., Lovell, J., Chasmer, L., Jupp, D., Kljun, N., & van Gorsel, E. (2013). Integrating terrestrial and airborne lidar to calibrate a 3D canopy model of effective leaf area index. *Remote Sensing of Environment*, *136*, 301–314. https://doi.org/10.1016/j.rse.2013.05.012
Hosseini, M., McNairn, H., Merzouki, A., & Pacheco, A. (2015). Estimation of leaf area index (LAI) in corn and soybeans using multi-polarization C- and L-band radar data. *Remote Sensing of Environment*, *170*, 77–89. https://doi.org/10.1016/j.rse.2015.09.002
Houborg, R., Anderson, M., & Daughtry, C. (2009). Utility of an image-based canopy reflectance modeling tool for remote estimation of LAI and leaf chlorophyll content at the field scale. *Remote Sensing of Environment*, *113*(1), 259–274. https://doi.org/10.1016/j.rse.2008.09.014
Houborg, R., & Boegh, E. (2008). Mapping leaf chlorophyll and leaf area index using inverse and forward canopy reflectance modeling and SPOT reflectance data. *Remote Sensing of Environment*, *112*(1), 186–202.
Houborg, R., McCabe, M., Cescatti, A., Gao, F., Schull, M., & Gitelson, A. (2015). Joint leaf chlorophyll content and leaf area index retrieval from Landsat data using a regularized model inversion system (REGFLEC). *Remote Sensing of Environment*, *159*(0), 203–221. https://doi.org/10.1016/j.rse.2014.12.008
Houborg, R., McCabe, M. F., & Gao, F. (2016). A Spatio-Temporal Enhancement Method for medium resolution LAI (STEM-LAI). *International Journal of Applied Earth Observation and Geoinformation*, *47*, 15–29. https://doi.org/10.1016/j.jag.2015.11.013
Houborg, R., Soegaard, H., & Boegh, E. (2007). Combining vegetation index and model inversion methods for the extraction of key vegetation biophysical parameters using Terra and Aqua MODIS reflectance data. *Remote Sensing of Environment*, *106*(1), 39–58.
Hu, B., Miller, J. R., Chen, J. M., & Hollinger, A. (2004). Retrieval of the canopy leaf area index in the BOREAS flux tower sites using linear spectral mixture analysis. *Remote Sensing of Environment*, *89*(2), 176–188.
Hu, J., Tan, B., Shabanov, N., Crean, K. A., Martonchik, J. V., Diner, D. J., et al. (2003). Performance of the MISR LAI and FPAR algorithm: A case study in Africa. *Remote Sensing of Environment*, *88*(3), 324–340. https://doi.org/10.1016/j.rse.2003.05.002
Hu, Z., & Islam, S. (1997). A framework for analyzing and designing scale invariant remote sensing algorithms. *IEEE Transactions on Geoscience and Remote Sensing*, *35*(3), 747–755.
Huang, D., Knyazikhin, Y., Wang, W., Deering, D. W., Stenberg, P., Shabanov, N., et al. (2008). Stochastic transport theory for investigating the three-dimensional canopy structure from space measurements. *Remote Sensing of Environment*, *112*(1), 35–50. https://doi.org/10.1016/j.rse.2006.05.026
Huang, H., Qin, W., & Liu, Q. (2013). RAPID: A Radiosity Applicable to Porous IndiviDual Objects for directional reflectance over complex vegetated scenes. *Remote Sensing of Environment*, *132*, 221–237. https://doi.org/10.1016/j.rse.2013.01.013
Huang, H., Zhang, Z., Ni, W., Chai, L., Qin, W., Liu, G., et al. (2018). Extending RAPID model to simulate forest microwave backscattering. *Remote Sensing of Environment*, *217*, 272–291. https://doi.org/10.1016/j.rse.2018.08.011
Huang, X., Jiao, Z., Dong, Y., Zhang, H., & Li, X. (2013). Analysis of BRDF and albedo retrieved by Kernel-driven models using field measurements. *IEEE Journal of Selected Topics in Applied Earth Observations and Remote Sensing*, *6*(1), 149–161. https://doi.org/10.1109/jstars.2012.2208264
Huete, A., Didan, K., Miura, T., Rodriguez, E. P., Gao, X., & Ferreira, L. G. (2002). Overview of the radiometric and biophysical performance of the MODIS vegetation indices. *Remote Sensing of Environment*, *83*(1-2), 195–213.
Huete, A. R. (1988). A soil-adjusted vegetation index (SAVI). *Remote Sensing of Environment*, *25*, 295–309.
Hyde, P., Dubayah, R., Peterson, B., Blair, J. B., Hofton, M., Hunsaker, C., et al. (2005). Mapping forest structure for wildlife habitat analysis using waveform lidar: Validation of montane ecosystems. *Remote Sensing of Environment*, *96*(3-4), 427–437. https://doi.org/10.1016/j.rse.2005.03.005
Iio, A., Hikosaka, K., Anten, N. P. R., Nakagawa, Y., & Ito, A. (2014). Global dependence of field-observed leaf area index in woody species on climate: A systematic review. *Global Ecology and Biogeography*, *23*(3), 274–285. https://doi.org/10.1111/geb.12133
Imbach, P., Molina, L., Locatelli, B., Roupsard, O., Ciais, P., Corrales, L., & Mahé, G. (2010). Climatology-based regional modelling of potential vegetation and average annual long-term runoff for Mesoamerica. *Hydrology and Earth System Sciences*, *14*(10), 1801–1817. https://doi.org/10.5194/hess-14-1801-2010
Inoue, Y., Sakaiya, E., & Wang, C. (2014). Capability of C-band backscattering coefficients from high-resolution satellite SAR sensors to assess biophysical variables in paddy rice. *Remote Sensing of Environment*, *140*(0), 257–266. https://doi.org/10.1016/j.rse.2013.09.001

Inoue, Y., Uratsuka, S., Kozu, T., Dabrowska-Zielinska, K., Qi, J., Kurosu, T., & Maeno, H. (2002). Season-long daily measurements of multifrequency (Ka, Ku, X, C, and L) and full-polarization backscatter signatures over paddy rice field and their relationship with biological variables. *Remote Sensing of Environment*, *81*(2-3), 194–204.

Iwata, H., Ueyama, M., Iwama, C., & Harazono, Y. (2013). A variation in the fraction of absorbed photosynthetically active radiation and a comparison with MODIS data in burned black spruce forests of interior Alaska. *Polar Science*, *7*, 113–124.

Jacquemoud, S. (1993). Inversion of the PROSPECT+SAIL canopy reflectance models from AVIRIS equivalent spectra: theoretical study. *Remote Sensing of Environment*, *44*, 281–292.

Jacquemoud, S., & Baret, F. (1990). PROSPECT: A model of leaf optical properties spectra. *Remote Sensing of Environment*, *34*(2), 75–91.

Jacquemoud, S., Baret, F., & Hanocq, J. F. (1992). Modeling spectral and bidirectional soil reflectance. *Remote Sensing of Environment*, *41*(2-3), 123–132.

Jacquemoud, S., Verhoef, W., Baret, F., Bacour, C., Zarco-Tejada, P. J., Asner, G. P., et al. (2009). PROSPECT + SAIL models: A review of use for vegetation characterization. *Remote Sensing of Environment*, *113*(Supplement 1), S56–S66. https://doi.org/10.1016/j.rse.2008.01.026

Jarlan, L., Balsamo, G., Lafont, S., Beljaars, A., Calvet, J. C., & Mougin, E. (2008). Analysis of leaf area index in the ECMWF land surface model and impact on latent heat and carbon fluxes: Application to West Africa. *Journal of Geophysical Research*, *113*, D24117. https://doi.org/10.1029/2007JD009370

Jégo, G., Pattey, E., & Liu, J. (2012). Using leaf area index, retrieved from optical imagery, in the STICS crop model for predicting yield and biomass of field crops. *Field Crops Research*, *131*, 63–74. https://doi.org/10.1016/j.fcr.2012.02.012

Jensen, J. L. R., Humes, K. S., Hudak, A. T., Vierling, L. A., & Delmelle, E. (2011). Evaluation of the MODIS LAI product using independent lidar-derived LAI: A case study in mixed conifer forest. *Remote Sensing of Environment*, *115*(12), 3625–3639. https://doi.org/10.1016/j.rse.2011.08.023

Jensen, J. L. R., Humes, K. S., Vierling, L. A., & Hudak, A. T. (2008). Discrete return lidar-based prediction of leaf area index in two conifer forests. *Remote Sensing of Environment*, *112*(10), 3947–3957.

Jiang, C., Ryu, Y., Fang, H., Myneni, R., Claverie, M., & Zhu, Z. (2017). Inconsistencies of interannual variability and trends in long-term satellite leaf area index products. *Global Change Biology*. https://doi.org/10.1111/gcb.13787

Jiapaer, G., Yi, Q., Yao, F., & Zhang, P. (2017). Comparison of non-destructive LAI determination methods and optimization of sampling schemes in an open Populus euphratica ecosystem. *Urban Forestry & Urban Greening*, *26*(Supplement C), 114–123. https://doi.org/10.1016/j.ufug.2017.06.010

Jin, H. A., Li, A. N., Bian, J. H., Nan, X., Zhao, W., Zhang, Z. J., & Yin, G. F. (2017). Intercomparison and validation of MODIS and GLASS leaf area index (LAI) products over mountain areas: A case study in southwestern China. *International Journal of Applied Earth Observation and Geoinformation*, *55*, 52–67. https://doi.org/10.1016/j.jag.2016.10.008

Jin, H. X., & Eklundh, L. (2014). A physically based vegetation index for improved monitoring of plant phenology. *Remote Sensing of Environment*, *152*, 512–525. https://doi.org/10.1016/j.rse.2014.07.010

Jin, X. L., Kumar, L., Li, Z. H., Feng, H. K., Xu, X. G., Yang, G. J., & Wang, J. H. (2018). A review of data assimilation of remote sensing and crop models. *European Journal of Agronomy*, *92*, 141–152. https://doi.org/10.1016/j.eja.2017.11.002

Johansen, K., & Phinn, S. (2006). Mapping structural parameters and species composition of riparian vegetation Using IKONOS and Landsat ETM+ data in Australian Tropical Savannahs. *Photogrammetric Engineering and Remote Sensing*, *72*(1), 71–80.

Jonckheere, I., Fleck, S., Nackaerts, K., Muys, B., Coppin, P., Weiss, M., & Baret, F. (2004). Review of methods for in situ leaf area index determination part I. Theories, sensors and hemispherical photography. *Agricultural and Forest Meteorology*, *121*(1-2), 19–35.

Jongschaap, R. E. E. (2006). Run-time calibration of simulation models by integrating remote sensing estimates of leaf area index and canopy nitrogen. *European Journal of Agronomy*, *24*(4), 316–324.

Jönsson, P., & Eklundh, L. (2002). Seasonality extraction by function fitting to time-series of satellite sensor data. *IEEE Transactions on Geoscience and Remote Sensing*, *40*(8), 1824–1832.

Julien, Y., & Sobrino, J. A. (2010). Comparison of cloud-reconstruction methods for time series of composite NDVI data. *Remote Sensing of Environment*, *114*(3), 618–625.

Jupp, D. L. B., Culvenor, D. S., Lovell, J. L., Newnham, G. J., Strahler, A. H., & Woodcock, C. E. (2009). Estimating forest LAI profiles and structural parameters using a ground-based laser called 'Echidna®☆. *Tree Physiology*, *29*(2), 171–181. https://doi.org/10.1093/treephys/tpn022

Kala, J., Decker, M., Exbrayat, J. F., Pitman, A. J., Carouge, C., Evans, J. P., et al. (2014). Influence of leaf area index prescriptions on simulations of heat, moisture, and carbon fluxes. *Journal of Hydrometeorology*, *15*(1), 489–503. https://doi.org/10.1175/jhm-d-13-063.1

Kalácska, M., Calvo-Alvarado, J. C., Journet, A. R. P., Arroyo-Mora, J. P., Ortiz-Ortiz, D., Sánchez-Azofeifa, G. A., & Rivard, B. (2004). Leaf area index measurements in a tropical moist forest: A case study from Costa Rica. *Remote Sensing of Environment*, *91*(2), 134–152.

Kalácska, M., Calvo-Alvarado, J. C., & Sánchez-Azofeifa, G. A. (2005). Calibration and assessment of seasonal changes in leaf area index of a tropical dry forest in different stages of succession. *Tree Physiology*, *25*, 733–744.

Kamal, M., Phinn, S., & Johansen, K. (2016). Assessment of multi-resolution image data for mangrove leaf area index mapping. *Remote Sensing of Environment*, *176*, 242–254. https://doi.org/10.1016/j.rse.2016.02.013

Kandasamy, S., Baret, F., Verger, A., Neveux, P., & Weiss, M. (2013). A comparison of methods for smoothing and gap filling time series of remote sensing observations—Application to MODIS LAI products. *Biogeosciences*, *10*(6), 4055–4071. https://doi.org/10.5194/bg-10-4055-2013

Kandasamy, S., Verger, A., & Baret, F. (2017). Assessment of three methods for near real-time estimation of leaf area index from AVHRR data. *IEEE Transactions on Geoscience and Remote Sensing*, *55*(3), 1489–1497. https://doi.org/10.1109/TGRS.2016.2626307

Kang, H.-S., Xue, Y., & Collatz, G. J. (2007). Impact assessment of satellite-derived leaf area index datasets using a general circulation model. *Journal of Climate*, *20*(6), 993–1015. https://doi.org/10.1175/jcli4054.1

Kang, Y., Özdoğan, M., Zipper, S., Román, M., Walker, J., Hong, S., et al. (2016). How universal is the relationship between remotely sensed vegetation indices and crop leaf area index? A global assessment. *Remote Sensing*, *8*(7), 597. https://doi.org/10.3390/rs8070597

Kaptue Tchuente, A. T., Roujean, J.-L., & Faroux, S. (2010). ECOCLIMAP-II: An ecosystem classification and land surface parameters database of Western Africa at 1 km resolution for the African Monsoon Multidisciplinary Analysis (AMMA) project. *Remote Sensing of Environment*, *114*(5), 961–976. https://doi.org/10.1016/j.rse.2009.12.008

Kaufman, Y. J., & Tanré, D. (1992). Atmospherically Resistant Vegetation Index (ARVI) for EOS-MODIS. *IEEE Transaction of Geoscience and Remote Sensing*, *30*, 261–270.

Kimes, D. S., Knyazikhin, Y., Privette, J. L., Abuelgasim, A. A., & Gao, F. (2000). Inversion methods for physically-based models. *Remote Sensing Reviews*, *18*, 381–440.

Kimura, R., Kamichika, M., Okada, S., & Miura, H. (2004). Relationships among the leaf area index, moisture availability, and spectral reflectance in an upland rice field. *Agricultural Water Management*, *69*(2), 83–100.
Kira, O., Nguy-Robertson, A. L., Arkebauer, T. J., Linker, R., & Gitelson, A. A. (2016). Informative spectral bands for remote green LAI estimation in C3 and C4 crops. *Agricultural and Forest Meteorology*, *218–219*, 243–249. https://doi.org/10.1016/j.agrformet.2015.12.064
Knote, C., Bonafe, G., & Giuseppe, F. D. (2009). Leaf area index specification for use in mesoscale weather prediction systems. *Monthly Weather Review*, *137*, 3535–3550. https://doi.org/10.1175/2009MWR2891.1
Knyazikhin, Y., Glassy, J., Privette, J. L., Tian, Y., Lotsch, A., Zhang, Y., et al. (1999). MODIS leaf area index (LAI) and Fraction of Photosynthetically Active Radiation Absorbed by Vegetation (FPAR) product (MOD15) algorithm theoretical basis document. Retrieved from http://modis.gsfc.nasa.gov/data/atbd/land_atbd.php
Kobayashi, H., Delbart, N., Suzuki, R., & Kushida, K. (2010). A satellite-based method for monitoring seasonality in the overstory leaf area index of Siberian larch forest. *Journal of Geophysical Research*, *115*, G01002. https://doi.org/10.1029/2009JG000939
Kobayashi, H., Suzuki, R., & Kobayashi, S. (2007). Reflectance seasonality and its relation to the canopy leaf area index in an eastern Siberian larch forest: Multi-satellite data and radiative transfer analyses. *Remote Sensing of Environment*, *106*(2), 238–252. https://doi.org/10.1016/j.rse.2006.08.011
Koetz, B., Baret, F., Poilvé, H., & Hill, J. (2005). Use of coupled canopy structure dynamic and radiative transfer models to estimate biophysical canopy characteristics. *Remote Sensing of Environment*, *95*(1), 115–124.
Koetz, B., Morsdorf, F., Sun, G., Ranson, K. J., Itten, K., & Allgower, B. (2006). Inversion of a lidar waveform model for forest biophysical parameter estimation. *IEEE Geoscience and Remote Sensing Letters*, *3*(1), 49–53.
Koetz, B., Sun, G., Morsdorf, F., Ranson, K. J., Kneubuhler, M., Itten, K., & Allgower, B. (2007). Fusion of imaging spectrometer and LIDAR data over combined radiative transfer models for forest canopy characterization. *Remote Sensing of Environment*, *106*(4), 449–459.
Kolari, P., Lappalainen, H. K., Hanninen, H., & Hari, P. (2007). Relationship between temperature and the seasonal course of photosynthesis in Scots pine at northern timberline and in southern boreal zone. *Tellus Series B: Chemical and Physical Meteorology*, *59*(3), 542–552. https://doi.org/10.1111/j.1600-0889.2007.00262.x
Korhonen, L., Korpela, I., Heiskanen, J., & Maltamo, M. (2011). Airborne discrete-return LIDAR data in the estimation of vertical canopy cover, angular canopy closure and leaf area index. *Remote Sensing of Environment*, *115*(4), 1065–1080. https://doi.org/10.1016/j.rse.2010.12.011
Kötz, B., Baret, F., Poilvé, H., & Hill, J. (2005). Use of coupled canopy structure dynamic and radiative transfer models to estimate biophysical canopy characteristics. *Remote Sensing of Environment*, *95*, 115–124.
Kouadio, L., Duveiller, G., Djaby, B., El Jarroudi, M., Defourny, P., & Tychon, B. (2012). Estimating regional wheat yield from the shape of decreasing curves of green area index temporal profiles retrieved from MODIS data. *International Journal of Applied Earth Observation and Geoinformation*, *18*, 111–118. https://doi.org/10.1016/j.jag.2012.01.009
Kraus, T., Schmidt, M., Dech, S. W., & Samimi, C. (2009). The potential of optical high resolution data for the assessment of leaf area index in East African rainforest ecosystems. *International Journal of Remote Sensing*, *30*(19), 5039–5059.
Kumagai, T. o., Ichie, T., Yoshimura, M., Yamashita, M., Kenzo, T., Saitoh, T. M., et al. (2006). Modeling CO_2 exchange over a Bornean tropical rain forest using measured vertical and horizontal variations in leaf-level physiological parameters and leaf area densities. *Journal of Geophysical Research*, *111*, D10107. https://doi.org/10.1029/2005JD006676
Kumar, V., Kumari, M., & Saha, S. K. (2013). Leaf area index estimation of lowland rice using semi-empirical backscattering model. *Journal of Applied Remote Sensing*, *7*(1), 073474–073474. https://doi.org/10.1117/1.jrs.7.073474
Kuusk, A. (1998). Monitoring of vegetation parameters on large areas by the inversion of a canopy reflectance model. *International Journal of Remote Sensing*, *19*(15), 2893–2905.
Kuusk, A. (2001). A two-layer canopy reflectance model. *Journal of Quantitative Spectroscopy and Radiative Transfer*, *71*(1), 1–9.
Kuusk, A., & Nilson, T. (2000). A directional multispectral forest reflectance model. *Remote Sensing of Environment*, *72*(2), 244–252.
Lacaze, R., Chen, J. M., Roujean, J. L., & Leblanc, S. G. (2002). Retrieval of vegetation clumping index using hot spot signatures measured by POLDER instrument. *Remote Sensing of Environment*, *79*(1), 84–95.
Lacherade, S., Fougnie, B., Henry, P., & Gamet, P. (2013). Cross calibration over desert sites: Description, methodology, and operational implementation. *IEEE Transactions on Geoscience and Remote Sensing*, *51*(3), 1098–1113.
Lafont, S., Zhao, Y., Calvet, J. C., Peylin, P., Ciais, P., Maignan, F., & Weiss, M. (2012). Modelling LAI, surface water and carbon fluxes at high-resolution over France: Comparison of ISBA-A-gs and ORCHIDEE. *Biogeosciences*, *9*(1), 439–456. https://doi.org/10.5194/bg-9-439-2012
Lang, A. R. G. (1987). Simplified estimate of leaf area index from transmittance of the Sun's beam. *Agricultural and Forest Meteorology*, *41*, 179–186.
Lang, A. R. G., McMurtrie, R. E., & Benson, M. L. (1991). Validity of surface area indices of Pinus radiata estimated from transmittance of the sun's beam. *Agricultural and Forest Meteorology*, *57*(1–3), 157–170. https://doi.org/10.1016/0168-1923(91)90084-4
Lang, A. R. G., & Xiang, Y. (1986). Estimation of leaf area index from transmission of direct sunlight in discontinuous canopies. *Agricultural and Forest Meteorology*, *37*(3), 229–243. https://doi.org/10.1016/0168-1923(86)90033-x
Laurent, V. C. E., Schaepman, M. E., Verhoef, W., Weyermann, J., & Chávez, R. O. (2014). Bayesian object-based estimation of LAI and chlorophyll from a simulated Sentinel-2 top-of-atmosphere radiance image. *Remote Sensing of Environment*, *140*(0), 318–329. https://doi.org/10.1016/j.rse.2013.09.005
Laurent, V. C. E., Verhoef, W., Schaepman, M. E., Damm, A., & Clevers, J. G. P. W. (2012). Mapping LAI and chlorophyll content from at-sensor APEX data using a Bayesian optimization of a coupled canopy-atmosphere model. Paper presented at the IGARSS, Munich, Germany.
Lauvernet, C., Baret, F., Hascoët, L., Buis, S., & Le Dimet, F. X. (2008). Multitemporal-patch ensemble inversion of coupled surface-atmosphere radiative transfer models for land surface characterization. *Remote Sensing of Environment*, *112*(3), 851–861.
Law, B. E., van Tuyl, S., & Baldocchi, D. D. (2001). Estimation of leaf area index in open-canopy ponderosa pine forests at different successional stages and management regimes in Oregon. *Agricultural and Forest Meteorology*, *108*(1), 1–14.
Law, B. E., & Waring, R. H. (1994). Remote sensing of leaf area index and radiation intercepted by understory vegetation. *Ecological Applications*, *4*(2), 272–279. https://doi.org/10.2307/1941933
Lawrence, P. J., & Chase, T. N. (2007). Representing a new MODIS consistent land surface in the Community Land Model (CLM 3.0). *Journal of Geophysical Research*, *112*, G01023. https://doi.org/10.1029/2006JG000168
Lawrence, P. J., Feddema, J. J., Bonan, G. B., Meehl, G. A., O'Neill, B. C., Oleson, K. W., et al. (2012). Simulating the biogeochemical and biogeophysical impacts of transient land cover change and wood harvest in the Community Climate System Model (CCSM4) from 1850 to 2100. *Journal of Climate*, *25*(9), 3071–3095. https://doi.org/10.1175/jcli-d-11-00256.1

Lazaro-Gredilla, M., Titsias, M. K., Verrelst, J., & Camps-Valls, G. (2014). Retrieval of biophysical parameters with heteroscedastic Gaussian processes. *IEEE Geoscience and Remote Sensing Letters*, *11*(4), 838–842. https://doi.org/10.1109/lgrs.2013.2279695

le Maire, G., François, C., Soudani, K., Berveiller, D., Pontailler, J.-Y., Bréda, N., et al. (2008). Calibration and validation of hyperspectral indices for the estimation of broadleaved forest leaf chlorophyll content, leaf mass per area, leaf area index and leaf canopy biomass. *Remote Sensing of Environment*, *112*(10), 3846–3864. https://doi.org/10.1016/j.rse.2008.06.005

le Maire, G., Marsden, C., Verhoef, W., Ponzoni, F. J., Lo Seen, D., Bégué, A., et al. (2011). Leaf area index estimation with MODIS reflectance time series and model inversion during full rotations of Eucalyptus plantations. *Remote Sensing of Environment*, *115*(2), 586–599. https://doi.org/10.1016/j.rse.2010.10.004

Leblanc, S. G. (2002). Correction to the plant canopy gap-size analysis theory used by the tracing radiation and architecture of canopies instrument. *Applied Optics*, *41*(36), 7667–7670.

Leblanc, S. G., & Chen, J. M. (2001). A practical scheme for correcting multiple scattering effects on optical LAI measurements. *Agricultural and Forest Meteorology*, *110*(2), 125–139. https://doi.org/10.1016/S0168-1923(01)00284-2

Leblanc, S. G., Chen, J. M., Fernandes, R., Deering, D. W., & Conley, A. (2005). Methodology comparison for canopy structure parameters extraction from digital hemispherical photography in boreal forests. *Agricultural and Forest Meteorology*, *129*(3-4), 187–297.

Leblanc, S. G., & Fournier, R. A. (2014). Hemispherical photography simulations with an architectural model to assess retrieval of leaf area index. *Agricultural and Forest Meteorology*, *194*(0), 64–76. https://doi.org/10.1016/j.agrformet.2014.03.016

Lee, B., Kwon, H., Miyata, A., Lindner, S., & Tenhunen, J. (2017). Evaluation of a phenology-dependent response method for estimating leaf area index of rice across climate gradients. *Remote Sensing*, *9*(1), 16. https://doi.org/10.3390/rs9010020

Lee, K.-S., Cohen, W. B., Kennedy, R. E., Maiersperger, T. K., & Gower, S. T. (2004). Hyperspectral versus multispectral data for estimating leaf area index in four different biomes. *Remote Sensing of Environment*, *91*(3-4), 508–520.

Lelong, C., Burger, P., Jubelin, G., Roux, B., Labbé, S., & Baret, F. (2008). Assessment of unmanned aerial vehicles imagery for quantitative monitoring of wheat crop in small plots. *Sensors*, *8*(5), 3557–3585.

Leonenko, G., Los, S., & North, P. (2013a). Statistical distances and their applications to biophysical parameter estimation: Information measures, M-estimates, and minimum contrast methods. *Remote Sensing*, *5*(3), 1355.

Leonenko, G., Los, S. O., & North, P. R. J. (2013b). Retrieval of leaf area index from MODIS surface reflectance by model inversion using different minimization criteria. *Remote Sensing of Environment*, *139*, 257–270. https://doi.org/10.1016/j.rse.2013.07.012

Leuning, R., Cleugh, H. A., Zegelin, S. J., & Hughes, D. (2005). Carbon and water fluxes over a temperate Eucalyptus forest and a tropical wet/dry savanna in Australia: Measurements and comparison with MODIS remote sensing estimates. *Agricultural and Forest Meteorology*, *129*(3-4), 151–173.

Lewis, P., Gómez-Dans, J., Kaminski, T., Settle, J., Quaife, T., Gobron, N., et al. (2012). An Earth Observation Land Data Assimilation System (EO-LDAS). *Remote Sensing of Environment*, *120*, 219–235. https://doi.org/10.1016/j.rse.2011.12.027

Li, A. H., Bo, Y. C., & Chen, L. (2013). Bayesian maximum entropy data fusion of field-observed leaf area index (LAI) and Landsat Enhanced Thematic Mapper Plus-derived LAI. *International Journal of Remote Sensing*, *34*(1), 227–246. https://doi.org/10.1080/01431161.2012.712234

Li, C., Xu, Y., Liu, Z., Tao, S., Li, F., & Fang, J. (2016). Estimation of forest topsoil properties using airborne LiDAR-derived intensity and topographic factors. *Remote Sensing*, *8*(7), 561. https://doi.org/10.3390/rs8070561

Li, S., Ganguly, S., Dungan, J., Zhang, G., Ju, J., & Claverie, M. (2015). Improving the frequency of high spatial resolution leaf area index maps using Landsat OLI and Sentinel-2 MSI. Paper presented at the AGU'15, San Francisco. Retrieved from https://agu.confex.com/agu/fm15/meetingapp.cgi/Paper/84805

Li, X., Gao, F., Wang, J., & Strahler, A. (2001). A priori knowledge accumulation and its application to linear BRDF model inversion. *Journal of Geophysical Research*, *106*(D11), 11925–11935.

Li, X., & Strahler, A. (1985). Geometric-optical modeling of a coniferous forest canopy. *IEEE Transactions on Geoscience and Remote Sensing*, *23*, 705–721.

Li, X., Zhang, Y., Bao, Y., Luo, J., Jin, X., Xu, X., et al. (2014). Exploring the best hyperspectral features for LAI estimation using partial least squares regression. *Remote Sensing*, *6*(7), 6221–6241. https://doi.org/10.3390/rs6076221

Li, Z., Strahler, A., Schaaf, C., Jupp, D., Schaefer, M., & Olofsson, P. (2018). Seasonal change of leaf and woody area profiles in a midlatitude deciduous forest canopy from classified dual-wavelength terrestrial lidar point clouds. *Agricultural and Forest Meteorology*, *262*, 279–297. https://doi.org/10.1016/j.agrformet.2018.07.014

Li, Z., Tang, H., Xin, X., Zhang, B., & Wang, D. (2014). Assessment of the MODIS LAI product using ground measurement data and HJ-1A/1B Imagery in the meadow steppe of Hulunber, China. *Remote Sensing*, *6*(7), 6242–6265.

Liang, L., Di, L., Zhang, L., Deng, M., Qin, Z., Zhao, S., & Lin, H. (2015). Estimation of crop LAI using hyperspectral vegetation indices and a hybrid inversion method. *Remote Sensing of Environment*, *165*(0), 123–134. https://doi.org/10.1016/j.rse.2015.04.032

Liang, S. (2004). *Quantitative remote sensing of land surfaces*. New York: John Wiley and Sons, Inc.

Lin, A., Zhu, H., Wang, L., Gong, W., & Zou, L. (2016). Characteristics of long-term climate change and the ecological responses in Central China. *Earth Interactions*, *20*(2), 1–24. https://doi.org/10.1175/ei-d-15-0004.1

Liu, J., Pattey, E., & Jégo, G. (2012). Assessment of vegetation indices for regional crop green LAI estimation from Landsat images over multiple growing seasons. *Remote Sensing of Environment*, *123*, 347–358. https://doi.org/10.1016/j.rse.2012.04.002

Liu, Q., Liang, S., Xiao, Z., & Fang, H. (2014). Retrieval of leaf area index using temporal, spectral, and angular information from multiple satellite data. *Remote Sensing of Environment*, *145*(0), 25–37. https://doi.org/10.1016/j.rse.2014.01.021

Liu, R. G., Shang, R., Liu, Y., & Lu, X. L. (2017). Global evaluation of gap-filling approaches for seasonal NDVI with considering vegetation growth trajectory, protection of key point, noise resistance and curve stability. *Remote Sensing of Environment*, *189*, 164–179. https://doi.org/10.1016/j.rse.2016.11.023

Liu, Y., Liu, R., & Chen, J. M. (2012). Retrospective retrieval of long-term consistent global leaf area index (1981–2011) from combined AVHRR and MODIS data. *Journal of Geophysical Research*, *117*, G04003. https://doi.org/10.1029/2012JG002084

Liu, Y., Liu, R., Pisek, J., & Chen, J. M. (2017). Separating overstory and understory leaf area indices for global needleleaf and deciduous broadleaf forests by fusion of MODIS and MISR data. *Biogeosciences*, *14*(5), 1093–1110. https://doi.org/10.5194/bg-14-1093-2017

Liu, Z., Chen, J. M., Jin, G., & Qi, Y. (2015). Estimating seasonal variations of leaf area index using litterfall collection and optical methods in four mixed evergreen–deciduous forests. *Agricultural and Forest Meteorology*, *209–210*, 36–48. https://doi.org/10.1016/j.agrformet.2015.04.025

Locherer, M., Hank, T., Danner, M., & Mauser, W. (2015). Retrieval of seasonal leaf area index from simulated EnMAP data through optimized LUT-based inversion of the PROSAIL model. *Remote Sensing*, *7*(8), 10321–10346.

Loew, A., Bell, W., Brocca, L., Bulgin, C. E., Burdanowitz, J., Calbet, X., et al. (2017). Validation practices for satellite based earth observation data across communities. *Reviews of Geophysics*, *55*, 779–817. https://doi.org/10.1002/2017RG000562

Loew, A., van Bodegom, P. M., Widlowski, J. L., Otto, J., Quaife, T., Pinty, B., & Raddatz, T. (2014). Do we (need to) care about canopy radiation schemes in DGVMs? Caveats and potential impacts. *Biogeosciences*, *11*(7), 1873–1897. https://doi.org/10.5194/bg-11-1873-2014

López-Serrano, F. R., Landete-Castillejos, T., Martínez-Millán, J., & del Cerro-Barja, A. (2000). LAI estimation of natural pine forest using a non-standard sampling technique. *Agricultural and Forest Meteorology*, *101*(2-3), 95–111.

Los, S. O., Collatz, G. J., Sellers, P. J., Malmstršm, C. M., Pollack, N. H., DeFries, R. S., et al. (2000). A global 9-year biophysical land-surface data set from NOAA AVHRR data. *Journal of Hydrometeorology*, *1*(2), 183–199. https://doi.org/10.1175/1525-7541(2000)001<0183:AGYBLS>2.0.CO;2

Lotsch, A., Friedl, M. A., Anderson, B. T., & Tucker, C. J. (2003). Coupled vegetation-precipitation variability observed from satellite and climate records. *Geophysical Research Letters*, *30*(14), 1774. https://doi.org/10.1029/2003GL017506

LSA SAF (2008). Validation report vegetation parameters (FVC, LAI, FAPAR). (SAF/LAND/UV/VR_VEGA/2.1).Valencia, Spain: Universitat de Valencia.

Lucas, D. D. P., Heldwein, A. B., Hinnah, F. D., Maldaner, I. C., & Loose, L. H. (2015). Estimation of leaf area index in the sunflower as a function of thermal time. *Revista Ciência Agronômica*, *46*(2), 404–411. https://doi.org/10.5935/1806-6690.20150020

Luo, S. Z., Wang, C., Li, G. C., & Xi, X. H. (2013). Retrieving leaf area index using ICESat/GLAS full-waveform data. *Remote Sensing Letters*, *4*(8), 745–753. https://doi.org/10.1080/2150704x.2013.790573

Luo, S. Z., Wang, C., Pan, F. F., Xi, X. H., Li, G. C., Nie, S., & Xia, S. B. (2015). Estimation of wetland vegetation height and leaf area index using airborne laser scanning data. *Ecological Indicators*, *48*, 550–559. https://doi.org/10.1016/j.ecolind.2014.09.024

Luo, S.-Z., Wang, C., Zhang, G.-B., Xi, X.-H., & Li, G.-C. (2013). Forest leaf area index (LAI) estimation using airborne discrete-return lidar data. *Chinese Journal of Geophysics*, *56*(3), 233–242. https://doi.org/10.1002/cjg2.20024

Ma, H., Song, J., & Wang, J. (2015). Forest canopy LAI and vertical FAVD profile inversion from airborne full-waveform LiDAR data based on a radiative transfer model. *Remote Sensing*, *7*(2), 1897–1914.

Ma, H., Song, J. L., Wang, J. D., Xiao, Z. Q., & Fu, Z. (2014). Improvement of spatially continuous forest LAI retrieval by integration of discrete airborne LiDAR and remote sensing multi-angle optical data. *Agricultural and Forest Meteorology*, *189*, 60–70. https://doi.org/10.1016/j.agrformet.2014.01.009

Ma, L., Zheng, G., Eitel, J. U. H., Magney, T. S., & Moskal, L. M. (2016). Determining woody-to-total area ratio using terrestrial laser scanning (TLS). *Agricultural and Forest Meteorology*, *228–229*, 217–228. https://doi.org/10.1016/j.agrformet.2016.06.021

Ma, M., Che, T., Li, X., Xiao, Q., Zhao, K., & Xin, X. (2015). A prototype network for remote sensing validation in China. *Remote Sensing*, *7*(5), 5187.

Macfarlane, C., Grigg, A., & Evangelista, C. (2007). Estimating forest leaf area using cover and fullframe fisheye photography: Thinking inside the circle. *Agricultural and Forest Meteorology*, *146*(1-2), 1–12. https://doi.org/10.1016/j.agrformet.2007.05.001

Magnussen, S., Næsset, E., & Wulder, M. A. (2008). Efficient multiresolution spatial predictions for large data arrays. *Remote Sensing of Environment*, *109*(4), 451–463.

Mahowald, N., Lo, F. N., Zheng, Y., Harrison, L., Funk, C., Lombardozzi, D., & Goodale, C. (2016). Projections of leaf area index in earth system models. *Earth System Dynamics*, *7*(1), 211–229. https://doi.org/10.5194/esd-7-211-2016

Mailly, D., Turbis, S., & Chazdon, R. L. (2013). SOLARCALC 7.0: An enhanced version of a program for the analysis of hemispherical canopy photographs. *Computers and Electronics in Agriculture*, *97*, 15–20. https://doi.org/10.1016/j.compag.2013.06.004

Majasalmi, T., Rautiainen, M., Stenberg, P., & Lukes, P. (2013). An assessment of ground reference methods for estimating LAI of boreal forests. *Forest Ecology and Management*, *292*, 10–18. https://doi.org/10.1016/j.foreco.2012.12.017

Majasalmi, T., Rautiainen, M., Stenberg, P., & Rita, H. (2012). Optimizing the sampling scheme for LAI-2000 measurements in a boreal forest. *Agricultural and Forest Meteorology*, *154*, 38–43. https://doi.org/10.1016/j.agrformet.2011.10.002

Malenovský, Z., Martin, E., Homolová, L., Gastellu-Etchegorry, J.-P., Zurita-Milla, R., Schaepman, M. E., et al. (2008). Influence of woody elements of a Norway spruce canopy on nadir reflectance simulated by the DART model at very high spatial resolution. *Remote Sensing of Environment*, *112*(1), 1–18. https://doi.org/10.1016/j.rse.2006.02.028

Manninen, T., Korhonen, L., Riihelä, A., Lahtinen, P., Stenberg, P., Roujean, J.-L., & Hautecoeur, O. (2012). Boreal forest albedo and LAI in SNORTEX 2008-2010. Paper presented at the IGARSS, Munich, Germany. https://doi.org/10.1109/IGARSS.2012.6350589

Manninen, T., Korhonen, L., Voipio, P., Lahtinen, P., & Stenberg, P. (2012). Airborne estimation of boreal forest LAI in winter conditions: A test using summer and winter ground truth. *IEEE Transactions on Geoscience and Remote Sensing*, *50*(1), 68–74. https://doi.org/10.1109/TGRS.2011.2173939

Manninen, T., Stenberg, P., Rautiainen, M., Smolander, H., Voipio, P., & Ahola, H. (2005). Boreal forest LAI retrieval using both optical and microwave data of ENVISAT. Paper presented at the IEEE International Geoscience and Remote Sensing Symposium, Seoul, Korea.

Manninen, T., Stenberg, P., Rautiainen, M., & Voipio, P. (2013). Leaf area index estimation of boreal and subarctic forests using VV/HH ENVISAT/ASAR data of various swaths. *IEEE Transactions on Geoscience and Remote Sensing*, *51*(7), 3899–3909. https://doi.org/10.1109/TGRS.2012.2227327

Mannschatz, T., Pflug, B., Borg, E., Feger, K. H., & Dietrich, P. (2014). Uncertainties of LAI estimation from satellite imaging due to atmospheric correction. *Remote Sensing of Environment*, *153*, 24–39. https://doi.org/10.1016/j.rse.2014.07.020

Mao, J., Ribes, A., Yan, B., Shi, X., Thornton, P. E., Seferian, R., et al. (2016). Human-induced greening of the northern extratropical land surface. *Nature Climate Change*, *6*(10), 959–963. https://doi.org/10.1038/nclimate3056, http://www.nature.com/nclimate/journal/vaop/ncurrent/abs/nclimate3056.html#supplementary-information

Mao, J., Shi, X., Thornton, P., Hoffman, F., Zhu, Z., & Myneni, R. (2013). Global latitudinal-asymmetric vegetation growth trends and their driving mechanisms: 1982–2009. *Remote Sensing*, *5*(3), 1484–1497.

María Luisa, E., Frédéric, B., & Marie, W. (2008). Slope correction for LAI estimation from gap fraction measurements. *Agricultural and Forest Meteorology*, *148*(10), 1553–1562. https://doi.org/10.1016/j.agrformet.2008.05.005

Martinez, B., Cassiraga, E., Camacho, F., & Garcia-Haro, J. (2010). Geostatistics for mapping leaf area index over a cropland landscape: Efficiency sampling assessment. *Remote Sensing*, *2*(11), 2584–2606.

Martinez, B., García-Haro, F. J., & Camacho-de Coca, F. (2009). Derivation of high-resolution leaf area index maps in support of validation activities: Application to the cropland Barrax site. *Agricultural and Forest Meteorology*, *149*(1), 130–145. https://doi.org/10.1016/j.agrformet.2008.07.014

Mathews, A., & Jensen, J. (2013). Visualizing and quantifying vineyard canopy LAI using an unmanned aerial vehicle (UAV) collected high density structure from motion point cloud. *Remote Sensing*, *5*(5), 2164–2183.

Mayaux, P., Eva, H., Gallego, J., Strahler, A. H., Herold, M., Agrawal, S., et al. (2006). Validation of the global land cover 2000 map. *IEEE Transactions on Geoscience and Remote Sensing*, *44*(7), 1728–1739. https://doi.org/10.1109/TGRS.2006.864370

Mayr, M., & Samimi, C. (2015). Comparing the dry season in-situ leaf area index (LAI) derived from high-resolution RapidEye imagery with MODIS LAI in a Namibian savanna. *Remote Sensing*, *7*(4), 4834–4857.
McCallum, I., Wagner, W., Schmullius, C., Shvidenko, A., Obersteiner, M., Fritz, S., & Nilsson, S. (2010). Comparison of four global FAPAR datasets over Northern Eurasia for the year 2000. *Remote Sensing of Environment*, *114*(5), 941–949. https://doi.org/10.1016/j.rse.2009.12.009
Melaas, E. K., Friedl, M. A., & Zhu, Z. (2013). Detecting interannual variation in deciduous broadleaf forest phenology using Landsat TM/ETM+ data. *Remote Sensing of Environment*, *132*(0), 176–185. https://doi.org/10.1016/j.rse.2013.01.011
Militino, A. F., Ugarte, M. D., & Perez-Goya, U. (2017). Stochastic spatio-temporal models for analysing NDVI distribution of GIMMS NDVI3g Images. *Remote Sensing*, *9*(1), 17. https://doi.org/10.3390/rs9010076
Miller, J. B. (1967). A formula for average foliage density. *Australian Journal of Botany*, *15*, 141–144.
Miralles, D. G., Crow, W. T., & Cosh, M. H. (2010). Estimating spatial sampling errors in coarse-scale soil moisture estimates derived from point-scale observations. *Journal of Hydrometeorology*, *11*(6), 1423–1429. https://doi.org/10.1175/2010jhm1285.1
Moore, N., Torbick, N., Lofgren, B., Wang, J., Pijanowski, B., Andresen, J., et al. (2010). Adapting MODIS-derived LAI and fractional cover into the RAMS in East Africa. *International Journal of Climatology*, *30*(13), 1954–1969. https://doi.org/10.1002/joc.2011
Moorthy, I., Miller, J. R., Hu, B., Chen, J. M., & Li, Q. (2008). Retrieving crown leaf area index from an individual tree using ground-based lidar data. *Canadian Journal of Remote Sensing*, *34*(3), 320–332.
Moreno, Á., García-Haro, F., Martínez, B., & Gilabert, M. (2014). Noise reduction and gap filling of fAPAR time series using an adapted local regression filter. *Remote Sensing*, *6*(9), 8238–8260.
Morisette, J., Heinsch, F., & Running, S. (2006). Monitoring global vegetation. *EOS Transactions*, *87*(50), 568.
Morsdorf, F., Nichol, C., Malthus, T., & Woodhouse, I. H. (2009). Assessing forest structural and physiological information content of multi-spectral LiDAR waveforms by radiative transfer modelling. *Remote Sensing of Environment*, *113*(10), 2152–2163. https://doi.org/10.1016/j.rse.2009.05.019
Moskal, L. M., & Franklin, S. E. (2004). Relationship between airborne multispectral image texture and aspen defoliation. *International Journal of Remote Sensing*, *25*(14), 2701–2711.
Moulin, S., Bondeau, A., & Delécolle, R. (1998). Combining agricultural crop models and satellite observations; from field to regional scales. *International Journal of Remote Sensing*, *19*(6), 1021–1036.
Mousivand, A., Menenti, M., Gorte, B., & Verhoef, W. (2015). Multi-temporal, multi-sensor retrieval of terrestrial vegetation properties from spectral–directional radiometric data. *Remote Sensing of Environment*, *158*(0), 311–330. https://doi.org/10.1016/j.rse.2014.10.030
Mu, Q., Heinsch, F. A., Zhao, M., & Running, S. W. (2007). Development of a global evapotranspiration algorithm based on MODIS and global meteorology data. *Remote Sensing of Environment*, *111*(4), 519–536. https://doi.org/10.1016/j.rse.2007.04.015
Munier, S., Carrer, D., Planque, C., Camacho, F., Albergel, C., & Calvet, J.-C. (2018). Satellite leaf area index: Global scale analysis of the tendencies per vegetation type over the last 17 years. *Remote Sensing*, *10*(3), 424. https://doi.org/10.3390/rs10030424
Murray-Tortarolo, G., Anav, A., Friedlingstein, P., Sitch, S., Piao, S., Zhu, Z., et al. (2013). Evaluation of land surface models in reproducing satellite-derived LAI over the high-latitude northern hemisphere. Part I: Uncoupled DGVMs. *Remote Sensing*, *5*(10), 4819–4838. https://doi.org/10.3390/rs5104819
Myneni, R., Yang, W., Nemani, R. R., Huete, A. R., Dickinson, R. E., Knyazikhin, Y., et al. (2007). Large seasonal changes in leaf area of amazon rainforests. *Proceedings of the National Academy of Sciences*, *104*(12), 4820–4823. https://doi.org/10.1073/pnas.0611338104
Myneni, R., Yang, W., Tan, B., Shabanov, N., & Knyazikhin, Y. (2005). Global products of vegetation leaf area and fraction absorbed PAR from MODIS sensors onboard NASA Terra and Aqua satellites. Paper presented at the The 9th International Symposium on Physical Measurements and Signatures in Remote Sensing, Beijing, China.
Myneni, R. B., Hoffman, S., Knyazikhin, Y., Privette, J. L., Glassy, J., Tian, Y., et al. (2002). Global products of vegetation leaf area and fraction absorbed PAR from year one of MODIS data. *Remote Sensing of Environment*, *83*(1-2), 214–231. https://doi.org/10.1016/S0034-4257(02)00074-3
Myneni, R. B., Los, S. O., & Tucker, C. J. (1996). Satellite-based identification of linked vegetation index and sea surface temperature anomaly areas from 1982–1990 for Africa, Australia and South America. *Geophysical Research Letters*, *23*(7), 729–732. https://doi.org/10.1029/96GL00266
Nackaerts, K., Coppin, P., Muys, B., & Hermy, M. (2000). Sampling methodology for LAI measurements with LAI-2000 in small forest stands. *Agricultural and Forest Meteorology*, *101*(2-3), 95–111.
Nasahara, K. N., Muraoka, H., Nagai, S., & Mikami, H. (2008). Vertical integration of leaf area index in a Japanese deciduous broad-leaved forest. *Agricultural and Forest Meteorology*, *148*(6-7), 1136–1146. https://doi.org/10.1016/j.agrformet.2008.02.011
Nearing, G. S., Crow, W. T., Thorp, K. R., Moran, M. S., Reichle, R. H., & Gupta, H. V. (2012). Assimilating remote sensing observations of leaf area index and soil moisture for wheat yield estimates: An observing system simulation experiment. *Water Resources Research*, *48*, W05525. https://doi.org/10.1029/2011WR011420
Neilson, R. P. (1995). A model for predicting continental-scale vegetation distribution and water balance. *Ecological Applications*, *5*(2), 362–385. https://doi.org/10.2307/1942028
Ni, W., & Woodcock, C. E. (2000). Effect of canopy structure and the presence of snow on the albedo of boreal conifer forests. *Journal of Geophysical Research*, *105*(D9), 11,879–11,888. https://doi.org/10.1029/1999JD901158
Nie, S., Wang, C., Dong, P., & Xi, X. (2016). Estimating leaf area index of maize using airborne full-waveform lidar data. *Remote Sensing Letters*, *7*(2), 111–120. https://doi.org/10.1080/2150704X.2015.1111536
Nigam, R., Bhattacharya, B. K., Vyas, S., & Oza, M. P. (2014). Retrieval of wheat leaf area index from AWiFS multispectral data using canopy radiative transfer simulation. *International Journal of Applied Earth Observation and Geoinformation*, *32*, 173–185. https://doi.org/10.1016/j.jag.2014.04.003
Nikolov, N., & Zeller, K. (2006). Efficient retrieval of vegetation leaf area index and canopy clumping factor from satellite data to support pollutant deposition assessments. *Environmental Pollution*, *141*(3), 539–549.
Nilson, T. (1971). A theoretical analysis of the frequency of gaps in plant stands. *Agricultural Meteorology*, *8*, 25–38.
Ni-Meister, W., Jupp, D. L. B., & Dubayah, R. (2001). Modeling lidar waveforms in heterogeneous and discrete canopies. *IEEE Transactions on Geoscience and Remote Sensing*, *39*(9), 1943–1958.
Niu, G., Yang, Z., Mitchell, K. E., Chen, F., Ek, M. B., Barlage, M., et al. (2011). The community Noah land surface model with multiparameterization options (Noah-MP): 1. Model description and evaluation with local-scale measurements. *Journal of Geophysical Research*, *116*, D12109. https://doi.org/10.1029/2010JD015139
North, P. R. J., Rosette, J. A. B., Suárez, J. C., & Los, S. O. (2010). A Monte Carlo radiative transfer model of satellite waveform LiDAR. *International Journal of Remote Sensing*, *31*(5), 1343–1358.

Ogutu, B., Dash, J., & Dawson, T. P. (2011). Evaluation of leaf area index estimated from medium spatial resolution remote sensing data in a broadleaf deciduous forest in southern England, UK. *Canadian Journal of Remote Sensing*, *37*(4), 333–347. https://doi.org/10.5589/m11-043

Olivas, P. C., Oberbauer, S. F., Clark, D. B., Clark, D. A., Ryan, M. G., O'Brien, J. J., & Ordoñez, H. (2013). Comparison of direct and indirect methods for assessing leaf area index across a tropical rain forest landscape. *Agricultural and Forest Meteorology*, *177*, 110–116. https://doi.org/10.1016/j.agrformet.2013.04.010

Olsoy, P. J., Mitchell, J. J., Levia, D. F., Clark, P. E., & Glenn, N. F. (2016). Estimation of big sagebrush leaf area index with terrestrial laser scanning. *Ecological Indicators*, *61*, 815–821. https://doi.org/10.1016/j.ecolind.2015.10.034

Olthof, I., King, D. J., & Lautenschlager, R. A. (2003). Overstory and understory leaf area index as indicators of forest response to ice storm damage. *Ecological Indicators*, *3*(1), 49–64.

Omer, G., Mutanga, O., Abdel-Rahman, E., & Adam, E. (2016). Empirical prediction of leaf area index (LAI) of endangered tree species in intact and fragmented indigenous forests ecosystems using WorldView-2 data and two robust machine learning algorithms. *Remote Sensing*, *8*(4), 324. https://doi.org/10.3390/rs8040324

Pandya, M. R., Singh, R. P., Chaudhari, K. N., Bairagi, G. D., Sharma, R., Dadhwal, V. K., & Parihar, J. S. (2006). Leaf area index retrieval using IRS LISS-III sensor data and validation of the MODIS LAI product over central India. *IEEE Transactions on Geoscience and Remote Sensing*, *44*(7), 1858–1865.

Pasolli, E., Melgani, F., Alajlan, N., & Bazi, Y. (2012). Active learning methods for biophysical parameter estimation. *IEEE Transactions on Geoscience and Remote Sensing*, *50*(10), 4071–4084.

Pasolli, L., Asam, S., Castelli, M., Bruzzone, L., Wohlfahrt, G., Zebisch, M., & Notarnicola, C. (2015). Retrieval of leaf area index in mountain grasslands in the Alps from MODIS satellite imagery. *Remote Sensing of Environment*, *165*(0), 159–174. https://doi.org/10.1016/j.rse.2015.04.027

Pauwels, V. R. N., Verhoest, N. E. C., De Lannoy, G. J. M., Guissard, V., Lucau, C., & Defourny, P. (2007). Optimization of a coupled hydrology–crop growth model through the assimilation of observed soil moisture and leaf area index values using an ensemble Kalman filter. *Water Resources Research*, *43*, W04421. https://doi.org/10.1029/2006WR004942

Pearse, G. D., Watt, M. S., & Morgenroth, J. (2016). Comparison of optical LAI measurements under diffuse and clear skies after correcting for scattered radiation. *Agricultural and Forest Meteorology*, *221*, 61–70. https://doi.org/10.1016/j.agrformet.2016.02.001

Peddle, R. D., Davidson, D. P., Johnson, R. L., & Hall, R. J. (1999). Spectral mixture analysis and geometric-optical reflectance modelling of boreal forest biophysical structure. *Remote Sensing of Environment*, *67*, 288–297.

Pfeifer, M., Gonsamo, A., Disney, M., Pellikka, P., & Marchant, R. (2012). Leaf area index for biomes of the Eastern Arc Mountains: Landsat and SPOT observations along precipitation and altitude gradients. *Remote Sensing of Environment*, *118*, 103–115. https://doi.org/10.1016/j.rse.2011.11.009

Pfeifer, M., Lefebvre, V., Gonsamo, A., Pellikka, P., Marchant, R., Denu, D., & Platts, P. (2014). Validating and linking the GIMMS leaf area index (LAI3g) with environmental controls in tropical Africa. *Remote Sensing*, *6*(3), 1973–1990.

Piao, S., Yin, G., Tan, J., Cheng, L., Huang, M., Li, Y., et al. (2015). Detection and attribution of vegetation greening trend in China over the last 30 years. *Global Change Biology*, *21*(4), 1601–1609. https://doi.org/10.1111/gcb.12795

Pinty, B., Andredakis, I., Clerici, M., Kaminski, T., Taberner, M., Verstraete, M. M., et al. (2011). Exploiting the MODIS albedos with the Two-stream Inversion Package (JRC-TIP): 1. Effective leaf area index, vegetation, and soil properties. *Journal of Geophysical Research*, *116*, D09105. https://doi.org/10.1029/2010JD015372

Pinty, B., Widlowski, J. L., Taberner, M., Gobron, N., Verstraete, M. M., Disney, M., et al. (2004). The RAdiation transfer Model Intercomparison (RAMI) exercise: Results from the second phase. *Journal of Geophysical Research*, *109*, D06210. https://doi.org/10.1029/2003JD004252

Pisek, J., Chen, J. M., Alikas, K., & Deng, F. (2010). Impacts of including forest understory brightness and foliage clumping information from multiangular measurements on leaf area index mapping over North America. *Journal of Geophysical Research*, *115*, G03023. https://doi.org/10.1029/2009JG001138

Pisek, J., Chen, J. M., & Deng, F. (2007). Assessment of a global leaf area index product from SPOT-4 VEGETATION data over selected sites in Canada. *Canadian Journal of Remote Sensing*, *33*(4), 341–356.

Pisek, J., Lang, M., Nilson, T., Korhonen, L., & Karu, H. (2011). Comparison of methods for measuring gap size distribution and canopy nonrandomness at Järvselja RAMI (RAdiation transfer Model Intercomparison) test sites. *Agricultural and Forest Meteorology*, *151*(3), 365–377. https://doi.org/10.1016/j.agrformet.2010.11.009

Plummer, S., Arino, O., Simon, M., & Steffen, W. (2006). Establishing a earth observation product service For The terrestrial carbon community: The globcarbon initiative. *Mitigation and Adaptation Strategies for Global Change*, *11*(1), 97–111. https://doi.org/10.1007/s11027-006-1012-8

Pocewicz, A., Vierling, L. A., Lentile, L. B., & Smith, R. (2007). View angle effects on relationships between MISR vegetation indices and leaf area index in a recently burned ponderosa pine forest. *Remote Sensing of Environment*, *107*(1-2), 322–333.

Potithep, S., Nagai, S., Nasahara, K. N., Muraoka, H., & Suzuki, R. (2013). Two separate periods of the LAI–VIs relationships using in situ measurements in a deciduous broadleaf forest. *Agricultural and Forest Meteorology*, *169*(0), 148–155. https://doi.org/10.1016/j.agrformet.2012.09.003

Price, J. C. (1990). On the information content of soil reflectance spectra. *Remote Sensing of Environment*, *33*(2), 113–121.

Privette, J., Myneni, R., Morisette, J., & Justice, C. (1998). Global validation of EOS LAI and FPAR products. *Earth Observer*, *10*(6), 39–42.

Privette, J. L., Myneni, R. B., Knyazikhin, Y., Mukelabai, M., Roberts, G., Tian, Y., et al. (2002). Early spatial and temporal validation of MODIS LAI product in the Southern Africa Kalahari. *Remote Sensing of Environment*, *83*(1-2), 232–243. https://doi.org/10.1016/S0034-4257(02)00075-5

Pu, R., & Cheng, J. (2015). Mapping forest leaf area index using reflectance and textural information derived from WorldView-2 imagery in a mixed natural forest area in Florida, US. *International Journal of Applied Earth Observation and Geoinformation*, *42*(0), 11–23. https://doi.org/10.1016/j.jag.2015.05.004

Pu, R., Yu, Q., Gong, P., & Biging, G. S. (2005). EO-1 Hyperion, ALI and Landsat 7 ETM+ data comparison for estimating forest crown closure and leaf area index. *International Journal of Remote Sensing*, *26*(3), 457–474.

Pulliainen, J., Salminen, M., Heinilä, K., Cohen, J., & Hannula, H.-R. (2015). Semi-empirical modeling of the scene reflectance of snow-covered boreal forest: Validation with airborne spectrometer and LIDAR observations. *Remote Sensing of Environment*, *155*, 303–311. https://doi.org/10.1016/j.rse.2014.09.004

Qi, J., Chehbouni, A., Huete, A. R., Kerr, Y., & Sorooshian, S. (1994). A modified soil adjusted vegetation index (MSAVI). *Remote Sensing of Environment*, *48*, 119–126.

Qi, Y., Li, F., Liu, Z., & Jin, G. (2014). Impact of understorey on overstorey leaf area index estimation from optical remote sensing in five forest types in northeastern China. *Agricultural and Forest Meteorology*, *198–199*, 72–80. https://doi.org/10.1016/j.agrformet.2014.08.001

Qin, J., Liang, S., Li, X., & Wang, J. (2008). Development of the adjoint model of a canopy radiative transfer model for sensitivity study and inversion of leaf area index. *IEEE Transactions on Geoscience and Remote Sensing*, *46*(7), 2028–2037.

Qin, W. H., & Xiang, Y. Q. (1994). On the hotspot effect of leaf canopies—Modelling study and influence of leaf shape. *Remote Sensing of Environment*, *50*(2), 95–106.

Qu, Y., Han, W., Fu, L., Li, C., Song, J., Zhou, H., et al. (2014). LAINet—A wireless sensor network for coniferous forest leaf area index measurement: Design, algorithm and validation. *Computers and Electronics in Agriculture*, *108*(0), 200–208. https://doi.org/10.1016/j.compag.2014.08.003

Qu, Y., Meng, J., Wan, H., & Li, Y. (2016). Preliminary study on integrated wireless smart terminals for leaf area index measurement. *Computers and Electronics in Agriculture*, *129*, 56–65. https://doi.org/10.1016/j.compag.2016.09.011

Qu, Y., Zhang, Y., & Xue, H. (2014). Retrieval of 30-m-resolution leaf area index from China HJ-1 CCD data and MODIS products through a dynamic Bayesian network. *IEEE Journal of Selected Topics in Applied Earth Observations and Remote Sensing*, *7*(1), 222–228. https://doi.org/10.1109/jstars.2013.2259472

Qu, Y., Zhu, Y., Han, W., Wang, J., & Ma, M. (2014). Crop leaf area index observations with a wireless sensor network and its potential for validating remote sensing products. *IEEE Journal of Selected Topics in Applied Earth Observations and Remote Sensing*, *7*(2), 431–444. https://doi.org/10.1109/JSTARS.2013.2289931

Quan, X., He, B., & Li, X. (2015). A Bayesian network-based method to alleviate the ill-posed inverse problem: A case study on leaf area index and canopy water content retrieval. *IEEE Transactions on Geoscience and Remote Sensing*, *53*(12), 6507–6517. https://doi.org/10.1109/TGRS.2015.2442999

Rahman, H., Pinty, B., & Verstraete, M. M. (1993). Coupled surface-atmosphere reflectance (CSAR) model, 2, semiempirical surface model usable with NOAA advanced very high resolution radiometer data. *Journal of Geophysical Research*, *98*, 20,791–20,801.

Randerson, J. T., Hoffman, F. M., Thornton, P. E., Mahowald, N. M., Lindsay, K., Lee, Y.-H., et al. (2009). Systematic assessment of terrestrial biogeochemistry in coupled climate–carbon models. *Global Change Biology*, *15*(10), 2462–2484. https://doi.org/10.1111/j.1365-2486.2009.01912.x

Raymaekers, D., Garcia, A., Di Bella, C., Beget, M. E., Llavallol, C., Oricchio, P., et al. (2014). SPOT-VEGETATION GEOV1 biophysical parameters in semi-arid agro-ecosystems. *International Journal of Remote Sensing*, *35*(7), 2534–2547. https://doi.org/10.1080/01431161.2014.883096

Revill, A., Sus, O., Barrett, B., & Williams, M. (2013). Carbon cycling of European croplands: A framework for the assimilation of optical and microwave Earth observation data. *Remote Sensing of Environment*, *137*(0), 84–93. https://doi.org/10.1016/j.rse.2013.06.002

Riaño, D., Valladares, F., Condés, S., & Chuvieco, E. (2004). Estimation of leaf area index and covered ground from airborne laser scanner (Lidar) in two contrasting forests. *Agricultural and Forest Meteorology*, *124*(3-4), 269–275.

Richardson, A. D., Anderson, R. S., Arain, M. A., Barr, A. G., Bohrer, G., Chen, G., et al. (2012). Terrestrial biosphere models need better representation of vegetation phenology: Results from the North American Carbon Program Site Synthesis. *Global Change Biology*, *18*(2), 566–584. https://doi.org/10.1111/j.1365-2486.2011.02562.x

Richardson, A. D., Dail, D. B., & Hollinger, D. Y. (2011). Leaf area index uncertainty estimates for model-data fusion applications. *Agricultural and Forest Meteorology*, *151*(9), 1287–1292. https://doi.org/10.1016/j.agrformet.2011.05.009

Richardson, J. J., Moskal, L. M., & Kim, S.-H. (2009). Modeling approaches to estimate effective leaf area index from aerial discrete-return LIDAR. *Agricultural and Forest Meteorology*, *149*(6–7), 1152–1160. https://doi.org/10.1016/j.agrformet.2009.02.007

Richter, K., Atzberger, C., Hank, T. B., & Mauser, W. (2012). Derivation of biophysical variables from Earth observation data: Validation and statistical measures. *Journal of Applied Remote Sensing*, *6*. https://doi.org/10.1117/1.JRS.6.063557

Richter, K., Atzberger, C., Vuolo, F., & D'Urso, G. (2011). Evaluation of Sentinel-2 spectral sampling for radiative transfer model based LAI estimation of wheat, sugar beet, and maize. *IEEE Journal of Selected Topics in Applied Earth Observations and Remote Sensing*, *4*(2), 458–464. https://doi.org/10.1109/JSTARS.2010.2091492

Richter, K., Hank, T. B., Vuolo, F., Mauser, W., & D'Urso, G. (2012). Optimal exploitation of the Sentinel-2 spectral capabilities for crop leaf area index mapping. *Remote Sensing*, *4*(3), 561–582.

Ritchie, J. C. (1996). Remote sensing applications to hydrology: Airborne laser altimeters. *Hydrological Sciences Journal*, *41*, 625–636.

Rivera, J., Verrelst, J., Leonenko, G., & Moreno, J. (2013). Multiple cost functions and regularization options for improved retrieval of leaf chlorophyll content and LAI through Inversion of the PROSAIL model. *Remote Sensing*, *5*(7), 3280–3304.

Román, M., Justice, C., & Csiszar, I. (2014). Land, cryosphere, and nighttime environmental products from Suomi NPP VIIRS: Overview and status. Paper presented at the IEEE International Geoscience and Remote Sensing Symposium (IGARSS), Quebec, Canada.

Román, M. O., Gatebe, C. K., Shuai, Y., Wang, Z., Gao, F., Masek, J. G., et al. (2013). Use of in situ and airborne multiangle data to assess MODIS- and Landsat-based estimates of directional reflectance and albedo. *IEEE Transactions on Geoscience and Remote Sensing*, *51*(3), 1393–1404. https://doi.org/10.1109/TGRS.2013.2243457

Roujean, J. L., & Lacaze, R. (2002). Global mapping of vegetation parameters from POLDER multiangular measurements for studies of surface-atmosphere interactions: A pragmatic method and its validation. *Journal of Geophysical Research*, *107*(D12), 4150. https://doi.org/10.1029/2001JD000751

Roujean, J. L., Leroy, M., & Deschamps, P. Y. (1992). A bi-directional reflectance model of the Earth's surface for the correction of remote sensing data. *Journal of Geophysical Research*, *D97*, 20,455–20,468.

Roumenina, E., Kazandjiev, V., Dimitrov, P., Filchev, L., Vassilev, V., Jelev, G., et al. (2013). Validation of LAI and assessment of winter wheat status using spectral data and vegetation indices from SPOT VEGETATION and simulated PROBA-V images. *International Journal of Remote Sensing*, *34*(8), 2888–2904. https://doi.org/10.1080/01431161.2012.755276

Roupsard, O., Dauzat, J., Nouuellon, Y., Deueau, A., Feintrenie, L., Saint-Andre, L., et al. (2008). Cross-validating Sun-shade and 3D models of light absorption by a tree-crop canopy. *Agricultural and Forest Meteorology*, *148*(4), 549–564. https://doi.org/10.1016/j.agrformet.2007.11.002

Rüdiger, C., Albergel, C., Mahfouf, J.-F., Calvet, J.-C., & Walker, J. P. (2010). Evaluation of the observation operator Jacobian for leaf area index data assimilation with an extended Kalman filter. *Journal of Geophysical Research*, *115*, D09111. https://doi.org/10.1029/2009JD012912

Running, S. W., Nemani, R. R., Heinsch, F. A., Zhao, M., Reeves, M. C., & Hashimoto, H. (2004). A continuous satellite-derived measure of global terrestrial primary production. *BioScience*, *54*, 547–560.

Ryu, Y., Nilson, T., Kobayashi, H., Sonnentag, O., Law, B. E., & Baldocchi, D. D. (2010). On the correct estimation of effective leaf area index: Does it reveal information on clumping effects? *Agricultural and Forest Meteorology*, *150*(3), 463–472. https://doi.org/10.1016/j.agrformet.2010.01.009

Ryu, Y., Sonnentag, O., Nilson, T., Vargas, R., Kobayashi, H., Wenk, R., & Baldocchi, D. D. (2010). How to quantify tree leaf area index in an open savanna ecosystem: A multi-instrument and multi-model approach. *Agricultural and Forest Meteorology*, *150*, 63–76.

Ryu, Y., Verfaillie, J., Macfarlane, C., Kobayashi, H., Sonnentag, O., Vargas, R., et al. (2012). Continuous observation of tree leaf area index at ecosystem scale using upward-pointing digital cameras. *Remote Sensing of Environment*, *126*, 116–125. https://doi.org/10.1016/j.rse.2012.08.027

Sabater, J. M., Rüdiger, C., Calvet, J.-C., Fritz, N., Jarlan, L., & Kerr, Y. (2008). Joint assimilation of surface soil moisture and LAI observations into a land surface model. *Agricultural and Forest Meteorology*, *148*(8-9), 1362–1373. https://doi.org/10.1016/j.agrformet.2008.04.003

Sakamoto, T., Gitelson, A. A., & Arkebauer, T. J. (2013). MODIS-based corn grain yield estimation model incorporating crop phenology information. *Remote Sensing of Environment*, *131*(0), 215–231. https://doi.org/10.1016/j.rse.2012.12.017

Sánchez-Azofeifa, G. A., Kalácska, M., Espírito-Santo, M. M. d., Fernandes, G. W., & Schnitzer, S. (2009). Tropical dry forest succession and the contribution of lianas to wood area index (WAI). *Forest Ecology and Management*, *258*(6), 941–948. https://doi.org/10.1016/j.foreco.2008.10.007

Savoy, P., & Mackay, D. S. (2015). Modeling the seasonal dynamics of leaf area index based on environmental constraints to canopy development. *Agricultural and Forest Meteorology*, *200*(0), 46–56. https://doi.org/10.1016/j.agrformet.2014.09.019

Schlerf, M., Atzberger, C., & Hill, J. (2005). Remote sensing of forest biophysical variables using HyMap imaging spectrometer data. *Remote Sensing of Environment*, *95*(2), 177–194.

Scurlock, J. M. O., Asner, G. P., & Gower, S. T. (2001). Worldwide historical estimates of leaf area index, 1932–2000 (ORNL/TM-2001/268). Oak Ridge, Tenn: Oak Ridge National Laboratory. Retrieved from https://daac.ornl.gov/VEGETATION/LAI_des.html

Sea, W. B., Choler, P., Beringer, J., Weinmann, R. A., Hutley, L. B., & Leuning, R. (2011). Documenting improvement in leaf area index estimates from MODIS using hemispherical photos for Australian savannas. *Agricultural and Forest Meteorology*, *151*(11), 1453–1461. https://doi.org/10.1016/j.agrformet.2010.12.006

Seixas, J., Carvalhais, N., Nunes, C., & Benali, A. (2009). Comparative analysis of MODIS-FAPAR and MERIS-MGVI datasets: Potential impacts on ecosystem modeling. *Remote Sensing of Environment*, *113*(12), 2547–2559. https://doi.org/10.1016/j.rse.2009.07.018

Sellers, P. J., Mintz, Y., Sud, Y. C., & Dalcher, A. (1986). A simple biosphere model (SiB) for use within general circulation models. *Journal of the Atmopsheric Science*, *43*, 505–531.

Sellers, P. J., Tucker, C. J., Collatz, G. J., Los, S. O., Justice, C. O., Dazlich, D. A., & Randall, D. A. (1994). A global 1° by 1° NDVI data set for climate studies. Part 2: The generation of global fields of terrestrial biophysical parameters from the NDVI. *International Journal of Remote Sensing*, *15*, 3519–3545.

Senf, C., Pflugmacher, D., Heurich, M., & Krueger, T. (2017). A Bayesian hierarchical model for estimating spatial and temporal variation in vegetation phenology from Landsat time series. *Remote Sensing of Environment*, *194*, 155–160. http://doi.org/10.1016/j.rse.2017.03.020

Serbin, S. P., Ahl, D. E., & Gower, S. T. (2013). Spatial and temporal validation of the MODIS LAI and FPAR products across a boreal forest wildfire chronosequence. *Remote Sensing of Environment*, *133*, 71–84. https://doi.org/10.1016/j.rse.2013.01.022

Shabanov, N. V., Kotchenova, S., Huang, D., Yang, W., Tan, B., Knyazikhin, Y., et al. (2005). Analysis and optimization of the MODIS leaf area index algorithm retrievals over broadleaf forests. *IEEE Transactions on Geoscience and Remote Sensing*, *43*(8), 1855–1865. https://doi.org/10.1109/TGRS.2005.852477

Shabanov, N. V., Wang, Y., Buermann, W., Dong, J., Hoffman, S., Smith, G. R., et al. (2003). Effect of foliage spatial heterogeneity in the MODIS LAI and FPAR algorithm over broadleaf forests. *Remote Sensing of Environment*, *85*(4), 410–423. https://doi.org/10.1016/S0034-4257(03)00017-8

Sheue, C. R., Pao, S. H., Chien, L. F., Chesson, P., & Peng, C. I. (2012). Natural foliar variegation without costs? The case of Begonia. *Annals of Botany*, *109*(6), 1065–1074. https://doi.org/10.1093/aob/mcs025

Shi, H., Xiao, Z., Liang, S., & Zhang, X. (2016). Consistent estimation of multiple parameters from MODIS top of atmosphere reflectance data using a coupled soil-canopy-atmosphere radiative transfer model. *Remote Sensing of Environment*, *184*, 40–57. https://doi.org/10.1016/j.rse.2016.06.008

Shibayama, M., Sakamoto, T., Takada, E., Inoue, A., Morita, K., Takahashi, W., & Kimura, A. (2011). Estimating paddy rice leaf area index with fixed point continuous observation of near infrared reflectance using a calibrated digital camera. *Plant Production Science*, *14*(1), 30–46.

Shibayama, M., Sakamoto, T., Takada, E., Inoue, A., Morita, K., Yamaguchi, T., et al. (2011). Regression-based models to predict rice leaf area index using biennial fixed point continuous observations of near infrared digital images. *Plant Production Science*, *14*(4), 365–376. https://doi.org/10.1626/pps.14.365

Si, Y., Schlerf, M., Zurita-Milla, R., Skidmore, A., & Wang, T. (2012). Mapping spatio-temporal variation of grassland quantity and quality using MERIS data and the PROSAIL model. *Remote Sensing of Environment*, *121*, 415–425. https://doi.org/10.1016/j.rse.2012.02.011

Skidmore, A. K., Pettorelli, N., Coops, N. C., Geller, G. N., Hansen, M., Lucas, R., et al. (2015). Agree on biodiversity metrics to track from space. *Nature*, *523*(7561), 403–405. https://doi.org/10.1038/523403a

Soenen, S. A., Peddle, D. R., & Coburn, C. A. (2005). SCS+C: A modified sun-canopy-sensor topographic correction in forested terrain. *IEEE Transactions on Geoscience and Remote Sensing*, *43*(9), 2148–2159.

Solberg, S., Naesset, E., Hanssen, K. H., & Christiansen, E. (2006). Mapping defoliation during a severe insect attack on Scots pine using airborne laser scanning. *Remote Sensing of Environment*, *102*(3-4), 364–376.

Sonnentag, O., Talbot, J., Chen, J. M., & Roulet, N. T. (2007). Using direct and indirect measurements of leaf area index to characterize the shrub canopy in an ombrotrophic peatland. *Agricultural and Forest Meteorology*, *144*(3-4), 200–212. https://doi.org/10.1016/j.agrformet.2007.03.001

Soudani, K., François, C., Maire, G. l., Dantec, V. L., & Dufrêne, E. (2006). Comparative analysis of IKONOS, SPOT, and ETM+ data for leaf area index estimation in temperate coniferous and deciduous forest stands. *Remote Sensing of Environment*, *102*(1-2), 161–175.

Stagakis, S., Markos, N., Sykioti, O., & Kyparissis, A. (2010). Monitoring canopy biophysical and biochemical parameters in ecosystem scale using satellite hyperspectral imagery: An application on a Phlomis fruticosa Mediterranean ecosystem using multiangular CHRIS/PROBA observations. *Remote Sensing of Environment*, *114*(5), 977–994. https://doi.org/10.1016/j.rse.2009.12.006

Stehman, S. V., Olofsson, P., Woodcock, C. E., Herold, M., & Friedl, M. A. (2012). A global land-cover validation data set, II: Augmenting a stratified sampling design to estimate accuracy by region and land-cover class. *International Journal of Remote Sensing*, *33*(22), 6975–6993. https://doi.org/10.1080/01431161.2012.695092

Stenberg, P. (2006). A note on the G-function for needle leaf canopies. *Agricultural and Forest Meteorology*, *136*(1-2), 76–79.
Stenberg, P., Lukeš, P., Rautiainen, M., & Manninen, T. (2013). A new approach for simulating forest albedo based on spectral invariants. *Remote Sensing of Environment*, *137*, 12–16. https://doi.org/10.1016/j.rse.2013.05.030
Stern, A. J., Doraiswamy, P. C., & Hunt, E. R. (2014). Comparison of different MODIS data product collections over an agricultural area. *Remote Sensing Letters*, 1–9. https://doi.org/10.1080/2150704x.2013.862600
Sumnall, M., Peduzzi, A., Fox, T. R., Wynne, R. H., Thomas, V. A., & Cook, B. (2016). Assessing the transferability of statistical predictive models for leaf area index between two airborne discrete return LiDAR sensor designs within multiple intensely managed Loblolly pine forest locations in the south-eastern USA. *Remote Sensing of Environment*, *176*, 308–319. https://doi.org/10.1016/j.rse.2016.02.012
Sumnall, M. J., Fox, T. R., Wynne, R. H., Blinn, C., & Thomas, V. A. (2016). Estimating leaf area index at multiple heights within the understorey component of Loblolly pine forests from airborne discrete-return lidar. *International Journal of Remote Sensing*, *37*(1), 78–99. https://doi.org/10.1080/01431161.2015.1117683
Sun, G. Q., & Ranson, K. J. (2000). Modeling lidar returns from forest canopies. *IEEE Transactions on Geoscience and Remote Sensing*, *38*(6), 2617–2626.
Sun, L. Y., & Schulz, K. (2017). Spatio-temporal LAI modelling by integrating climate and MODIS LAI data in a mesoscale catchment. *Remote Sensing*, *9*(2), 21. https://doi.org/10.3390/rs9020144
Szczypta, C., Calvet, J. C., Maignan, F., Dorigo, W., Baret, F., & Ciais, P. (2014). Suitability of modelled and remotely sensed essential climate variables for monitoring Euro-Mediterranean droughts. *Geoscientific Model Development*, *7*(3), 931–946. https://doi.org/10.5194/gmd-7-931-2014
Takeda, T., Oguma, H., Sano, T., Yone, Y., & Fujinuma, Y. (2008). Estimating the plant area density of a Japanese larch (Larix kaempferi Sarg.) plantation using a ground-based laser scanner. *Agricultural and Forest Meteorology*, *148*(3), 428–438. https://doi.org/10.1016/j.agrformet.2007.10.004
Tan, B., Hu, J., Zhang, P., Huang, D., Shabanov, N., Weiss, M., et al. (2005). Validation of MOderate Resolution Imaging Spectroradiometer leaf area index product in croplands of Alpilles, France. *Journal of Geophysical Research*, *110*, D01107. https://doi.org/10.1029/2004JD004860
Tang, H., Brolly, M., Zhao, F., Strahler, A. H., Schaaf, C. L., Ganguly, S., et al. (2014). Deriving and validating Leaf Area Index (LAI) at multiple spatial scales through lidar remote sensing: A case study in Sierra National Forest, CA. *Remote Sensing of Environment*, *143*, 131–141. https://doi.org/10.1016/j.rse.2013.12.007
Tang, H., Dubayah, R., Swatantran, A., Hofton, M., Sheldon, S., Clark, D. B., & Blair, B. (2012). Retrieval of vertical LAI profiles over tropical rain forests using waveform lidar at La Selva, Costa Rica. *Remote Sensing of Environment*, *124*, 242–250. https://doi.org/10.1016/j.rse.2012.05.005
Tang, H., Ganguly, S., Zhang, G., Hofton, M. A., Nelson, R. F., & Dubayah, R. (2016). Characterizing leaf area index (LAI) and vertical foliage profile (VFP) over the United States. *Biogeosciences*, *13*(1), 239–252. https://doi.org/10.5194/bg-13-239-2016
Tansey, K., Selmes, N., Anstee, A., Tate, N. J., & Denniss, A. (2009). Estimating tree and stand variables in a Corsican Pine woodland from terrestrial laser scanner data. *International Journal of Remote Sensing*, *30*(19), 5195–5209. https://doi.org/10.1080/01431160902882587
Tao, L., Li, J., Jiang, J., & Chen, X. (2016). Leaf area index inversion of winter wheat using modified water-cloud model. *IEEE Geoscience and Remote Sensing Letters*, *13*(6), 816–820. https://doi.org/10.1109/LGRS.2016.2546945
Tesemma, Z. K., Wei, Y., Peel, M. C., & Western, A. W. (2015). The effect of year-to-year variability of leaf area index on variable infiltration capacity model performance and simulation of runoff. *Advances in Water Resources*, *83*, 310–322. https://doi.org/10.1016/j.advwatres.2015.07.002
Tesemma, Z. K., Wei, Y. P., Western, A. W., & Peel, M. C. (2014). Leaf area index variation for crop, pasture, and tree in response to climatic variation in the Goulburn-Broken Catchment, Australia. *Journal of Hydrometeorology*, *15*(4), 1592–1606. https://doi.org/10.1175/jhm-d-13-0108.1
Thomas, V., Noland, T., Treitz, P., & McCaughey, J. H. (2011). Leaf area and clumping indices for a boreal mixed-wood forest: Lidar, hyperspectral, and Landsat models. *International Journal of Remote Sensing*, *32*(23), 8271–8297. https://doi.org/10.1080/01431161.2010.533211
Thomasson, J. A., Sui, R., Cox, M. S., & Al-Rajehy, A. (2001). Soil reflectance sensing for determining soil properties in precision agriculture. *Transactions of ASAE*, *44*(6), 1445–1453.
Tian, Y., Dickinson, R. E., Zhou, L., & Shaikh, M. (2004). Impact of new land boundary conditions from Moderate Resolution Imaging Spectroradiometer (MODIS) data on the climatology of land surface variables. *Journal of Geophysical Research*, 109, D20115. https://doi.org/10.1029/2003JD004499
Tian, Y., Dickinson, R. E., Zhou, L., Zeng, X., Dai, Y., Myneni, R. B., et al. (2004). Comparison of seasonal and spatial variations of leaf area index and fraction of absorbed photosynthetically active radiation from Moderate Resolution Imaging Spectroradiometer (MODIS) and Common Land Model. *Journal of Geophysical Research*, *109*, D01103. https://doi.org/10.1029/2003JD003777
Tian, Y., Wang, Y., Zhang, Y., Knyazikhin, Y., Bogaert, J., & Myneni, R. B. (2003). Radiative transfer based scaling of LAI retrievals from reflectance data of different resolutions. *Remote Sensing of Environment*, *84*(1), 143–159.
Tian, Y., Woodcock, C. E., Wang, Y., Privette, J. L., Shabanov, N. V., Zhou, L., et al. (2002). Multiscale analysis and validation of the MODIS LAI product I. Uncertainty assessment. *Remote Sensing of Environment*, *83*(3), 414–430. https://doi.org/10.1016/S0034-4257(02)00047-0
Tian, Y., Zhang, Y., Knyazikhin, Y., Myneni, R. B., Glassy, J. M., Dedieu, D., & Running, S. W. (2000). Prototyping of MODIS LAI and FPAR algorithm with LASUR and LANDSAT data. *IEEE Transactions on Geoscience and Remote Sensing*, *38*(5), 2387–2401.
Tillack, A., Clasen, A., Kleinschmit, B., & Förster, M. (2014). Estimation of the seasonal leaf area index in an alluvial forest using high-resolution satellite-based vegetation indices. *Remote Sensing of Environment*, *141*(0), 52–63. https://doi.org/10.1016/j.rse.2013.10.018
Tong, A., & He, Y. H. (2013). Comparative analysis of SPOT, Landsat, MODIS, and AVHRR normalized difference vegetation index data on the estimation of leaf area index in a mixed grassland ecosystem. *Journal of Applied Remote Sensing*, *7*, 15. https://doi.org/10.1117/1.jrs.7.073599
Tum, M., Günther, K., Böttcher, M., Baret, F., Bittner, M., Brockmann, C., & Weiss, M. (2016). Global gap-free MERIS LAI time series (2002–2012). *Remote Sensing*, *8*(1), 69. https://doi.org/10.3390/rs8010069
Turner, D. P., Acker, S. A., Means, J. E., & Garman, S. L. (2000). Assessing alternative allometric algorithms for estimating leaf area of Douglas-fir trees and stands. *Forest Ecology and Management*, *126*(1), 61–76. https://doi.org/10.1016/S0378-1127(99)00083-3
Turner, D. P., Cohen, W. B., Kennedy, R. E., Fassnacht, K. S., & Briggs, J. M. (1999). Relationships between leaf area index and Landsat TM spectral vegetation indices across three temperate zone sites. *Remote Sensing of Environment*, *70*, 52–68.

Uto, K., Seki, H., Saito, G., & Kosugi, Y. (2013). Characterization of rice paddies by a UAV-mounted miniature hyperspectral sensor system. *IEEE Journal of Selected Topics in Applied Earth Observations and Remote Sensing*, *6*(2), 851–860. https://doi.org/10.1109/jstars.2013.2250921

Vaesen, K., Gilliams, S., Nackaerts, K., & Coppin, P. (2001). Ground-measured spectral signatures as indicators of ground cover and leaf area index: The case of paddy rice. *Field Crops Research*, *69*(1), 13–25.

Valderrama-Landeros, L. H., Espana-Boquera, M. L., & Baret, F. (2016). Deforestation in Michoacan, Mexico, from CYCLOPES-LAI time series (2000-2006). *IEEE Journal of Selected Topics in Applied Earth Observations and Remote Sensing*, *9*(12), 5398–5405. https://doi.org/10.1109/jstars.2016.2597742

van den Hurk, B. J. J. M., Viterbo, P., & Los, S. O. (2003). Impact of leaf area index seasonality on the annual land surface evaporation in a global circulation model. *Journal of Geophysical Research*, *108*(D6), 4191. https://doi.org/10.1029/2002JD002846

van Dijk, A. I. J. M., & Bruijnzeel, L. A. (2001). Modelling rainfall interception by vegetation of variable density using an adapted analytical model. Part 1. Model description. *Journal of Hydrology*, *247*(3–4), 230–238. https://doi.org/10.1016/S0022-1694(01)00392-4

van Gardingen, P. R., Jackson, G. E., Hernandez-Daumas, S., Russell, G., & Sharp, L. (1999). Leaf area index estimates obtained for clumped canopies using hemispherical photography. *Agricultural and Forest Meteorology*, *94*(3-4), 243–257. https://doi.org/10.1016/s0168-1923(99)00018-0

van Leeuwen, M., & Nieuwenhuis, M. (2010). Retrieval of forest structural parameters using LiDAR remote sensing. *European Journal of Forest Research*, *129*(4), 749–770. https://doi.org/10.1007/s10342-010-0381-4

Vazifedoust, M., van Dam, J. C., Bastiaanssen, W. G. M., & Reddes, R. A. (2009). Assimilation of satellite data into agrohydrological models to improve crop yield forecasts. *International Journal of Remote Sensing*, *30*(10), 2523–2545.

Verbyla, D. L. (2005). Assessment of the MODIS Leaf Area Index Product (MOD15) in Alaska. *International Journal of Remote Sensing*, *26*(6), 1277–1284.

Verger, A., Baret, F., & Camacho, F. (2011). Optimal modalities for radiative transfer-neural network estimation of canopy biophysical characteristics: Evaluation over an agricultural area with CHRIS/PROBA observations. *Remote Sensing of Environment*, *115*(2), 415–426. https://doi.org/10.1016/j.rse.2010.09.012

Verger, A., Baret, F., & Weiss, M. (2008). Performances of neural networks for deriving LAI estimates from existing CYCLOPES and MODIS products. *Remote Sensing of Environment*, *112*(6), 2789–2803.

Verger, A., Baret, F., & Weiss, M. (2011). A multisensor fusion approach to improve LAI time series. *Remote Sensing of Environment*, *115*(10), 2423–2750.

Verger, A., Baret, F., Weiss, M., Kandasamy, S., & Vermote, E. (2013). The CACAO method for smoothing, gap filling, and characterizing seasonal anomalies in satellite time series. *IEEE Transactions on Geoscience and Remote Sensing*, *51*(4), 1963–1972.

Verger, A., Camacho, F., García-Haro, F. J., & Meliá, J. (2009). Prototyping of Land-SAF leaf area index algorithm with VEGETATION and MODIS data over Europe. *Remote Sensing of Environment*, *113*(11), 2285–2297. https://doi.org/10.1016/j.rse.2009.06.009

Verger, A., Filella, I., Baret, F., & Peñuelas, J. (2016). Vegetation baseline phenology from kilometric global LAI satellite products. *Remote Sensing of Environment*, *178*, 1–14. https://doi.org/10.1016/j.rse.2016.02.057

Verger, A., Martinez, B., Camacho-de Coca, F., & Garcia-Haro, F. J. (2009). Accuracy assessment of fraction of vegetation cover and leaf area index estimates from pragmatic methods in a cropland area. *International Journal of Remote Sensing*, *30*(10), 2685–2704. https://doi.org/10.1080/01431160802555804

Verger, A., Vigneau, N., Chéron, C., Gilliot, J.-M., Comar, A., & Baret, F. (2014). Green area index from an unmanned aerial system over wheat and rapeseed crops. *Remote Sensing of Environment*, *152*(0), 654–664. https://doi.org/10.1016/j.rse.2014.06.006

Verhoef, W. (1984). Light scattering by leaf layers with application to canopy reflectance modeling: The SAIL model. *Remote Sensing of Environment*, *16*, 125–141.

Vermote, E. F., El Saleous, N. Z., & Justice, C. O. (2002). Atmospheric correction of MODIS data in the visible to middle infrared: First results. *Remote Sensing of Environment*, *83*, 97–111.

Vermote, E. F., Roger, J. C., & Ray, J. P. (2015). MODIS surface reflectance user's guide: Collection 6. Retrieved from. https://lpdaac.usgs.gov/sites/default/files/public/product_documentation/mod09_user_guide_v1.4.pdf

Verrelst, J., Alonso, L., Camps-Valls, G., Delegido, J., & Moreno, J. (2012). Retrieval of vegetation biophysical parameters using Gaussian process techniques. *IEEE Transactions on Geoscience and Remote Sensing*, *50*(5), 1832–1843.

Verrelst, J., Camps-Valls, G., Munoz-Mari, J., Rivera, J. P., Veroustraete, F., Clevers, J., & Moreno, J. (2015). Optical remote sensing and the retrieval of terrestrial vegetation bio-geophysical properties—A review. *ISPRS Journal of Photogrammetry and Remote Sensing*, *108*, 273–290. https://doi.org/10.1016/j.isprsjprs.2015.05.005

Verrelst, J., Clevers, J. G. P. W., & Schaepman, M. E. (2010). Merging the Minnaert-k parameter with spectral unmixing to map forest heterogeneity with CHRIS/PROBA data. *IEEE Transactions on Geoscience and Remote Sensing*, *48*(11), 4014–4022. https://doi.org/10.1109/TGRS.2010.2047400

Verrelst, J., Muñoz, J., Alonso, L., Delegido, J., Rivera, J. P., Camps-Valls, G., & Moreno, J. (2012). Machine learning regression algorithms for biophysical parameter retrieval: Opportunities for Sentinel-2 and -3. *Remote Sensing of Environment*, *118*, 127–139. https://doi.org/10.1016/j.rse.2011.11.002

Verrelst, J., Rivera, J. P., Leonenko, G., Alonso, L., & Moreno, J. (2014). Optimizing LUT-based RTM inversion for semiautomatic mapping of crop biophysical parameters from Sentinel-2 and -3 data: Role of cost functions. *IEEE Transactions on Geoscience and Remote Sensing*, *52*(1), 257–269. https://doi.org/10.1109/TGRS.2013.2238242

Verrelst, J., Rivera, J. P., Veroustraete, F., Muñoz-Marí, J., Clevers, J. G. P. W., Camps-Valls, G., & Moreno, J. (2015). Experimental Sentinel-2 LAI estimation using parametric, non-parametric and physical retrieval methods—A comparison. *ISPRS Journal of Photogrammetry and Remote Sensing*, *108*, 260–272. https://doi.org/10.1016/j.isprsjprs.2015.04.013

Villa, P., Mousivand, A., & Bresciani, M. (2014). Aquatic vegetation indices assessment through radiative transfer modeling and linear mixture simulation. *International Journal of Applied Earth Observation and Geoinformation*, *30*, 113–127. https://doi.org/10.1016/j.jag.2014.01.017

Viña, A., Gitelson, A. A., Nguy-Robertson, A. L., & Peng, Y. (2011). Comparison of different vegetation indices for the remote assessment of green leaf area index of crops. *Remote Sensing of Environment*, *115*(12), 3468–3478. https://doi.org/10.1016/j.rse.2011.08.010

Viskari, T., Hardiman, B., Desai, A. R., & Dietze, M. C. (2015). Model-data assimilation of multiple phenological observations to constrain and predict leaf area index. *Ecological Applications*, *25*(2), 546–558. https://doi.org/10.1890/14-0497.1

Vuolo, F., Dini, L., & D'Urso, G. (2008). Retrieval of leaf area index from CHRIS/PROBA data: An analysis of the directional and spectral information content. *International Journal of Remote Sensing*, *29*(17), 5063–5072.

Vyas, D., Christian, B., & Krishnayya, N. S. R. (2013). Canopy level estimations of chlorophyll and LAI for two tropical species (teak and bamboo) from Hyperion (EO1) data. *International Journal of Remote Sensing*, *34*(5), 1676–1690. https://doi.org/10.1080/01431161.2012.725484

Vyas, D., Mehta, N., Dinakaran, J., & Krishnayya, N. S. R. (2010). Allometric equations for estimating leaf area index (LAI) of two important tropical species (Tectona grandis and Dendrocalamus strictus). *Journal of Forestry Research*, *21*(2), 197–200.
Walthall, C. L., Norman, J. M., Welles, J. M., Campbell, G., & Blad, B. L. (1985). Simple equation to approximate the bi-directional reflectance from vegetation canopies and bare soil surfaces. *Applied Optics*, *24*, 383–387.
Wang, C., Chen, J., Wu, J., Tang, Y., Shi, P., Black, T. A., & Zhu, K. (2017). A snow-free vegetation index for improved monitoring of vegetation spring green-up date in deciduous ecosystems. *Remote Sensing of Environment*, *196*, 1–12. https://doi.org/10.1016/j.rse.2017.04.031
Wang, C., Li, J., Liu, Q. H., Zhong, B., Wu, S. L., & Xia, C. F. (2017). Analysis of differences in phenology extracted from the enhanced vegetation index and the leaf area index. *Sensors*, *17*(9). https://doi.org/10.3390/s17091982
Wang, D., & Liang, S. (2010). Using multiresolution tree to integrate MODIS and MISR-L3 LAI products. Paper presented at the IEEE International Geoscience and Remote Sensing Symposium, Honolulu, Hawaii, USA.
Wang, D., & Liang, S. (2011). Integrating MODIS and CYCLOPES leaf area index products using empirical orthogonal functions. *IEEE Transactions on Geoscience and Remote Sensing*, *49*(5), 1513–1519.
Wang, D., & Liang, S. (2014). Improving LAI Mapping by Integrating MODIS and CYCLOPES LAI products using optimal interpolation. *IEEE Journal of Selected Topics in Applied Earth Observations and Remote Sensing*, *7*(2), 445–457. https://doi.org/10.1109/jstars.2013.2264870
Wang, J., Wang, J., Zhou, H., & Xiao, Z. (2017). Detecting forest disturbance in Northeast China from GLASS LAI time series data using a dynamic model. *Remote Sensing*, *9*(12), 1293. https://doi.org/10.3390/rs9121293
Wang, Q., Pang, Y., Li, Z., Chen, E., Sun, G., & Tan, B. (2013). Improvement and application of the conifer forest multiangular hybrid GORT model MGeoSAIL. *IEEE Transactions on Geoscience and Remote Sensing*, *in press*. https://doi.org/10.1109/TGRS.2012.2234466
Wang, Q., Tenhunen, J., Dinh, N. Q., Reichstein, M., Otieno, D., Granier, A., & Pilegarrd, K. (2005). Evaluation of seasonal variation of MODIS derived leaf area index at two European deciduous broadleaf forest sites. *Remote Sensing of Environment*, *96*(3-4), 475–484.
Wang, S., Li, X., Ge, Y., Jin, R., Ma, M., Liu, Q., et al. (2016). Validation of regional-scale remote sensing products in China: From site to network. *Remote Sensing*, *8*(12), 980. https://doi.org/10.3390/rs8120980
Wang, W. M., Li, Z. L., & Su, H. B. (2007). Comparison of leaf angle distribution functions: Effects on extinction coefficient and fraction of sunlit foliage. *Agricultural and Forest Meteorology*, *143*(1–2), 106–122. https://doi.org/10.1016/j.agrformet.2006.12.003
Wang, Y., Tian, Y., Zhang, Y., El-Saleous, N., Knyazikhin, Y., Vermote, E., & Myneni, R. B. (2001). Investigation of product accuracy as a function of input and model uncertainties: Case study with SeaWiFS and MODIS LAI/FPAR algorithm. *Remote Sensing of Environment*, *78*(3), 296–311.
Wang, Y., Woodcock, C. E., Buermann, W., Stenberg, P., Voipio, P., Smolander, H., et al. (2004). Evaluation of the MODIS LAI algorithm at a coniferous forest site in Finland. *Remote Sensing of Environment*, *91*(1), 114–127. https://doi.org/10.1016/j.rse.2004.02.007
Wang, Y.-P., Chang, K.-W., Chen, R.-K., Lo, J.-C., & Shen, Y. (2010). Large-area rice yield forecasting using satellite imageries. *International Journal of Applied Earth Observation and Geoinformation*, *12*(1), 27–35. https://doi.org/10.1016/j.jag.2009.09.009
Wang, Z., Schaaf, C. B., Strahler, A. H., Chopping, M. J., Román, M. O., Shuai, Y., et al. (2014). Evaluation of MODIS albedo product (MCD43A) over grassland, agriculture and forest surface types during dormant and snow-covered periods. *Remote Sensing of Environment*, *140*(0), 60–77. https://doi.org/10.1016/j.rse.2013.08.025
Warren Wilson, J. (1960). Inclined point quadrats. *New Phytologist*, *59*(1), 1–7.
Watson, D. J. (1947). Comparative physiological studies in the growth of field crops: I: Variation in net assimilation rate and leaf area between species and varieties, and within and between years. *Annals of Botany*, *11*(1), 41–76.
Wei, S., & Fang, H. (2016). Estimation of canopy clumping index from MISR and MODIS sensors using the normalized difference hotspot and darkspot (NDHD) method: The influence of BRDF models and solar zenith angle. *Remote Sensing of Environment*, *187*, 476–491. https://doi.org/10.1016/j.rse.2016.10.039
Weiskittel, A. R., & Maguire, D. A. (2006). Branch surface area and its vertical distribution in coastal Douglas-fir. *Trees-Structure and Function*, *20*(6), 657–667. https://doi.org/10.1007/s00468-006-0081-3
Weiss, M., & Baret, F. (2014). CAN-EYE V6.313 user manual. Retrieved from http://www6.paca.inra.fr/can-eye/Documentation-Publications/Documentation
Weiss, M., & Baret, F. (2017). Using 3D point clouds derived from UAV RGB Imagery to describe vineyard 3D macro-structure. *Remote Sensing*, *9*(2), 17. https://doi.org/10.3390/rs9020111
Weiss, M., Baret, F., Block, T., Koetz, B., Burini, A., Scholze, B., et al. (2014). On Line Validation Exercise (OLIVE): A web based service for the validation of medium resolution land products. Application to FAPAR Products. *Remote Sensing*, *6*(5), 4190–4216. https://doi.org/10.3390/rs6054190
Weiss, M., Baret, F., Garrigues, S., & Lacaze, R. (2007). LAI and fPAR CYCLOPES global products derived from VEGETATION. Part 2: Validation and comparison with MODIS collection 4 products. *Remote Sensing of Environment*, *110*(3), 317–331. https://doi.org/10.1016/j.rse.2007.03.001
Weiss, M., Baret, F., Myneni, R. B., Pragnere, A., & Knyazikhin, Y. (2000). Investigation of a model inversion technique to estimate canopy biophysical variables from spectral and directional reflectance data. *Agronomie*, *20*(1), 3–22.
Weiss, M., Baret, F., Smith, G. J., Jonckheere, I., & Coppin, P. (2004). Review of methods for in situ leaf area index (LAI) determination part II: Estimation of LAI, errors and sampling. *Agricultural and Forest Meteorology*, *121*(1-2), 37–53.
Weiss, M., Hurk, B., Haarsma, R., & Hazeleger, W. (2012). Impact of vegetation variability on potential predictability and skill of EC-Earth simulations. *Climate Dynamics*, *39*(11), 2733–2746. https://doi.org/10.1007/s00382-012-1572-0
White, J. D., Ryan, K. C., Running, S. W., Nemani, R., & Keane, R. E. (1997). Measurement and remote sensing of LAI in rocky mountain montane ecosystems. *Canadian Journal of Forest Research*, *27*(11), 1714–1727.
Widlowski, J.-L. (2015). Conformity testing of satellite-derived quantitative surface variables. *Environmental Science & Policy*, *51*, 149–169. https://doi.org/10.1016/j.envsci.2015.03.018
Widlowski, J.-L., Mio, C., Disney, M., Adams, J., Andredakis, I., Atzberger, C., et al. (2015). The fourth phase of the radiative transfer model intercomparison (RAMI) exercise: Actual canopy scenarios and conformity testing. *Remote Sensing of Environment*, *169*, 418–437. https://doi.org/10.1016/j.rse.2015.08.016
Widlowski, J. L., Taberner, M., Pinty, B., Bruniquel-Pinel, V., Disney, M., Fernandes, R., et al. (2007). Third Radiation Transfer Model Intercomparison (RAMI) exercise: Documenting progress in canopy reflectance models. *Journal of Geophysical Research*, *112*, D09111. https://doi.org/10.1029/2006JD007821
Williams, M., Kurpius, M. R., Schwarz, P. A., Law, B. E., & Irvine, J. (2005). An improved analysis of forest carbon dynamics using data assimilation. *Global Change Biology*, *11*(1), 89–105.

Wong, F. K. K., & Fung, T. (2013). Combining hyperspectral and radar imagery for mangrove leaf area index modeling. *Photogrammetric Engineering and Remote Sensing*, *79*(5), 479–490.
Woodgate, W., Armston, J. D., Disney, M., Jones, S. D., Suarez, L., Hill, M. J., et al. (2016). Quantifying the impact of woody material on leaf area index estimation from hemispherical photography using 3D canopy simulations. *Agricultural and Forest Meteorology*, *226-227*, 1–12. https://doi.org/10.1016/j.agrformet.2016.05.009
Woodgate, W., Jones, S. D., Suarez, L., Hill, M. J., Armston, J. D., Wilkes, P., et al. (2015). Understanding the variability in ground-based methods for retrieving canopy openness, gap fraction, and leaf area index in diverse forest systems. *Agricultural and Forest Meteorology*, *205*(0), 83–95. https://doi.org/10.1016/j.agrformet.2015.02.012
Wright, P., Bergin, M., Dibb, J., Lefer, B., Domine, F., Carman, T., et al. (2014). Comparing MODIS daily snow albedo to spectral albedo field measurements in Central Greenland. *Remote Sensing of Environment*, *140*(0), 118–129. https://doi.org/10.1016/j.rse.2013.08.044
Wu, H., & Li, Z. L. (2009). Scale issues in remote sensing: A review on analysis, processing and modeling. *Sensors*, *9*, 1768–1793. https://doi.org/10.3390/s90301768
Wu, M. Q., Niu, Z., Wang, C. Y., Wu, C. Y., & Wang, L. (2012). Use of MODIS and Landsat time series data to generate high-resolution temporal synthetic Landsat data using a spatial and temporal reflectance fusion model. *Journal of Applied Remote Sensing*, *6*. https://doi.org/10.1117/1.jrs.6.063507
Wythers, K. R., Reich, P. B., & Turner, D. P. (2003). Predicting leaf area index from scaling principles: Corroboration and consequences. *Tree Physiology*, *23*(17), 1171–1179.
Xiao, Z., Liang, S., & Jiang, B. (2017). Evaluation of four long time-series global leaf area index products. *Agricultural and Forest Meteorology*, *246*, 218–230. https://doi.org/10.1016/j.agrformet.2017.06.016
Xiao, Z., Liang, S., Wang, J., Chen, P., Yin, X., Zhang, L., & Song, J. (2014). Use of general regression neural networks for generating the GLASS leaf area index product from time-series MODIS surface reflectance. *IEEE Transactions on Geoscience and Remote Sensing*, *52*(1), 209–223. https://doi.org/10.1109/TGRS.2013.2237780
Xiao, Z., Liang, S., Wang, J., Jiang, B., & Li, X. (2011). Real-time retrieval of leaf area index from MODIS time series data. *Remote Sensing of Environment*, *115*(1), 97–106. https://doi.org/10.1016/j.rse.2010.08.009
Xiao, Z., Liang, S., Wang, J., Song, J., & Wu, X. (2009). A temporally integrated inversion method for estimating leaf area index from MODIS data. *IEEE Transactions on Geoscience and Remote Sensing*, *47*(8), 2536–2645.
Xiao, Z., Liang, S., Wang, J., Xiang, Y., Zhao, X., & Song, J. (2016). Long time-series global land surface satellite leaf area index product derived from MODIS and AVHRR surface reflectance. *IEEE Transactions on Geoscience and Remote Sensing*, *54*(9), 5301–5318. https://doi.org/10.1109/TGRS.2016.2560522
Xiao, Z., Wang, J., Liang, S., Zhou, H., Li, X., Zhang, L., et al. (2011). Variational retrieval of leaf area index from MODIS time series data: Examples from the Heihe river basin, north-west China. *International Journal of Remote Sensing*, *33*(3), 730–745. https://doi.org/10.1080/01431161.2011.577826
Xiao, Z., Wang, T., Liang, S., & Sun, R. (2016). Estimating the fractional vegetation cover from GLASS leaf area index product. *Remote Sensing*, *8*(4), 337. https://doi.org/10.3390/rs8040337
Xie, Q., Dash, J., Huang, W., Peng, D., Qin, Q., Mortimer, H., et al. (2018). Vegetation indices combining the red and red-edge spectral information for leaf area index retrieval. *IEEE Journal of Selected Topics in Applied Earth Observations and Remote Sensing*, *11*(5), 1482–1493. https://doi.org/10.1109/JSTARS.2018.2813281
Xie, Y., Wang, P., Bai, X., Khan, J., Zhang, S., Li, L., & Wang, L. (2017). Assimilation of the leaf area index and vegetation temperature condition index for winter wheat yield estimation using Landsat imagery and the CERES-Wheat model. *Agricultural and Forest Meteorology*, *246*, 194–206. https://doi.org/10.1016/j.agrformet.2017.06.015
Xie, Y., Wang, P., Sun, H., Zhang, S., & Li, L. (2017). Assimilation of leaf area index and surface soil moisture with the CERES-wheat model for winter wheat yield estimation using a particle filter algorithm. *IEEE Journal of Selected Topics in Applied Earth Observations and Remote Sensing*, *10*(4), 1303–1316. https://doi.org/10.1109/JSTARS.2016.2628809
Xu, B., Li, J., Park, T., Liu, Q., Zeng, Y., Yin, G., et al. (2018). An integrated method for validating long-term leaf area index products using global networks of site-based measurements. *Remote Sensing of Environment*, *209*, 134–151. https://doi.org/10.1016/j.rse.2018.02.049
Xu, B., Park, T., Yan, K., Chen, C., Zeng, Y., Song, W., et al. (2018). Analysis of global LAI/FPAR products from VIIRS and MODIS sensors for spatio-temporal consistency and uncertainty from 2012–2016. *Forests*, *9*(2), 73. https://doi.org/10.3390/f9020073
Xu, H., & Steven, M. D. (1996). Monitoring leaf area of sugar beet using ERS-1 SAR data. *International Journal of Remote Sensing*, *17*(17), 3401–3410.
Xu, R., Dai, J., Luo, W., Yin, X., Li, Y., Tai, X., et al. (2010). A photothermal model of leaf area index for greenhouse crops. *Agricultural and Forest Meteorology*, *150*(4), 541–552. https://doi.org/10.1016/j.agrformet.2010.01.019
Yan, H., Wang, S. Q., Billesbach, D., Oechel, W., Zhang, J. H., Meyers, T., et al. (2012). Global estimation of evapotranspiration using a leaf area index-based surface energy and water balance model. *Remote Sensing of Environment*, *124*(0), 581–595. https://doi.org/10.1016/j.rse.2012.06.004
Yan, K., Park, T., Chen, C., Xu, B., Song, W., Yang, B., et al. (2018). Generating global products of LAI and FPAR from SNPP-VIIRS Data: Theoretical background and implementation. *IEEE Transactions on Geoscience and Remote Sensing*, *56*(4), 2119–2137. https://doi.org/10.1109/TGRS.2017.2775247
Yan, K., Park, T., Yan, G., Liu, Z., Yang, B., Chen, C., et al. (2016). Evaluation of MODIS LAI/FPAR product collection 6. Part 2: Validation and intercomparison. *Remote Sensing*, *8*(6), 460. https://doi.org/10.3390/rs8060460
Yang, F., Sun, J., Fang, H., Yao, Z., Zhang, J., Zhu, Y., et al. (2012). Comparison of different methods for corn LAI estimation over northeastern China. *International Journal of Applied Earth Observation and Geoinformation*, *18*, 462–471. https://doi.org/10.1016/j.jag.2011.09.004
Yang, G., Zhao, C., Liu, Q., Huang, W., & Wang, J. (2011). Inversion of a radiative transfer model for estimating forest LAI from multisource and multiangular optical remote sensing data. *IEEE Transactions on Geoscience and Remote Sensing*, *49*(3), 988–1000.
Yang, P., Shibasaki, R., Wu, W., Zhou, Q., Chen, Z., Zha, Y., et al. (2007). Evaluation of MODIS land cover and LAI products in cropland of North China Plain using *in situ* measurements and Landsat TM images. *IEEE Transactions on Geoscience and Remote Sensing*, *45*(10), 3087–3097. https://doi.org/10.1109/TGRS.2007.902426
Yang, W., Shabanov, N. V., Huang, D., Wang, W., Dickinson, R. E., Nemani, R. R., et al. (2006). Analysis of leaf area index products from combination of MODIS Terra and Aqua data. *Remote Sensing of Environment*, *104*(3), 297–312.
Yao, Y., Liu, Q., Liu, Q., & Li, X. (2008). LAI retrieval and uncertainty evaluations for typical row-planted crops at different growth stages. *Remote Sensing of Environment*, *112*(1), 94–106. https://doi.org/10.1016/j.rse.2006.09.037
Yin, G. F., Li, A. N., Zeng, Y. L., Xu, B. D., Zhao, W., Nan, X., et al. (2016). A cost-constrained sampling strategy in support of LAI product validation in mountainous areas. *Remote Sensing*, *8*(9), 17. https://doi.org/10.3390/rs8090704

Yin, G. F., Li, J., Liu, Q. H., Zhong, B., & Li, A. N. (2016). Improving LAI spatio-temporal continuity using a combination of MODIS and MERSI data. *Remote Sensing Letters*, *7*(8), 771–780. https://doi.org/10.1080/2150704x.2016.1182657

Yoshida, H., Horie, T., Katsura, K., & Shiraiwa, T. (2007). A model explaining genotypic and environmental variation in leaf area development of rice based on biomass growth and leaf N accumulation. *Field Crops Research*, *102*(3), 228–238. https://doi.org/10.1016/j.fcr.2007.04.006

Yu, Y., Tarpley, D., Privette, J. L., Flynn, L. E., Xu, H., Chen, M., et al. (2012). Validation of GOES-R satellite land surface temperature algorithm using SURFRAD ground measurements and statistical estimates of error properties. *IEEE Transactions on Geoscience and Remote Sensing*, *50*(3), 704–713.

Yuan, H., Dai, Y., Xiao, Z., Ji, D., & Shangguan, W. (2011). Reprocessing the MODIS leaf area index products for land surface and climate modelling. *Remote Sensing of Environment*, *115*(5), 1171–1187. https://doi.org/10.1016/j.rse.2011.01.001

Zeng, X., Shaihk, M., Dai, Y., Dickinson, R. E., & Myneni, R. (2002). Coupling of the Common Land Model to the NCAR Community Climate Model. *Journal of Climate*, *15*(14), 1832–1854.

Zeng, Y., Li, J., Liu, Q., Li, L., Xu, B., Yin, G., & Peng, J. (2014). A sampling strategy for remotely sensed LAI product validation over heterogeneous land surfaces. *IEEE Journal of Selected Topics in Applied Earth Observations and Remote Sensing*, *7*(7), 3128–3142. https://doi.org/10.1109/JSTARS.2014.2312231

Zeng, Z., Piao, S., Li, L. Z. X., Wang, T., Ciais, P., Lian, X., et al. (2018). Impact of Earth greening on the terrestrial water cycle. *Journal of Climate*, *31*(7), 2633–2650. https://doi.org/10.1175/jcli-d-17-0236.1

Zeng, Z. Z., Zhu, Z. C., Lian, X., Li, L. Z. X., Chen, A. P., He, X. G., & Piao, S. L. (2016). Responses of land evapotranspiration to Earth's greening in CMIP5 Earth system models. *Environmental Research Letters*, *11*(10). https://doi.org/10.1088/1748-9326/11/10/104006

Zhang, H. K., Chen, J. M., Huang, B., Song, H. H., & Li, Y. R. (2014). Reconstructing seasonal variation of Landsat vegetation index related to leaf area index by fusing with MODIS data. *IEEE Journal of Selected Topics in Applied Earth Observations and Remote Sensing*, *7*(3), 950–960. https://doi.org/10.1109/jstars.2013.2284528

Zhang, L. P., Zhang, L. F., & Du, B. (2016). Deep learning for remote sensing data—A technical tutorial on the state of the art. *IEEE Geoscience and Remote Sensing Magazine*, *4*(2), 22–40. https://doi.org/10.1109/mgrs.2016.2540798

Zhang, P., Anderson, B., Barlow, M., Tan, B., & Myneni, R. B. (2004). Climate-related vegetation characteristics derived from Moderate Resolution Imaging Spectroradiometer (MODIS) leaf area index and normalized difference vegetation index. *Journal of Geophysical Research*, *109*, D20105. https://doi.org/10.1029/2004JD004720

Zhang, P., Anderson, B., Tan, B., Huang, D., & Myneni, R. (2005). Potential monitoring of crop production using a satellite-based climate-variability impact index. *Agricultural and Forest Meteorology*, *132*, 344–358.

Zhang, Q., Xiao, X., Braswell, B., Linder, E., Baret, F., & Moore, B. III (2005). Estimating light absorption by chlorophyll, leaf and canopy in a deciduous broadleaf forest using MODIS data and a radiative transfer model. *Remote Sensing of Environment*, *99*, 357–371.

Zhang, X., Yan, G., Li, Q., Li, Z. L., Wan, H., & Guo, Z. (2006). Evaluating the fraction of vegetation cover based on NDVI spatial scale correction model. *International Journal of Remote Sensing*, *27*(24), 5359–5372.

Zhao, D., Yang, T., & An, S. (2012). Effects of crop residue cover resulting from tillage practices on LAI estimation of wheat canopies using remote sensing. *International Journal of Applied Earth Observation and Geoinformation*, *14*(1), 169–177. https://doi.org/10.1016/j.jag.2011.09.003

Zhao, F., Strahler, A. H., Schaaf, C. L., Yao, T., Yang, X., Wang, Z., et al. (2012). Measuring gap fraction, element clumping index and LAI in Sierra Forest stands using a full-waveform ground-based lidar. *Remote Sensing of Environment*, *125*, 73–79. https://doi.org/10.1016/j.rse.2012.07.007

Zhao, F., Yang, X., Schull, M. A., Román-Colón, M. O., Yao, T., Wang, Z., et al. (2011). Measuring effective leaf area index, foliage profile, and stand height in New England forest stands using a full-waveform ground-based lidar. *Remote Sensing of Environment*, *115*(11), 2954–2964. https://doi.org/10.1016/j.rse.2010.08.030

Zhao, K., García, M., Liu, S., Guo, Q., Chen, G., Zhang, X., et al. (2015). Terrestrial lidar remote sensing of forests: Maximum likelihood estimates of canopy profile, leaf area index, and leaf angle distribution. *Agricultural and Forest Meteorology*, *209–210*, 100–113. https://doi.org/10.1016/j.agrformet.2015.03.008

Zhao, K., & Popescu, S. (2009). Lidar-based mapping of leaf area index and its use for validating GLOBCARBON satellite LAI product in a temperate forest of the southern USA. *Remote Sensing of Environment*, *113*(8), 1628–1645.

Zhao, K. G., Popescu, S., Meng, X. L., Pang, Y., & Agca, M. (2011). Characterizing forest canopy structure with lidar composite metrics and machine learning. *Remote Sensing of Environment*, *115*(8), 1978–1996. https://doi.org/10.1016/j.rse.2011.04.001

Zheng, G., & Moskal, L. M. (2009). Retrieving leaf area index (LAI) using remote sensing: Theories, methods and sensors. *Sensors*, *9*(4), 2719–2745.

Zheng, G., Moskal, L. M., & Kim, S.-H. (2013). Retrieval of effective leaf area index in heterogeneous forests with terrestrial laser scanning. *IEEE Transactions on Geoscience and Remote Sensing*, *51*(2), 777–786.

Zhou, G., Niu, C., Xu, W., Yang, W., Wang, J., & Zhao, H. (2015). Canopy modeling of aquatic vegetation: A radiative transfer approach. *Remote Sensing of Environment*, *163*(0), 186–205. https://doi.org/10.1016/j.rse.2015.03.015

Zhou, J., Jia, L., Menenti, M., & Gorte, B. (2016). On the performance of remote sensing time series reconstruction methods—A spatial comparison. *Remote Sensing of Environment*, *187*, 367–384. http://doi.org/10.1016/j.rse.2016.10.025

Zhou, Y., Hilker, T., Ju, W., Coops, N. C., Black, T. A., Chen, J. M., & Wu, X. (2017). Modeling gross primary production for sunlit and shaded canopies across an evergreen and a deciduous site in Canada. *IEEE Transactions on Geoscience and Remote Sensing*, *55*(4), 1859–1873. https://doi.org/10.1109/TGRS.2016.2615102

Zhu, L., Chen, J. M., Tang, S., Li, G., & Guo, Z. (2014). Inter-comparison and validation of the FY-3A/MERSI LAI product over Mainland China. *IEEE Journal of Selected Topics in Applied Earth Observations and Remote Sensing*, *7*(2), 458–468. https://doi.org/10.1109/JSTARS.2013.2280466

Zhu, Z., Bi, J., Pan, Y., Ganguly, S., Anav, A., Xu, L., et al. (2013). Global data sets of vegetation leaf area index (LAI)3g and Fraction of Photosynthetically Active Radiation (FPAR)3g derived from Global Inventory Modeling and Mapping Studies (GIMMS) Normalized Difference Vegetation Index (NDVI3g) for the period 1981 to 2011. *Remote Sensing*, *5*(2), 927–948.

Zhu, Z., Fu, Y., Woodcock, C. E., Olofsson, P., Vogelmann, J. E., Holden, C., et al. (2016). Including land cover change in analysis of greenness trends using all available Landsat 5, 7, and 8 images: A case study from Guangzhou, China (2000–2014). *Remote Sensing of Environment*, *185*, 243–257. https://doi.org/10.1016/j.rse.2016.03.036

Zhu, Z., Piao, S., Myneni, R. B., Huang, M., Zeng, Z., Canadell, J. G., et al. (2016). Greening of the Earth and its drivers. *Nature Climate Change*, *6*(8), 791–795. https://doi.org/10.1038/nclimate3004, http://www.nature.com/nclimate/journal/vaop/ncurrent/abs/nclimate3004.html#supplementary-information

Zhu, Z., Woodcock, C. E., Holden, C., & Yang, Z. (2015). Generating synthetic Landsat images based on all available Landsat data: Predicting Landsat surface reflectance at any given time. *Remote Sensing of Environment*, *162*, 67–83. https://doi.org/10.1016/j.rse.2015.02.009

Zhu, Z. C., Piao, S. L., Lian, X., Myneni, R. B., Peng, S. S., & Yang, H. (2017). Attribution of seasonal leaf area index trends in the northern latitudes with "optimally" integrated ecosystem models. *Global Change Biology*, *23*(11), 4798–4813. https://doi.org/10.1111/gcb.13723

Zou, J., Yan, G., Zhu, L., & Zhang, W. (2009). Woody-to-total area ratio determination with a multispectral canopy imager. *Tree Physiology*, *29*(8), 1069–1080. https://doi.org/10.1093/treephys/tpp042

References From the Supporting Information

Abuelgasim, A. A., Fernandes, R. A., & Leblanc, S. G. (2006). Evaluation of national and global LAI products derived from optical remote sensing instruments over Canada. *IEEE Transactions on Geoscience and Remote Sensing*, *44*(7), 1872–1884. https://doi.org/10.1109/TGRS.2006.874794

Aguirre-Salado, C. A., Valdez-Lazalde, J. R., Ángeles-Pérez, G., de los Santos-Posadas, H. M., & Aguirre-Salado, A. I. (2011). Mapeo del índice de área foliar y cobertura arbórea mendiante fotografía hemisférica y datos SPOT 5 HRG: regresión y k-nn. *Agrociencia*, *45*, 105–119.

Amani, M., & Mobasheri, M. R. (2015). A parametric method for estimation of leaf area index using landsat ETM plus data. *Giscience & Remote Sensing*, *52*(4), 478–497. https://doi.org/10.1080/15481603.2015.1055540

Chaurasia, S., Parihar, J. S., Bhattacharya, B., & Dadhwal, V. K. (2006). Field-scale leaf area index estimation using IRS-1D LISS-III data. *International Journal of Remote Sensing*, *27*(4), 637–644.

De Kauwe, M. G., Disney, M. I., Quaife, T., Lewis, P., & Williams, M. (2011). An assessment of the MODIS collection 5 leaf area index product for a region of mixed coniferous forest. *Remote Sensing of Environment*, *115*(2), 767–780. https://doi.org/10.1016/j.rse.2010.11.004

Delegido, J., Fernández, G., Gandía, S., & Moreno, J. (2008). Retrieval of chlorophyll conent and LAI of crops using hyperspectral techniques: Application to PROBA/CHRIS data. *International Journal of Remote Sensing*, *29*(24), 7107–7127.

Demarty, J., Chevallier, F., Friend, A. D., Viovy, N., Piao, S., & Ciais, P. (2007). Assimilation of global MODIS leaf area index retrievals within a terrestrial biosphere model. *Geophysical Research Letters*, *34*, L15402. https://doi.org/10.1029/2007GL030014

Fang, H., Liang, S., & Hoogenboom, G. (2011). Integration of MODIS LAI and vegetation index products with the CSM-CERES-Maize model for corn yield estimation. *International Journal of Remote Sensing*, *32*(4), 1039–1065. https://doi.org/10.1080/01431160903505310

Fang, H., Liang, S., Hoogenboom, G., Teasdale, J., & Cavigelli, M. (2008). Corn yield estimation through assimilation of remote sensed data into the CSM-CERES-Maize model. *International Journal of Remote Sensing*, *29*(10), 3011–3032.

Gonsamo, A. (2010). Leaf area index retrieval using gap fractions obtained from high resolution satellite data: Comparisons of approaches, scales and atmospheric effects. *International Journal of Applied Earth Observation and Geoinformation*, *12*(4), 233–248. https://doi.org/10.1016/j.jag.2010.03.002

Gu, Z., Sanchez-Azofeifa, G. A., Feng, J., & Cao, S. (2015). Predictability of leaf area index using vegetation indices from multiangular CHRIS/PROBA data over eastern China. *Journal of Applied Remote Sensing*, *9*(1), 096085. https://doi.org/10.1117/1.JRS.9.096085

Harkonen, S., Lehtonen, A., Manninen, T., Tuominen, S., & Peltoniemi, M. (2015). Estimating forest leaf area index using satellite images: Comparison of k-NN based Landsat-NFI LAI with MODIS-RSR based LAI product for Finland. *Boreal Environment Research*, *20*(2), 181–195.

He, B., Li, X., Quan, X., & Qiu, S. (2015). Estimating the aboveground dry biomass of grass by assimilation of retrieved LAI into a crop growth model. *IEEE Journal of Selected Topics in Applied Earth Observations and Remote Sensing*, *8*(2), 550–561. https://doi.org/10.1109/JSTARS.2014.2360676

Heiskanen, J. (2006). Estimating aboveground tree biomass and leaf area index in a mountain birch forest using ASTER satellite data. *International Journal of Remote Sensing*, *27*(6), 1135–1158.

Huang, J., Sedano, F., Huang, Y., Ma, H., Li, X., Liang, S., et al. (2016). Assimilating a synthetic Kalman filter leaf area index series into the WOFOST model to improve regional winter wheat yield estimation. *Agricultural and Forest Meteorology*, *216*, 188–202. https://doi.org/10.1016/j.agrformet.2015.10.013

Huang, J., Tian, L., Liang, S., Ma, H., Becker-Reshef, I., Huang, Y., et al. (2015). Improving winter wheat yield estimation by assimilation of the leaf area index from Landsat TM and MODIS data into the WOFOST model. *Agricultural and Forest Meteorology*, *204*(0), 106–121. https://doi.org/10.1016/j.agrformet.2015.02.001

Huang, M., Chen, J. M., & Deng, F. (2011). Data-model fusion for improving LAI mapping: a case study over China's land mass. *International Journal of Remote Sensing*, *32*(22), 7279–7296. https://doi.org/10.1080/01431161.2010.520347

Kappas, M., Propastin, P., Degener, J., & Renchin, T. (2015). Inter-comparison and evaluation of the global LAI product (LAI3g) and the regional LAI product (GGRS-LAI) over the Area of Kazakhstan. *Remote Sensing*, *7*(4), 3760–3782.

Korhonen, L., Hadi, Packalen, P., & Rautiainen, M. (2017). Comparison of Sentinel-2 and Landsat 8 in the estimation of boreal forest canopy cover and leaf area index. *Remote Sensing of Environment*, *195*, 259–274. https://doi.org/10.1016/j.rse.2017.03.021

Lefsky, M. A., Hudak, A. T., Cohen, W. B., & Acker, S. A. (2005). Geographic variability in lidar predictions of forest stand structure in the Pacific Northwest. *Remote Sensing of Environment*, *95*(4), 532–548. https://doi.org/10.1016/j.rse.2005.01.010

Li, W., Weiss, M., Waldner, F., Defourny, P., Demarez, V., Morin, D., et al. (2015). A generic algorithm to estimate LAI, FAPAR and FCOVER variables from SPOT4_HRVIR and Landsat sensors: Evaluation of the consistency and comparison with ground measurements. *Remote Sensing*, *7*(11), 15494–15516. https://doi.org/10.3390/rs71115494

Li, X., Lu, H., Yu, L., & Yang, K. (2018). Comparison of the spatial characteristics of four remotely sensed leaf area index products over China: Direct validation and relative uncertainties. *Remote Sensing*, *10*(1), 148.

Li, X., Zhang, Y., Luo, J., Jin, X., Xu, Y., & Yang, W. (2016). Quantification winter wheat LAI with HJ-1CCD image features over multiple growing seasons. *International Journal of Applied Earth Observation and Geoinformation*, *44*, 104–112. https://doi.org/10.1016/j.jag.2015.08.004

Liu, Y., Xiao, J., Ju, W., Zhu, G., Wu, X., Fan, W., et al. (2018). Satellite-derived LAI products exhibit large discrepancies and can lead to substantial uncertainty in simulated carbon and water fluxes. *Remote Sensing of Environment*, *206*, 174–188. https://doi.org/10.1016/j.rse.2017.12.024

Masemola, C., Cho, M. A., & Ramoelo, A. (2016). Comparison of Landsat 8 OLI and Landsat 7 ETM+ for estimating grassland LAI using model inversion and spectral indices: Case study of Mpumalanga, South Africa. *International Journal of Remote Sensing*, *37*(18), 4401–4419. https://doi.org/10.1080/01431161.2016.1212421

Mokhtari, A., Noory, H., & Vazifedoust, M. (2018). Improving crop yield estimation by assimilating LAI and inputting satellite-based surface incoming solar radiation into SWAP model. *Agricultural and Forest Meteorology*, *250–251*, 159–170. https://doi.org/10.1016/j.agrformet.2017.12.250

Morsdorf, F., Kötz, B., Meier, E., Itten, K. I., & Allgöwer, B. (2006). Estimation of LAI and fractional cover from small footprint airborne laser scanning data based on gap fraction. *Remote Sensing of Environment*, *104*(1), 50–61.

Nguy-Robertson, A. L., & Gitelson, A. A. (2015). Algorithms for estimating green leaf area index in C3 and C4 crops for MODIS, Landsat TM/ETM+, MERIS, Sentinel MSI/OLCI, and Venμs sensors. *Remote Sensing Letters*, *6*(5), 360–369. https://doi.org/10.1080/2150704x.2015.1034888

Pearse, G. D., Morgenroth, J., Watt, M. S., & Dash, J. P. (2017). Optimising prediction of forest leaf area index from discrete airborne lidar. *Remote Sensing of Environment*, *200*(Supplement C), 220–239. https://doi.org/10.1016/j.rse.2017.08.002

Pisek, J., & Chen, J. M. (2007). Comparison and validation of MODIS and VEGETATION global LAI products over four BigFoot sites in North America. *Remote Sensing of Environment*, *109*(1), 81–94. https://doi.org/10.1016/j.rse.2006.12.004

Pope, G., & Treitz, P. (2013). Leaf area index (LAI) estimation in boreal mixedwood forest of Ontario, Canada using Light Detection and Ranging (LiDAR) and WorldView-2 Imagery. *Remote Sensing*, *5*(10), 5040–5063. https://doi.org/10.3390/rs5105040

Propastin, P., & Panferov, O. (2013). Retrieval of remotely sensed LAI using Landsat ETM+ data and ground measurements of solar radiation and vegetation structure: Implication of leaf inclination angle. *International Journal of Applied Earth Observation and Geoinformation*, *25*(0), 38–46. https://doi.org/10.1016/j.jag.2013.02.006

Pu, R. L. (2012). Mapping leaf area index over a mixed natural forest area in the flooding season using ground-based measurements and Landsat TM imagery. *International Journal of Remote Sensing*, *33*(20), 6600–6622. https://doi.org/10.1080/01431161.2012.692887

Pu, R. L., Gong, P., & Yu, Q. (2008). Comparative analysis of EO-1 ALI and Hyperion, and Landsat ETM+ data for mapping forest crown closure and leaf area index. *Sensors*, *8*(6), 3744–3766. https://doi.org/10.3390/s8063744

Roumenina, E., Dimitrov, P., Filchev, L., & Jelev, G. (2014). Validation of MERIS LAI and FAPAR products for winter wheat-sown test fields in North-East Bulgaria. *International Journal of Remote Sensing*, *35*(10), 3859–3874. https://doi.org/10.1080/01431161.2014.919681

Sasaki, T., Imanishi, J., Ioki, K., Morimoto, Y., & Kitada, K. (2008). Estimation of leaf area index and canopy openness in broad-leaved forest using an airborne laser scanner in comparison with high-resolution near-infrared digital photography. *Landscape and Ecological Engineering*, *4*(1), 47–55. https://doi.org/10.1007/s11355-008-0041-8

Siegmann, B., Jarmer, T., Beyer, F., & Ehlers, M. (2015). The potential of pan-sharpened EnMAP data for the assessment of wheat LAI. *Remote Sensing*, *7*(10), 12737.

Strahler, A. H., Jupp, D. L. B., Woodcock, C. E., Schaaf, C. B., Yao, T., Zhao, F., et al. (2008). Retrieval of forest structural parameters using a ground-based lidar instrument (Echidna®). *Canadian Journal of Remote Sensing*, *34*(sup2), S426–S440. https://doi.org/10.5589/m08-046

Tripathi, P., Patel, N. R., Kushwaha, S. P. S., & Dadhwal, V. K. (2014). Upscaling of leaf area index in Terai forest plantations using fine- and moderate-resolution satellite data. *International Journal of Remote Sensing*, *35*(22), 7749–7762. https://doi.org/10.1080/01431161.2014.976886

Vuolo, F., Neugebauer, N., Bolognesi, S., Atzberger, C., & D'Urso, G. (2013). Estimation of leaf area index using DEIMOS-1 data: Application and transferability of a semi-empirical relationship between two agricultural areas. *Remote Sensing*, *5*(3), 1274–1291.

Wang, C., & Qi, J. (2008). Biophysical estimation in tropical forests using JERS-1 VNIR imagery. I: Leaf area index. *International Journal of Remote Sensing*, *29*(23), 6811–6826.

Zhao, J., Li, J., Liu, Q., Wang, H., Chen, C., Xu, B., & Wu, S. (2018). Comparative analysis of Chinese HJ-1 CCD, GF-1 WFV and ZY-3 MUX sensor data for leaf area index estimations for maize. *Remote Sensing*, *10*(1), 68. https://doi.org/10.3390/rs10010068